Doctoral Thesis

Morphometric analysis of drainage basins in the Western Arabian Peninsula in relation to geomorphic processes and lithologic control

(アラビア半島西部の流域地形の計測と解析 ー地形プロセスと岩質との関連)

プルパダン ユヌス アリ

ABSTRACT

The Arabian Peninsula has a very long geological history, extending back to the Precambrian. The Tertiary Red Sea-Gulf of the Suez rift system is a prime example of active continental rifting and breakup. The uplift of the western margin of the Arabian Plate and the opening of the Red Sea led to the formation of well-developed mountain escarpments with the highest elevations over 3000 m. The resultant escarpments have been subjected to natural processes to form steep drainage systems in the Western Arabian Peninsula. Although the Peninsula has been studied from a geological perspective in relation to oil production, plate tectonics and eolian systems such as sand dunes, the steep mountainous drainage basins have received much less attention. The geomorphological studies exist regarding the Western Arabian Peninsula have mostly been carried out by petroleum geologists whose main interest is not geomorphology itself. Fluvial processes and landscape development there are poorly understood, in spite of some practical hydrological studies related to water availability. Considering the lack of comprehensive geomorphological research on the steep drainage basins in the mountainous terrain of the Western Arabian Peninsula, this study aims morphological quantification and comparisons of 36 drainage basins and their 1046 sub-basins.

A total of 21 morphometric parameters were extracted from the ASTER GDEM using geographic information systems (GIS) and multivariate statistical analyses were conducted to classify the basins and discuss the potential factors affecting drainage-basin form and development. Principal component analysis (PCA) and hierarchical cluster analysis (CA) were used to identify the variance distinguishing the morphometric parameters. Three major principal components (PC1 to PC3) were found to explain 73% of total variance. PC1 strongly reflects basin dimensions and drainage texture; their positive correlations indicate enhanced erosion in large basins as well as limited stream incision in small basins under an arid climate. PC2 mainly reflects the effect of bedrock geology, suggesting that volcanic rocks tend to produce more elongated and less eroded immature basins than crystalline rocks. PC3 mainly reflects the basin relief, slope and the length of each stream segment which may indicate the effect of mass wasting on stream development.

The erosional processes and depositional environment in the study area are analyzed from the alluvial fans at the mouth of the drainage basins. The commonly used power law expressions for the fan area–basin area relation and the fan slope–basin area relation were applied to examine the area and slope of alluvial fans and source areas. The

analysis shows the size of the alluvial fans tends to be large but it corresponds well to their large source basins. The fan slope is steep and variable, reflecting that fans formed the arid climate is less organized than those in humid regions.

This study as also evaluated the spatial controls on basin hypsometry by assessing factors that might influence the distribution of hypsometric integrals (*HI*). From the main basins defined, three sets of sub-basins were derived for each Strahler order ranging from 4 to 6. Then *HI* versus distance were plotted for each basin order for further analysis. Results reveal that basin hypsometry is independent of spatial variation and spatial scale. Furthermore, *HI* and hypsometric curves were analysed in terms of lithologic control on landforms. The result suggests that basin hypsometry is sensitive to lithological variation in the study area. At the largest scale, the *HI* values can be divided into two populations. More evenly distributed erosion in crystalline rocks and relatively uneven erosion in volcanic rocks are suggested from the results.

Longitudinal river profiles for the main channels of the 36 major basins were extracted from the DEM and the steepness and concavity indices were plotted using MathWorks Matlab codes. High steepness and low concavity in volcanic rocks and a reverse trend in crystalline rocks confirms the observation from the results of basin hypsometric analysis. For the first time in this region, knickzone analysis was conducted by using changing rate of river gradient at different scales; a total stream length of 5121 km was analysed and 325 knickzones were identified and interpreted. Knickzone frequency and knickzone density vary according to bedrock types. The effect of faults on knickzone abundance found weaker in relation to tectonics. The investigation suggests a coupled climatic and bedrock control for the origin of knickzones.

Table of Contents

List of figures

List of tables

CHAPTER 1: Introduction

River responses to different climatic, lithologic, and tectonic settings are fundamental to understand the evolution of topography (Jansen et al., 2011). Several geomorphometric indices characteristic of a river network have been formulated to describe the evolutionary stages of landforms. For instance, an analysis of river longitudinal profiles offers a promising means to understand the stages of drainage basin evolution (e.g., Gardner, 1983; Howard et al., 1994; Hurtrez et al., 1999; Whipple and Tucker, 1999; Kirby and Whipple, 2001; Ouimet et al., 2009), because they provide details on the primary mechanism of bed rock incision (Wobus et al., 2006; Kirby and Whipple, 2012). Such drainage or drainage basin morphometry has been widely studied around the globe (e.g., Dietrich et al., 2003; Crosby and Whipple, 2006; Olivetti et al., 2012). However, less attention is directed towards the landscape development in some particular areas including the steep drainage systems of the Western Arabian Peninsula. The peninsula has been much previously studied from the viewpoint of petroleum geology (e.g., McGillivray and Husseini, 1992; Cole et al., 1994), geological structures (e.g., Nehlig et al., 2002; Johnson and Woldehaimanot, 2003), eolian landforms (e.g., Holm, 1960; Fryberger et al., 1984; Sagga, 1993), and plate tectonics (Brown, 1972; Stern and Johnson, 2010). Yet, the geomorphology of the drainage basins in the peninsula and the fluvial processes acting there have received limited consideration (Vincent, 2008).

Although some geomorphological studies exist regarding the Western Arabian Peninsula, they have mostly been carried out by petroleum geologists whose main interest is not geomorphology itself (Chapman, 1978; Fourniguet et al., 1985) or in relation to a practical issue of water availability. The economic boom caused by the discovery of oil fields in the Peninsula during the 1960s attracted many geologists from around the world to Arabia. Intensive geological surveys on Western Arabia begun in 1963 by G.S Brown of the USGS, followed by the mineral occurrence mapping by the Japanese Geological Survey in 1964 under the direction of Dr. Shizuka Okumi, and later in 1965 for mineral prospecting by the BRGM, France, by Jacques Reneaux (Brown et al., 1989). However, a major concern for people in the Arabian Peninsula, an arid region with low intensity rainfall, high temperature and high evaporation rates, has been water scarcity. A reconnaissance survey in this regard was conducted in 1944 by Max Steinke and E.L Berg of the ARAMCO and Lt. G Wadsack of the American Military, successfully mapping ~10000 km^2 along the Red Sea coast (Brown et al., 1989). The ever increasing population and thus the urbanisation placed severe demands on water resources and therefore geomorphological attention in the 1980s and later focussed on water availability. The geomorphological characterisation of drainage basins for surface

water potential and ground water recharge were included in a number of studies (e.g., Hötzl and Zötl, 1978; Hötzl, 1995; Al-Turki, 1995; Subyani and Bayumi, 2001; Sen, 2008). Al-Turki (1995) investigated wells in the aquifers of Precambrian Crystalline rocks in the Arabian Shield and noted that they yield very limited water because of poor permeability and low intensity rainfall. Alluvial fans of several kilometres are present at the foot of the Red Sea escarpment and along the large drainages. Sen (2008) noted that these fans play an important role as potential aquifers and provide groundwater in coastal arid regions. The problem of saline intrusion in to ground water of the Wadi Yalamlam basin was addressed in Subyani (2005). Although the peninsula falls under arid to semi-arid climates (Koppen, 1936), occasional heavy rainstorms occur in some parts of the peninsula (Almazroui, 2011) and the recent literatures suggest an increase of interest in flood hazard and slope stability studies (Youssef et al., 2012; Alharbi et al., 2013).

Except the practical hydrological studies noted above, fluvial processes and landscape development in the western margin of the peninsula are poorly understood; because harsh terrain with low accessibility and limited mapping base made the benchmark research extremely difficult (Vincent, 2008). Nevertheless, some researchers such as Miller (1937), Brown (1970) and Vincent (2008) made interesting interpretations about ancient stream captures in the steep drainage basins and discussed the Tertiary drainage development in the Western Peninsula. The drainage pattern and their arrangement that determine the efficiency of drainage systems in the peninsula were discussed by Sen (2008). According to his study, these drainage patterns may be controlled by factors such as slope, climate, vegetation, soil and the nature of rocks. Chapman (1978) pointed out that during the Pleistocene epoch, rainfall was heavier and temperature was lower than today and such differences in climate may have left their imprints on the landforms. Hötzl et al., (1978) linked the sedimentation process of drainage basins in the peninsula to flash floods resulting from the occasional rainfall which set huge mass of sediments to motion. The timing and magnitude of denudation, role of extensional faults and orientation of drainages in the peninsula were discussed by Davison et al. (1998), but their study was limited to a small part of the Yemen region. General summaries of alluvial fill processes in the drainage basins of Arabia were provided by Glennie (1987) and Reineck and Singh (1973). However, none of these studies have quantitatively characterized the form and development of drainage basins in the Western Arabian Peninsula and therefore a full scientific understanding of landforms there is still lacking. Although Subyani et al., (2012) applied multivariate techniques to the geomorphology of steep basins in the Arabian Peninsula, they investigated only ten major basins, which places a limit on the statistical significance of the work. In addition, their paper is predominantly technical, with limited discussion regarding the

geomorphological implications of the results.

Considering the lack of comprehensive geomorphological research on the steep drainage basins in the mountainous terrain of the Western Arabian Peninsula, this study presents morphological quantification and comparisons of 36 basins and 1046 sub-basins there. The study also examines 21 DEM-derived morphometric parameters, and conducts multivariate statistical analyses to classify the basins and discuss the potential factors affecting drainage-basin form and development. The study also examines the influence of bedrock geology on various landforms by means of the hypsometric integral, river concavity, and the steepness index. Moreover, this study investigates knickzones in terms of their distribution and properties in the 36 main channels to discuss their forms and origin. As far as the author knows, no previous studies performed such geomorphometric analyses including knickzone characterization in the studied region.

CHAPTER 2: Review of previous studies on drainage basin morphometry

2.1 Brief history of drainage basin morphometric research

A drainage basin is defined as an extent of topographic boundary in which all the surface water diverts to a single point or outlet at a lower elevation. Drainage basin studies are important to understand the characteristics of stream habitats and surface water hydrology (e.g., Frissell et al., 1986; Sen, 2008), terrain characterization and evolutionary stages of topography (Nogami, 1995; Kirby and Whipple, 2001; Jansen et al., 2011), and climate changes (e.g., Tucker and Slingerland, 1997; Zaprowski, 2005). The present form and characteristics of drainage basins are the result of a long-term process of geomorphic evolution (Zavoianu, 1985). In the process, several factors such as underlying rock properties, climate, vegetation and relief contribute in the formation of drainage basins. However, it is very difficult to separate and quantify these factors because of their diverse nature.

Geomorphometry is the scientific field of quantitative land surface analysis (Pike, 1995, 2000). We refer to drainage basin morphometry as the quantitative evaluation of the size, shape and length of various basin elements. Quantitative morphometric analysis of drainage basins begun in the middle of the 20th century, based on manual analyses of printed topographic maps. Horton (1932, 1945), a hydraulic engineer who proposed the law of stream numbers and lengths, is considered as the pioneer in this field. Following his revolutionary ideas, fluvial geomorphology rapidly evolved in the 1950s and 1960s from the concepts of stream network topology and related geometric attributes of drainage basins. Most notable works during these period include Strahler (1950, 1952, 1957, and 1964), Miller (1953), Schumm (1956), Melton (1957), Morisawa (1957, 1962), Scheidegger (1961), and Gregory and Walling (1968). Work by Strahler (1952) is notable for the application of area–altitude analysis in drainage basin studies. The basin morphometric studies between the 1960s and 1980s sought to relate hillslopes to streams (Strahler 1964; Melton 1965; Schumm, 1967; Zavoianu, 1985) that began with Strahler's (1950) equilibrium theory of erosional slopes (Pike et al., 2009). Morisawa (1967) studied the relation between discharge and stream properties in the eastern United States and expressed the catchment stream flow pattern as a function of geomorphology of a drainage basin. Hack's (1973) stream gradient index (*SL*) from river longitudinal profiles in the Appalachians is another milestone in the quantitative morphometric analysis. The *SL* index has been used in evaluating tectonic activity in erosional landscapes including rock uplift rate (Seeber and Gornitz, 1983; Merritts and Vincent, 1989).

With the technological advancement of geographic information systems (GIS) since the 1980s, the digital extraction of morphometric parameters for the quantitative characterization of landforms became possible and popular among geomorphologists (Burrough and McDonnell, 1998; Pike, 2000, 2002; Wilson and Gallant, 2000). Such geomorphic analyses have been conducted using digital elevation models (DEMs). Although the concept of elevation contours to describe the topography dates to 1584 (Imhof, 2007), DEMs allowed more efficient topographic analyses. Major progress in this aspect of quantitative geomorphology has been made with the release of a high resolution near global digital elevation model (SRTM-DEM) developed by the United States National Aeronautical and Space Administration (NASA) and Consortium for Spatial Information of the Consultative Group for International Agricultural Research (CGIAR-CSI). Today, a large number of operational satellites in the earth's orbit with optical and radar payloads, manned and unmanned aircrafts with radar and laser equipment, and terrestrial LiDAR is capable of generating very high resolution DEMs to permit detailed morphometric analyses.

2.2 General basin morphometric parameters and their analysis

Each drainage basin possesses a quantifiable set of basic geometric properties that define the linear, aerial, and relief characteristics (e.g., Horton 1932, 1945; Strahler, 1952, 1964; Morisawa, 1957). Numerous studies have used these basin properties in relation to geomorphic processes such as sediment discharge and erosion rates (e.g., Gardiner, 1990; Barnes et al., 2006). Linear measurement allows the size comparisons of basin units. It includes basin length, basin perimeter, stream length, and the dimensionless parameters derived from ratios of length parameters (Ritter et al., 1995). Area of a basin itself is an important variable in drainage morphometry. Burkham (1966) suggested a high degree of correlation between basin area and discharge in semi-arid regions. Diaconu (1971) has thrown light on the relationships between drainage density, river length and basin area. Basin relief is another important parameter typically used in studying mountainous drainages. Relief representation includes elevation differences, slope, and dimensionless measurements such as the relief ratio (Schumm, 1956). Some basin properties are closely inter-related.

Basin hypsometry proposed by Strahler (1952) relates elevation with the basin area. Hypsometry refers to the frequency distribution of altitude. The hypsometric curve, the relative proportion of area below or above a given height, and the hypsometric integral, the standardized area below the hypsometric curve, are valuable tools in morphometric analysis especially for characterizing drainage basins, because they are correlated with the stage of

geomorphic development of the landscape (Strahler, 1952; Schumm 1956). Using the hypsometric curve and integral, it is possible to compare different areas in order to study the effects of different bedrock types, plate-tectonic settings, or the balance between tectonics and erosion. For example, the hypsometric integral of various river basins has been linked to lithological resistance (e.g., Lifton and Chase, 1992). Hurtrez et al. (1999) shows that the hypsometric integral in Siwalik Hills, Nepal Himalaya, is significantly correlated with the rock uplift rate. Ohmori (1993) inferred the hypsometric relationship between tectonics and denudation and found that Japanese drainage basins have a reversed shape of curves from that of original Strahler's diagram. Scale dependency of hypsometry is studied by Hurtrez et al. (1999) and Chen et al. (2003). According to them, smaller drainage basins tend to have larger hypsometric integral values. Some researchers even examined the effect of differences in precipitation and runoff on hypsometry (e.g., Masek et al., 1994; Montgomery et al., 2001).

2.2.1 Statistical Analysis in basin morphometry

Because various morphometric parameters can be derived from drainage basins, it is often difficult to ascertain which are the most effective for geomorphological reasoning. Statistical analysis aids in reducing this complexity in drainage basin research (e.g., Frissell et al., 1986; Bengraine and Marhaba, 2003) using a wide variety of pattern recognition operations, such as factor analysis, principal component analysis, cluster analysis, and discriminant analysis (Adams, 1998). Strahler (1954b), in relation to statistical analysis in geomorphic research, noted that "*it is a versatile and powerful tool for use in an intermediate stage of certain quantitative investigations*". Ehlen (1993) described two statistical approaches, correlation analysis and multivariate analysis, for geomorphic characterization of landforms of Dartmoor, southwest England. A systematic classification of large rivers based on their hydro-sedimentary components was successfully conducted using multivariate statistics, principal component analysis and cluster analysis (Miller et al., 1990; Raux et al., 2011). However, such studies on steep river basins have been relatively limited.

2.2.2 Alluvial fans – relationship with basin morphology

Depositional landforms, particularly alluvial fans, caused by river erosion are discussed in many studies. Alluvial fans are semi-conical depositional landforms created by the loose, water-transported material radiating from mountainous drainage outlets emerging into low-relief surface. The presence of alluvial fans are common in desert mountainous regions (Harvey, 1997), but they may occur in any climatic environment (e.g., Boothroyed and Nummendal, 1977; Kochel, 1988; Saito and Oguchi, 2005). Each fan is derived from a source basin area in which

the trunk stream transports erosional products to the fan apex (Bull, 1977). The coalescing or convergence of many alluvial fans is termed as bajada (Blackwelder, 1931). The factors influencing the development of alluvial fans is discussed by Blissencach (1954), Bull (1964), Hooke and Rohrer (1979), and Harvey (1989). Blissencach (1954) suggested that development of alluvial fans may be affected by varying base level, climatic changes, tectonic movements and slumping of fan deposits. Hooke (1968) studies suggested that steady-state slope of an alluvial fan is determined by debris size, depositional process and water discharge. Several researchers have studied the form and deposits of alluvial fans (e.g., Bull, 1964, Melton, 1965; Hooke, 1968; Harvey 1990; Willgoose et al., 1991; Lin et al., 2009) and suggested the positive relation between alluvial fan area and source basin area and; negative relationship between fan slope and basin area (Lin et al., 2009).

2.3 **Longitudinal river profile analysis**

Analysis of longitudinal river profiles provides an important tool for interpreting downstream changes in erosion–deposition regimes, rock uplift rate and lithological resistance to erosion. In this context, stream gradient and slope–area analysis have been widely applied to river profiles (Hack, 1973; Tarboton et al., 1989; Wobus et al., 2006). Hack (1973) demonstrated that river profile gradients can be related to upstream drainage area as a power law function. In this relation, the coefficient of proportionality is called the steepness index (K_s) and the power is the concavity index (θ) (Flint, 1974). With the widespread availability of digital topography and sophisticated computer programs in GIS, K_s and θ have been frequently used as indicators of river incision and erosion. Several studies have connected K_s to approximate the relationship between net uplift and net erosion (e.g., Howard, 1994; Whipple and Tucker, 1999; Snyder et al., 2000; Kirby and Whipple, 2001). Because different rivers have different K_s and θ values, K_s can be normalised (K_{sn}) for the sake of comparison, by using a reference concavity (Wobus et al., 2006). Van Laningham et al. (2006) noted that homogeneous substrate properties are required to derive a meaningful comparison of K_{sn} with rock uplift. Similarly, differences in K_{sn} values can also be attributed to lithological variations, particularly if no correlation is observed with tectonic elements. Hack (1973), in this aspect, has debated that steeper rivers are associated with more resistant lithologies. In general the channel slope is inversely proportional to drainage basin area. However, in areas where differential uplift is ongoing, the proportionality of drainage area and slope does not hold true (Ambili and Narayana, 2014).

Longitudinal profiles of rivers become concave over geomorphic time (Yatsu, 1955) and that concavity tends to be conserved and has a characteristic form (Bull, 1979). However, a river may adjust its concavity by incision or

aggradation under various circumstances (Zaprowski et al., 2005). Changes in the base level (Whipple et al., 1999), the rate of rock uplift (Snyder et al., 2000; Duvall et al., 2004), climatic influence particularly by changing hydrology and sediment control (Bull, 1991), and differences in bedrock condition or a combination of these can cause the adjustment in river concavity. Profile concavity is further influenced by drainage basin shape (Zaprowski et al., 2005). It has been noted that rivers in tectonically active regions have higher concavity indices than the equilibrium river profiles (Kirby and Whipple, 2001; Figueroa and Knott, 2010). The concavity index is typically in the range of 0.4–0.6; and reference concavity has been taken as 0.45 in most of the previous studies (e.g., Wobus, 2006).

Some other river longitudinal profile indices have been recently revitalized in landscape evolution studies (Sklar and Dietrich, 1998; Snyder et al., 2000; Kirby and Whipple, 2012). Using such indices, analyzing knickzones has become a key component in geomorphic research (Pederson and Tresslor, 2012). Knickpoints or knickzones are termed as marked increase in downstream channel gradient (Nanson and Gibling, 2004). Knickzones in the form of waterfalls often occur in bed-rock rivers (Wohl et al., 1999; Hayakawa and Oguchi, 2006), and are one of the most visually arresting indicators of channel adjustments to either regional or local perturbations (Ortega et al., 2013). Causative factors influencing knickzone origin have been interpreted in many studies; bedrock erosional resistance (e.g., Miller, 1991), transient response to base level fall (e.g., Bowman et al., 2007), tectonic activity (e.g., Bishop et al., 2005), and changes in sediment load from tributaries (e.g., Jansen et al., 2011) has been suggested as the dominant ones. Knickzones originate from a combination of these factors (Phillips et al., 2010). Knickzones are commonly convex or vertical reaches, although in extreme cases concave (Frankel et al., 2007), and their morphology include stepped, buttressed, and undercut forms (Young, 1985). Haviv et al. (2010) grouped knickzones into vertical step knickzones and slope break knickzones. Knickzones may migrate upstream and can maintain a constant geometry during the retreat (Crosby and Whipple, 2006). Due to enhanced erosion within its steepened reach, a knickzone often act as the front of stream incision (Wohl et al., 1994; Hayakawa and Matsukura, 2003). Knickzones have often been regarded as a key in discussing the geomorphological evolution of landscapes (Bishop et al., 2005; Hayakawa and Oguchi, 2009). In this context, models describing the evolution of knickzones in horizontally bedded strata (e.g., Gardner, 1983); in vertically bedded substrata (e.g., Frankel et al., 2007); numerical models of knickzone migration (e.g., Howard et al., 1994); and knickzones as transient features (e.g., Crosby and Whipple, 2006) have been postulated.

Despite such significant studies, most of them identified knickzones from visual inspection of longitudinal profiles, field observations and other data sources including topographic maps and high-resolution aerial photographs. **Table 2-1**is a brief overview of the previous studies knickzone investigations. Such studies based on visual interpretations tended to deal with only small numbers of knickzones. However, Hayakawa and Oguchi (2009) investigated 5753 knickzones in 1344 watersheds in Japan using a quantitative semi-automated method of identifying knickzones from 50-m DEMs with the help of GIS.

Table 2-1 Summary of previous studies on knickzone investigations

	Location	No of knickzones studied	Total drainage area/ length studied	No of watersheds	Identification source	References
1	South-Central Indiana, United States	20	--	9	Topographic maps, field observations	*Miller, 1991*
2	Black Hills, Laramide Rocky Mountains, United States	35	--	1	Topographic maps	*Zaprowski et al., 2001*
3	Waipaoa River, North Island, New Zealand	~ 350	2150 km^2	1	25 m DEM, Aerial photos and field observations	*Corsby and Whipple, 2006*
4	Central Japan	254	1966 km	86	50 m DEM	*Hayakawa and Oguchi, 2006*
5	Mukua, Liwu, and Hoping drainage basins, North Eastern, Taiwan	37	--	3	40 m DEM	*Wobus et al., 2006*
6	Roan Plateau, Colorado	33	1800 km^2	2	10 m and 30 m DEM	*Berlin and Anderson, 2007*
7	Susquehanna River, United States	2	~ 450 km	2	30 m SRTM DEM	*Frankel et al., 2007*
8	Western Ghats, India	--		30	Field observations	*Kale and Shejwalker, 2008*
9	Japan	5753	65468 km	1344	50 m DEM	*Hayakawa and Oguchi, 2009*
10	Big South Fork River basin, Kentucky–Tennessee	21	2082 km^2	1	10 m DEM, Aerial photos, field observations, and old maps	*Phillips et al., 2010*
11	Da-An River Gorge, Taiwan	5	100 km	1	2 m DEM, Aerial photos, field observations	*Chen, 2010*
12	Rio Piura, Rio Pisco, and Rio Lluta catchments, Andean mountain belt, South America	6	< 380 km	3	SRTM DEM 90 m	*Abbühl et al., 2011*

13	Yalu river, North Eastern, China	23	< 1150 km	23	90 m SRTM DEM	*Zhang et al., 2011*
14	Isle of Jura, Scotland	17	< 100 km^2	17	5 m Airborne InSAR DEM, Aerial photos	*Castillo et al., 2013*
15	South Fork Eel river, northern California	842	128 km	2	1 m LIDAR DEM	*Foster and Kelsey, 2012*
16	Hatay Graben, Southern Turkey, and Central Apennines, Italy	28	578.8 km^2	30	Field observations, DEM	*Whittaker and Boulton, 2012*
17	Paraná Basin, Brazil	63	61 km	1	Digital topographic maps, field observations	*Lima and Binda, 2013*

CHAPTER 3: Study area

3.1 Tectonic setting

The study area, comprising the Western Arabian Peninsula, corresponds to the western part of the Arabian Plate. The Arabian Peninsula has a very long geological history, extending back to the Precambrian. The peninsula measures ~7,800,000 km^2 and is surrounded by diverse plate boundaries; on the west by the Dead Sea transform and the Red Sea, on the north by the Zagros collision zone and the Bitlis suture, on the east by the Owen fracture zone, and on the south by the Gulf of Aden and the Arabian Sea **(Figure 3-1).** Long before the formation of the Red Sea, the Arabian Peninsula was a part of Africa as a part of the Nubian Shield. The Tertiary Red Sea-Gulf of the Suez rift system is a prime example of active continental rifting and breakup (e.g., Cochran, 1983; Bosworth et al., 2005). Since its separation from Africa, the Arabian Plate has undergone a series of uplift events which started from the Mesozoic period, with episodes of rotational tectonic movement, collision and subduction (Stern and Johnson, 2010). The thickness of the plate is estimated as 120 km (Reches and Schubert, 1987). The northern part of the plate has been moving in a northwest direction at a rate of approximately 15–20 mm/yr, whereas the southern part is moving more slowly and is subject to weak to moderate seismic activities (Vincent, 2008). The progressive uplift has caused well developed mountain escarpments on the western side with the highest elevations over 3000 m, while the rifting created a deep axial trough in the Red Sea basin (Bailey et al., 2007). The resultant mountains have been subjected to erosion to form steep drainage basins. Fractures developed as a part of the uplift have provided feeder fissures for the volcanic series (Coleman, 1974). The geodynamic processes acting in the Red Sea region largely control the geology of the Western Arabia (Sen and Al-Suba'i, 2002).

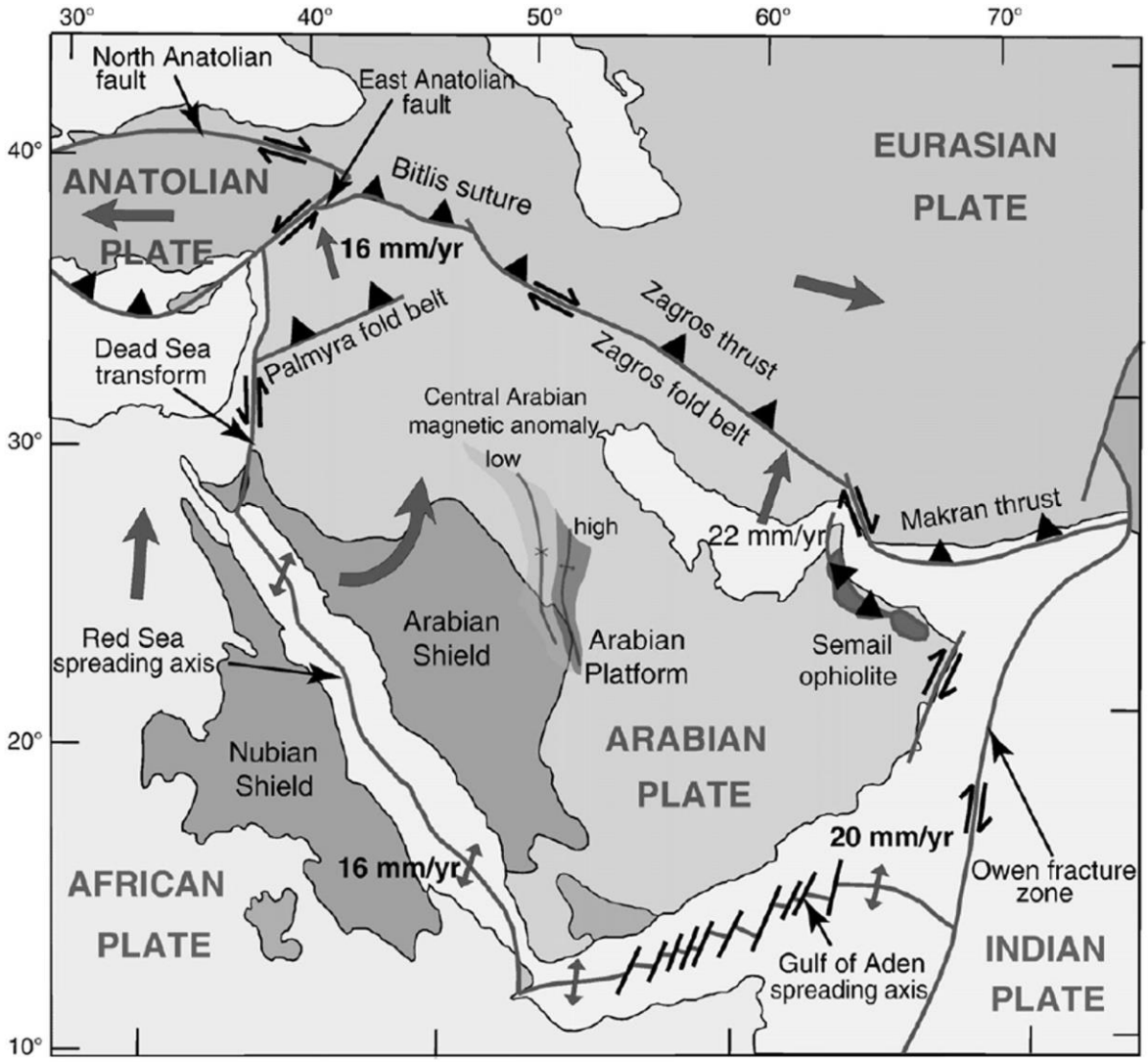

Figure 3-1 Simplified map of the Arabian Plate with plate boundaries (from Stern and Johnson, 2010 - reprinted by permission of Elsevier).

3.2 **Geology**

The geology of the Arabian Peninsula is dominated by the exposure of upper continental crust as a result of Oligo-Miocene uplift during the formation of the Red Sea (Stern and Johnson, 2010). Over 670,000 km^2 of the Peninsula comprises complex basement rocks, overlain by Tertiary and older volcanics to the west, and marine and continental sediments to the east (Brown, 1989; Reches and Schubert, 1987). The basement rocks are well exposed on the shield region, particularly on the uplands, scarp mountains, and coastal pediments (Brown, 1970).

These basement rocks in the Arabian shield are largely composed of metamorphosed sedimentary and volcanic rocks intruded by younger granites and gneisses (Vincent, 2008). Granitic rocks make up approximately 70% of

the plutons (Gettings et al., 1986). Isotopic data suggest that the rocks were formed during the Neoproterozoic and are of oceanic affinity (Stoeser and Frost, 2006). Radiometric data records a range of ~870–550 Ma for these rocks (Stern and Johnson, 2010). The shield region has been divided into various major tectonostratigraphic terrains, suture zones, fault zones and post accretionary basins (Johnson, 1998; Nehlig et al., 2002; Johnson and Woldehaimanot, 2003). Sutures between these terrains are marked by serpentinite-decorated faults, thrusts and brittle-ductile shear zones (Johnson, 1998). Basaltic rocks were exposed in the western Arabia as a result of sea floor spreading to form large volcanic lava fields (harrats). The oldest of these basalts are located in Yemen and southern Saudi Arabia (30 Ma), while the youngest are found in the north-west Saudi Arabia (700 yrs. AD). These flood basalts are predominately alkaline olivine basalt, with some interbedded silicic lavas, agglomerates, and pyroclastics (Baker et al., 1996). The Tertiary volcanic rocks over the Yemen and surroundings are one of the largest areas of alkaline basalts in the world (Coleman, 1974).

3.3 **Climate**

The Arabian Peninsula lies in the center of the great trade wind desert that encompasses Africa and Asia. Climatic data and models indicate that the Peninsula experienced both moist and arid phases in the geologic past (Burns et al., 1998; Fleitmann et al., 2004). Today, from north to south, the Arabian Peninsula exhibits relatively large climatic variations in terms of temperature, but is consistently arid to semi-arid. Temperature ranges from below freezing during the winter months to about 45°C during the summer. Diurnal variation of temperature sometime reaches as much as 16°C because of rapid heat exchange in the bare rocks as the desert passes from day to night (Brown, 1989). Relative humidity is as low as 10% in summer, away from the coast, to 45% in winter. Precipitation, otherwise meagre and episodic, increases with altitude on the slopes of the Red Sea escarpment; therefore vegetation is sparse except in the Hijaz Range and Yemen volcanic region. The annual average rainfall for Saudi Arabia is 93.5 mm (Almazroui et al., 2012) and that for Yemen is 492 mm (Rappold, 2005). In the south-western Peninsula, about 60% of the annual total precipitation occurs during the winter months under the influence of Indian Ocean monsoons (Almazroui, 2011). Thus, the basins studied here have only intermittent water flow, which is mostly restricted to the periods during and directly after occasional heavy precipitation events. Even one or two high-intensity, short-duration storms with little precipitation can produce flash floods because of low surface infiltration (Almazroui, 2011).

3.4 Drainage systems

Drainage ("wadi" in Arabic, pl "widyan") systems in the Arabian Peninsula, particularly those in the shield and adjacent coastal mountains, appear to be complex; they comprise two basic units (Vincent, 2008). One draining eastward across the shield onto the cover rocks, while the other, which forms the study area, comprises steep drainages originating in the Red Sea escarpments and adjacent mountains that flow westward onto the 20–60 km wide coastal plain. Perennial streams in the Peninsula are few due to the restricted rainfall. However, runoff occurs in most of the drainages because of diminished infiltration capacities and presence of bare rocks. The mean annual runoff in the whole of the Red Sea coastal area has been estimated at 39.8 m^3/sec (Vincent, 2008). Out of this, approximately 27 m^3/sec occurs south of Jeddah (Ministry of Agricultural and Water, 1984).

The 36 drainage basins were chosen for this study; they are major basins each with an area of more than 500 km^2 **(Figure 3-2)**. They are located in the Midyan, Hijaz and Asir terrains within the shield, and within an area of Tertiary volcanics in the Yemen region **(Figure 3-3).** Around 3/4 of the basins are located in the shield. All basins drain toward the west or southwest except for the southernmost basin (#1) draining toward the south. The maximum altitude of the study area is 3658 m in basin #4. The steep topography of the basins reflects the uplift along the Red Sea, whereas well-developed drainage systems there reflect long-term erosion by water.

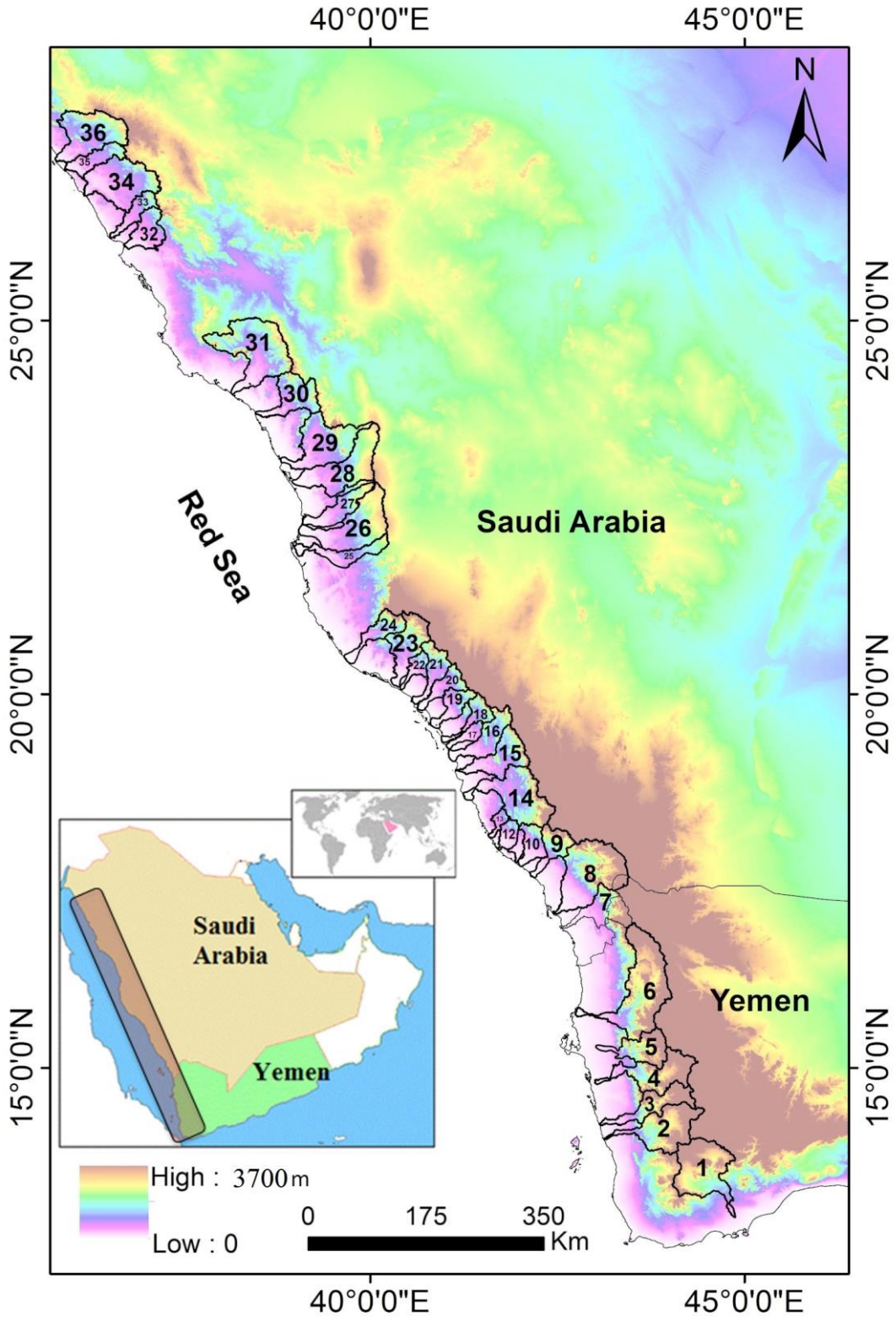

Figure 3-2 Location of the study area and outline of the 36 basins studied. Basins are numbered sequentially from 1 in the south to 36 in the north of the study area

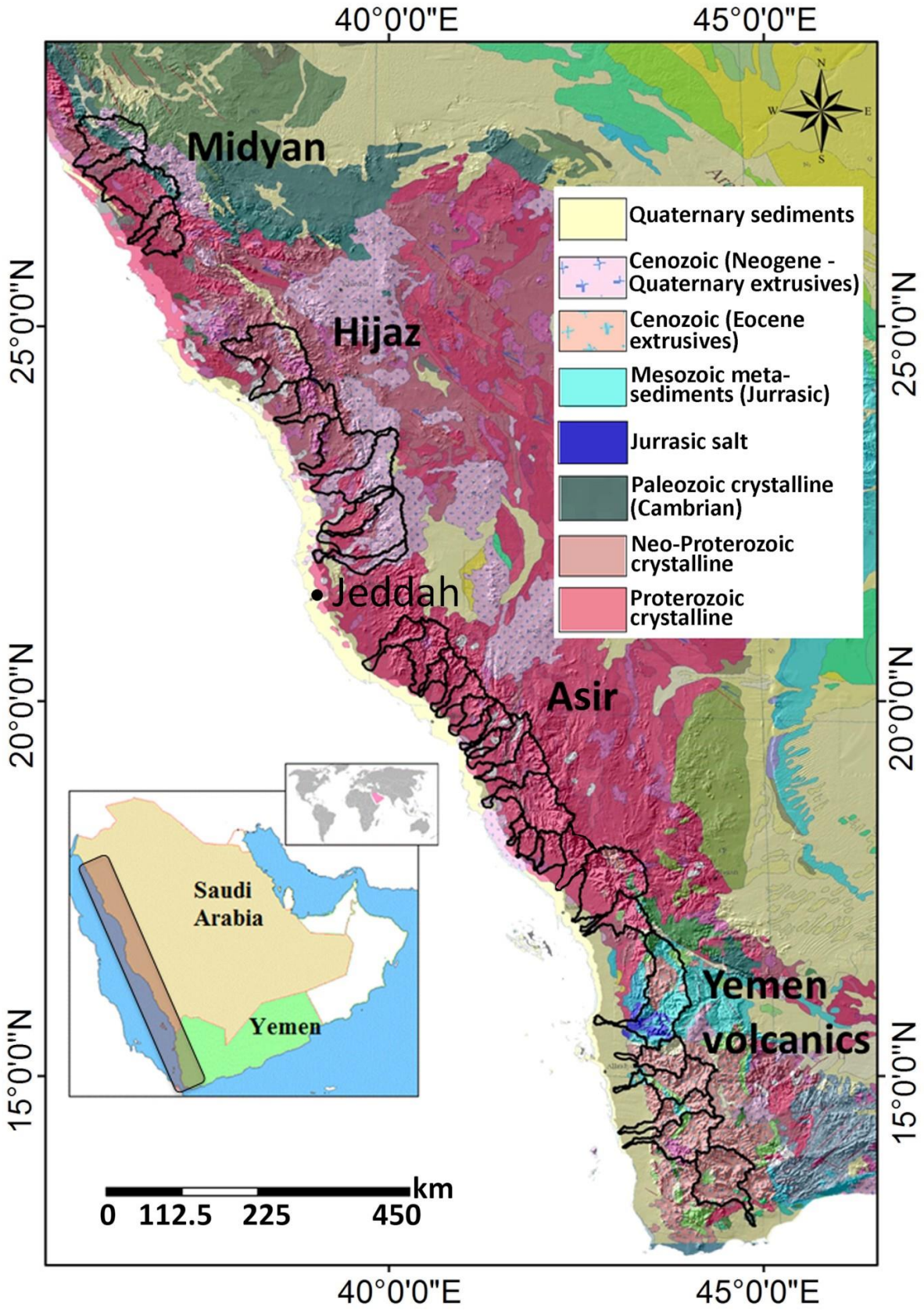

Figure 3-3 Geology map of study area (1:5,000,000 International Geological Map of Middle East).

CHAPTER 4: Materials and Methods

4.1 Digital elevation model and ancillary data

The global DEMs from the Shuttle Radar Topographic Mission (SRTM) and the Advanced Spaceborne Thermal Emission and Reflection Radiometer (ASTER) are available highest-resolution topographic data covering the whole of the study area. The National Aeronautics and Space Administration (NASA) produced the SRTM digital elevation data in 2000. The vertical accuracy of the SRTM DEM is less than 16 m and the horizontal resolution is 3 arc second for universal usage (http://www2.jpl.nasa.gov/srtm/statistics.html). The ASTER GDEM was developed jointly by the Ministry of Economy, Trade and Industry (METI) of Japan and NASA of the United States, from automated processing of ~1.5 million ASTER VNIR scenes. It has 20 m vertical accuracy at 95% confidence level, when compared to ~18,000 absolute geodetic references over the Conterminous US (CONUS), and a horizontal accuracy of 30 m at 95% confidence (Tachikawa et al., 2011). The first version of the ASTER GDEM was released in June 2009 and the improved GDEM v2 in October 2011.

Although both the SRTM and ASTER DEMs suffer from local artifacts, they have strong similarities (Frey and Paul, 2012; Li et al., 2012), and artifacts in the ASTER GDEM v2 are less for open or bare lands than forested areas (Tachikawa et al., 2011). Because the study area consists mostly of bare land under an arid climate, and the ASTER GDEM has a higher spatial resolution (30 m) than the SRTM DEM (90 m), this study chose the ASTER GDEM v2 for morphometric analyses. The ASTER GDEM tiles for the study area were downloaded from the J-spacesystems website http://gdem.ersdac.jspacesystems.or.jp. The DEM tiles were then mosaiced in ArcGIS and converted into the UTM projected coordinate system.

The 1:5,000,000 International Geological Map of the Middle East published by the Commission for the Geological Map of the World (CGMW) was used to categorize the major lithologic types: broadly crystalline and volcanic (**Figure 3-3**). Major faults in the study area were also delineated from the same geological map to analyse the relative effect of tectonics (**Figure 4-1**). For this analysis, presence or absence of a fault in the channel profile is considered; if the channel profile have a fault, it is called fault intersected channel and vice versa. The precipitation data were obtained from the TRMM v.7 3B43, averaged over January 1998 – January 2014. The spatial distribution of mean annual precipitation (mm) over the Arabian Peninsula is displayed in **Figure 4-2.**

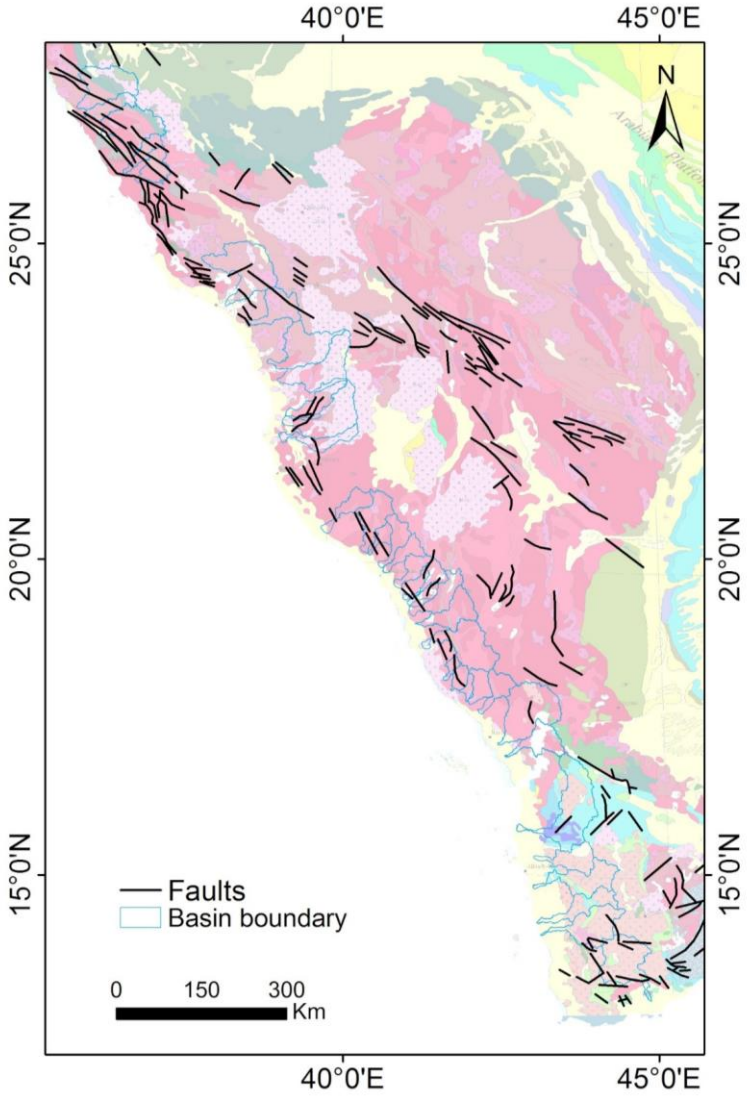

Figure 4-1 Faults delineated from the geological map of the Middle East (1:5,000,000 International Geological Map of the Middle East)

4.2 **Drainage basins and stream network extraction**

Extraction of drainage basins and stream networks is one of the preliminary tasks in a geomorphometric analysis. Since the advancement of GIS in hydrological modelling, several flow path algorithms including D8, FD8, Rho8, Frho8, DEMON, and D∞ have been developed to demarcate drainage basins and stream networks (O'Callaghan and Mark 1984; Jenson and Domingue 1988; Fairfield and Leymarie, 1991; Freeman, 1991; Moore et al., 1993; Costa-Cabral and Burges 1994, Tarboton, 1997).

The basins and stream networks of the 36 basins and 1046 sub-basins in the study area were delineated from the ASTER GDEM based on the threshold contributing-area method of Jenson and Domingue (1988) embedded in the ArcHydro Tools in ArcGIS. ArcHydro is an extension of water resource applications developed by the

University of Texas (Maidment, 2002). The tools were downloaded from https://mft.esri.com and were used for DEM pre-processing with terrain elevation correction, slope–area calculation for flow direction and flow accumulation, basin delineation, and stream network extraction.

The delineation of basins and stream networks using a DEM and ArcHydro tools is not a straightforward process. Some of the complications that can arise include insufficient or missing data present in the raw DEM. Such errors may be negligible in small and steep drainage basins; however, for flat areas of larger watersheds, DEM reconditioning with sink filling are necessary (Liang and Mackay, 2000). The reconditioning involves modifying the elevation data to be more consistent with the input vector stream network. The fill sinks function in the ArcHydro Tools permitted us to detect hollows in the elevation data and modify these *z* values to eliminate such DEM artifacts.

The flow direction function in the ArcHydro Tools was employed to determine the steepest downstream slope according to the 8-point pour flow model. The values in the cells of the flow direction grid indicate the direction of the steepest descent from that cell. After determining the flow of each grid point, a flow accumulation function was applied. This function computes the accumulated number of cells upstream of a cell, for each cell in the input grid. In order to determine the channel head and catchment morphology, it is required to provide a minimum contributing area in the ArcHydro Tools. A default value provided by the software represents 1% of the maximum flow accumulation. However, a careful trial and error method is necessary to accurately determine the channel heads. For this study, after several trials, a constant threshold contribution area of 0.45 km^2 was chosen, based on visual comparisons with the 1-m resolution World Imagery Map provided by Microsoft's Bing Maps. A comparison map showing the actual drainages and DEM derived drainages are shown in **Figure 4-3**. The stream networks were then ordered using Strahler's (1954a) method for the 36 drainage basins larger than 500 km^2 **(Figure 4-4)** and their 1046 sub-basins (Strahler order range from 4 to 6).

4.3 **Morphometric parameters of drainage basins**

Twenty-one morphometric parameters for all the 36 basins and thirteen parameters for the 1046 sub-basins (**Table 4-1**) were obtained from the DEM. The selected variables were previously used in the literature and they represents a wide range of hydrologic, geomorphic, geologic and climatic characteristics. It was difficult to compute all the 21 parameters for the sub-basins because their number is large. The parameters include several basic

morphometric parameters: the basin area (*A*), perimeter length (*P*), basin length (*Lb*), total number of streams (*Nu*) and total stream length (*Lu*). The remaining parameters, which were partly derived from the basic parameters, were mean stream length (*Ls*), bifurcation ratio (*Rb*), stream frequency (*Fs*), first order stream frequency (Fs_1), average length of first order streams (L_1), ratio of average lengths of first to second order streams (R_{12}), ratio of first order stream number to perimeter (R_{P1}), drainage density (*Dd*), maintenance coefficient (*Mc*), form factor (*Ff*), circularity ratio (*C*), elongation ratio (*Re*), relief ratio (*Rr*), relative relief (*Rl*), ruggedness number (*Rn*) and hypsometric integral (*HI*). The detailed definitions of the parameters are described in the following section and **Table 4-1**.

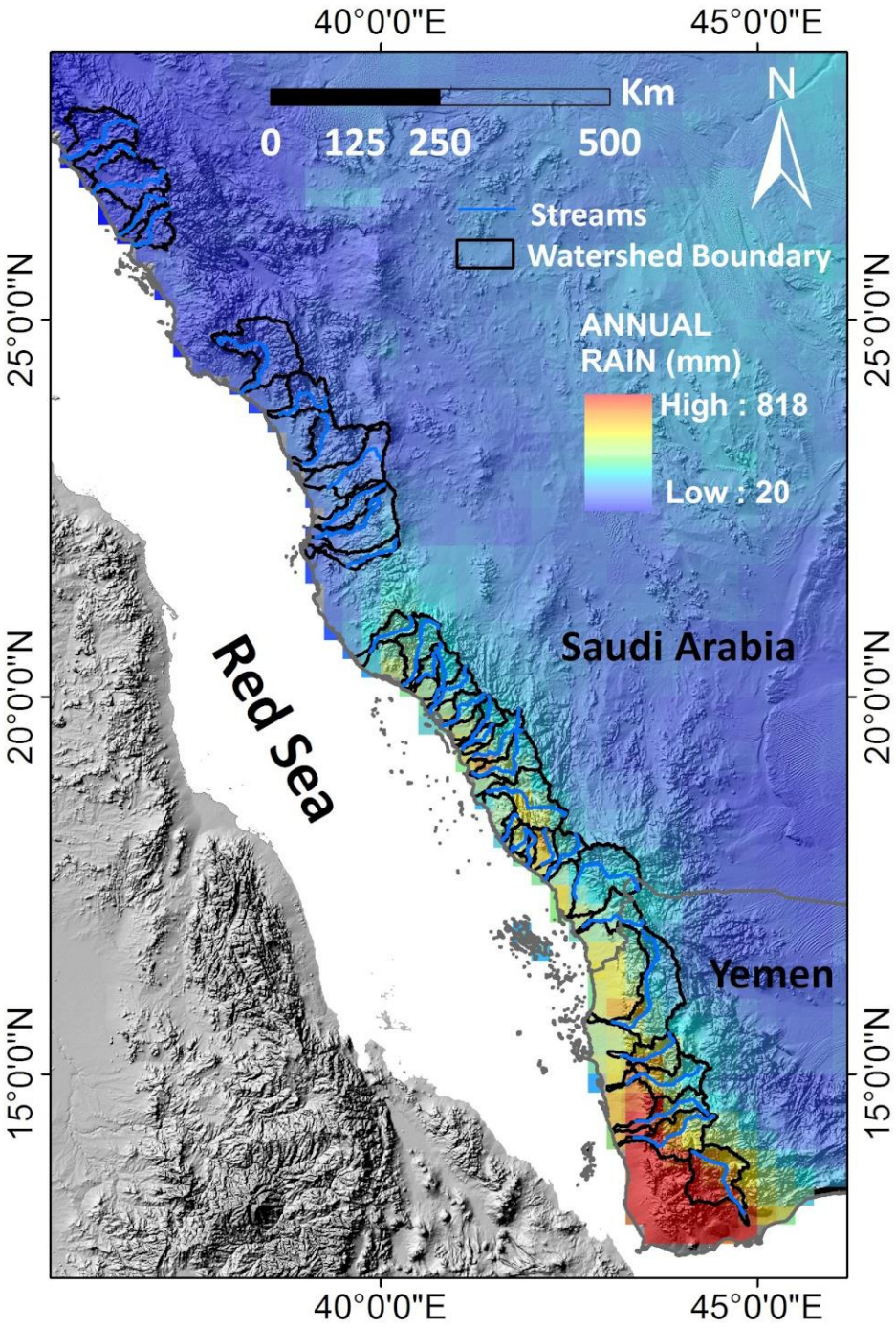

Figure 4-2 Map showing the spatial distribution of mean annual rainfall (mm) over the Western Arabian Peninsula obtained from the TRMM data averaged over 1998–2013.

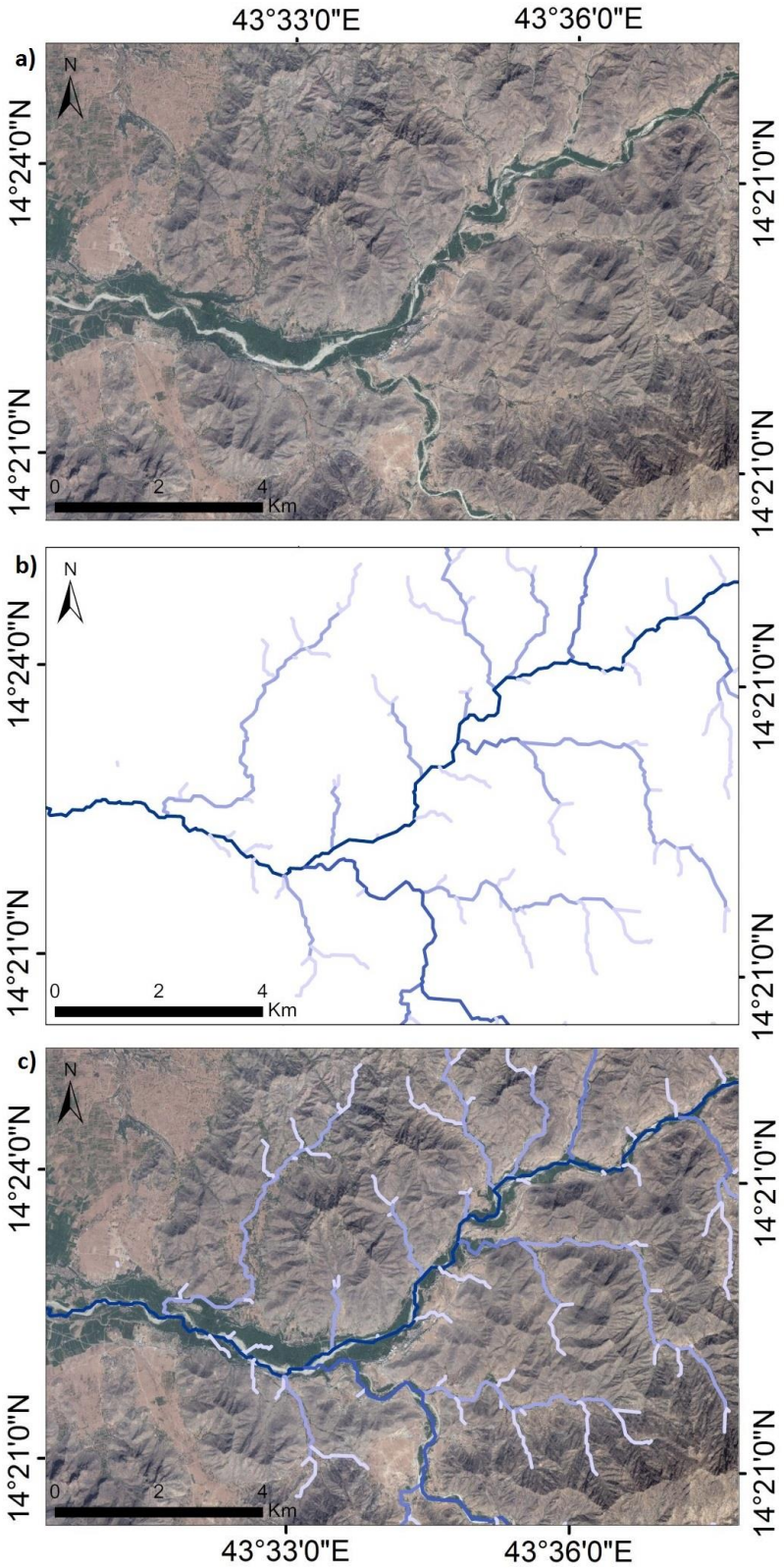

Figure 4-3 Example maps showing the comparison between the actual drainage networks and extracted drainage networks. a) Satellite image showing a part of the Western Arabian Peninsula, b) DEM derived drainage network for the same region, c) DEM derived drainage network super imposed on the satellite image.

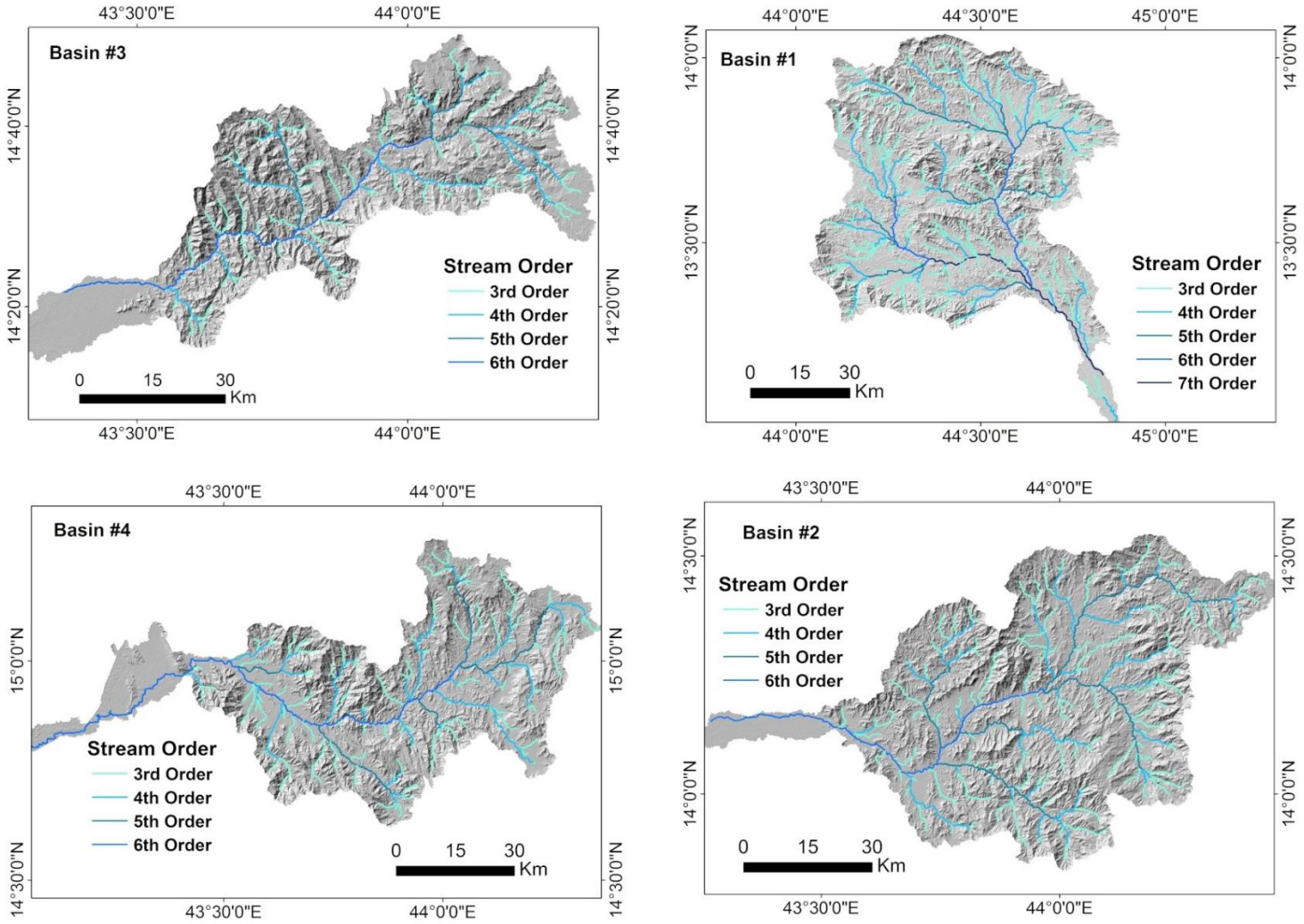

Figure 4-4 Main drainage basins and stream networks extracted from the ASTER GDEM using the ArcHydro Tools and ArcGIS. Basin #1 to #4

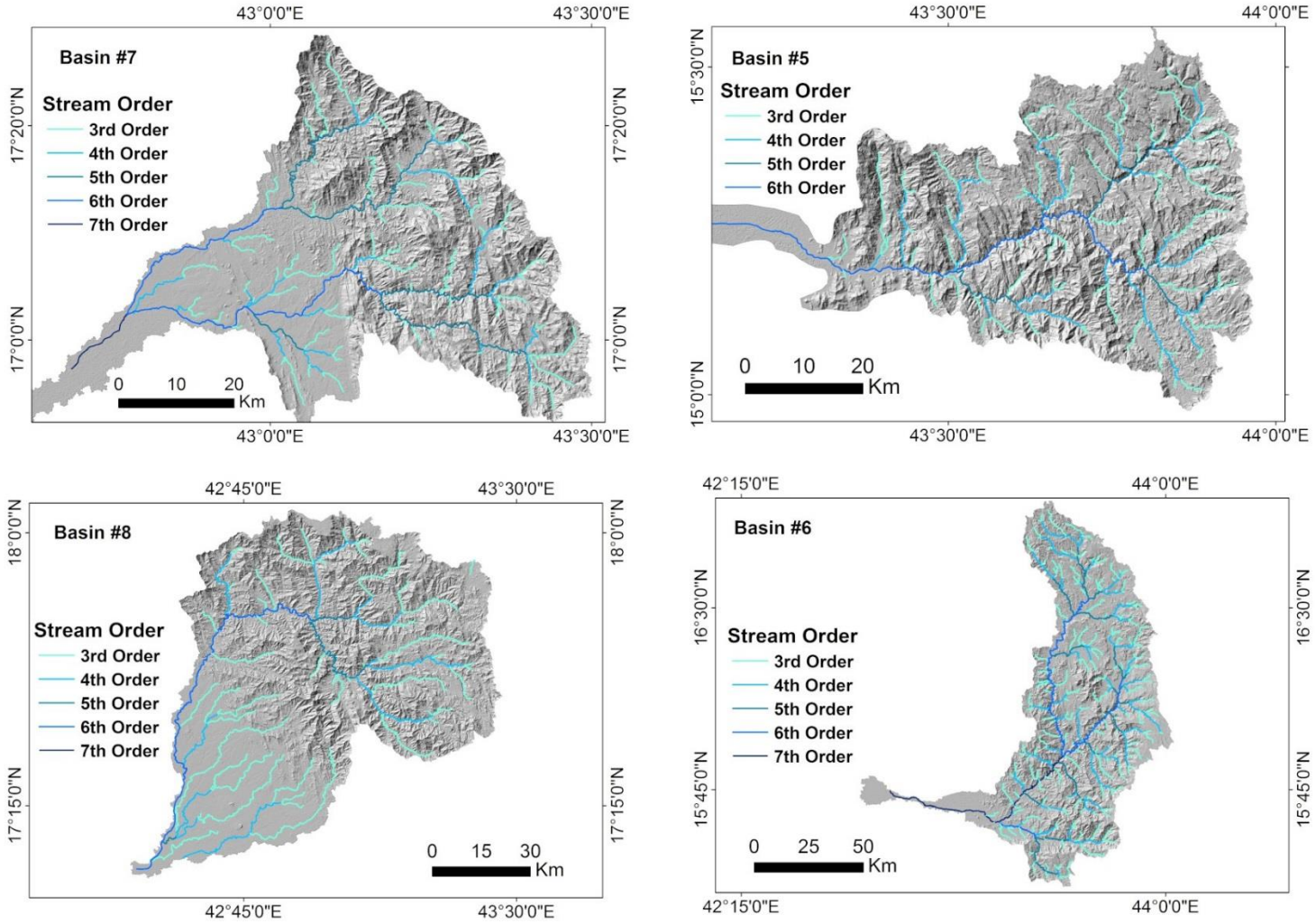

Figure 4-4 (continued). Basin #5 to #8

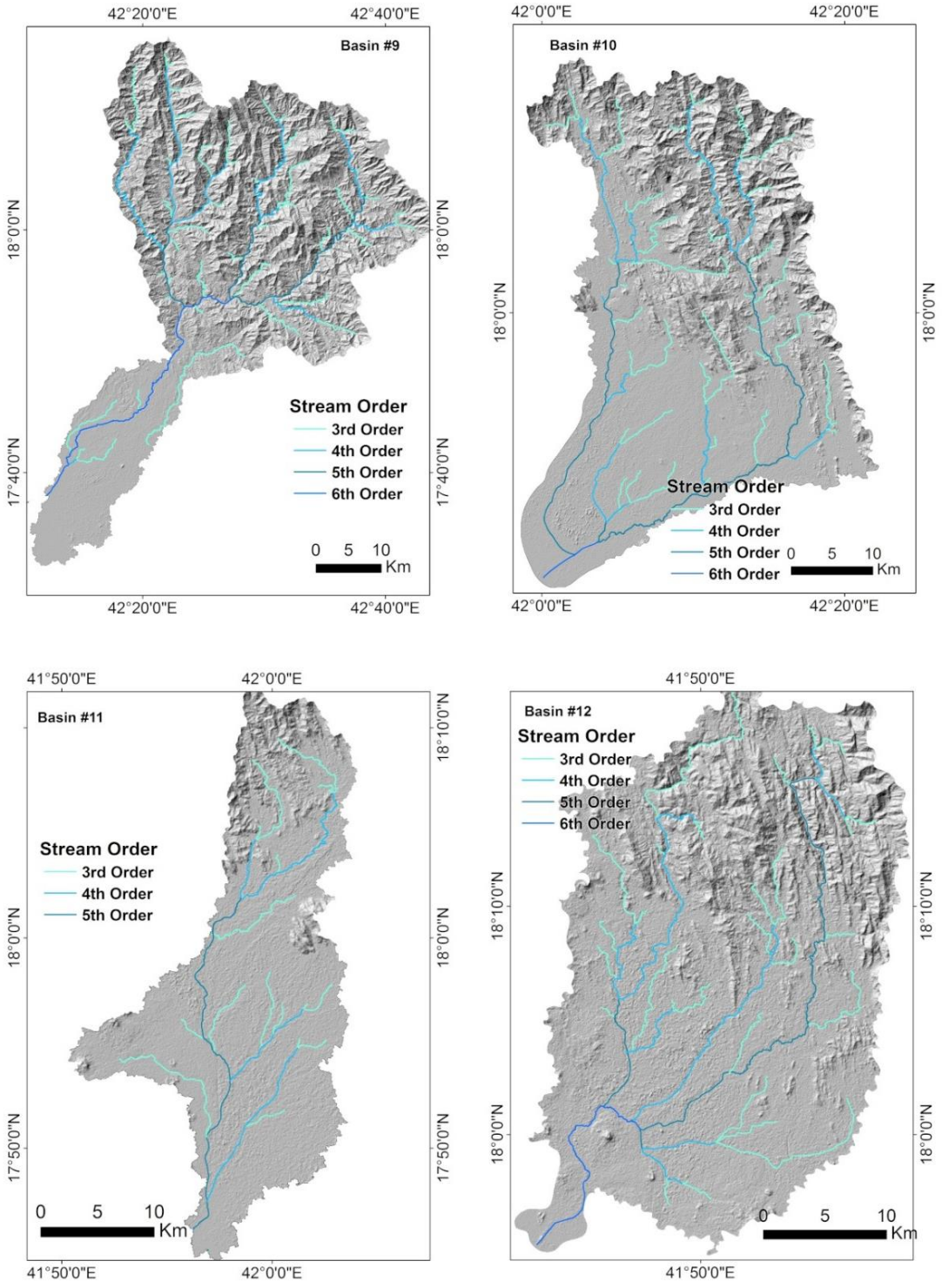

Figure 4-4 (continued). Basin #9 to #12

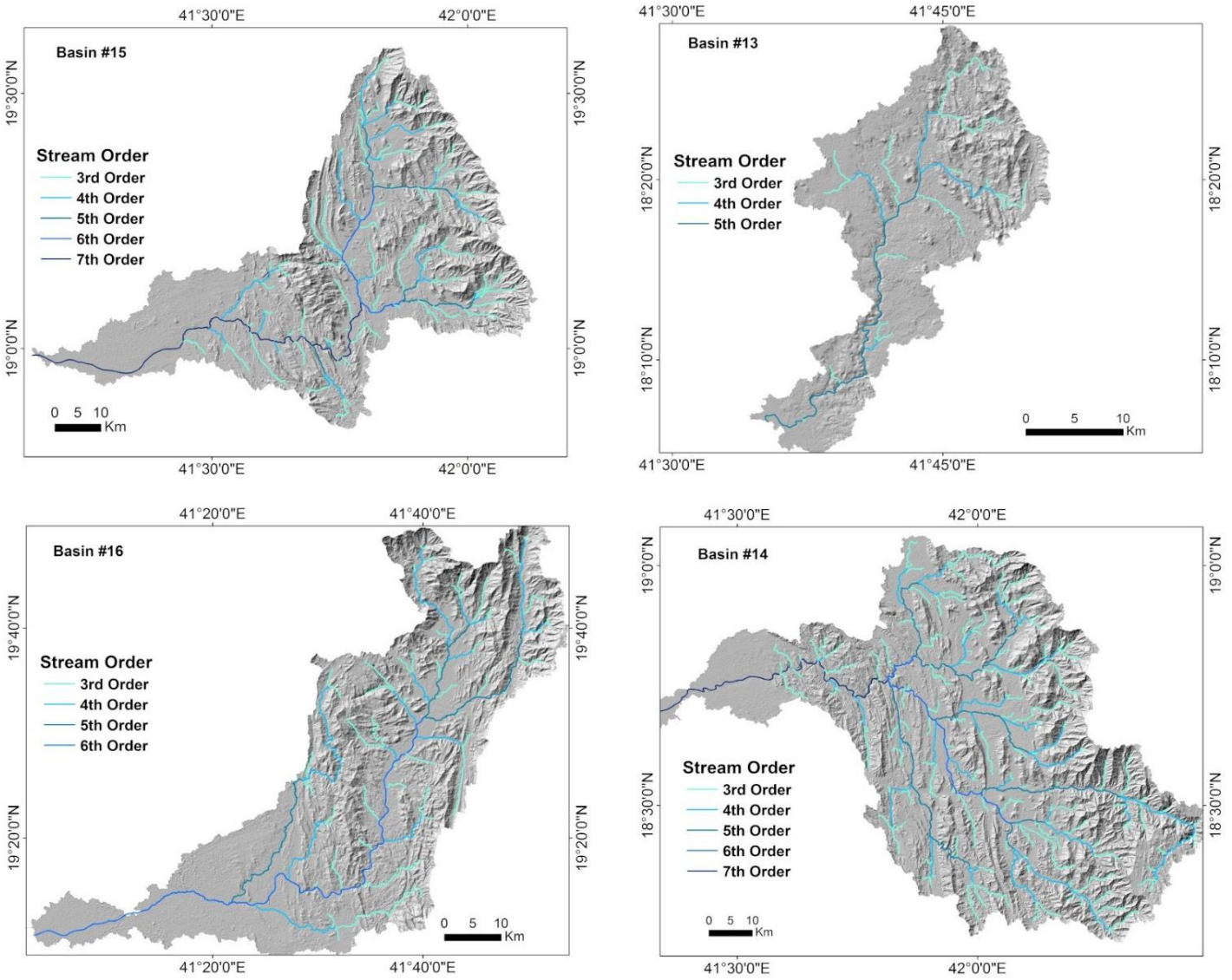

Figure 4-4 (continued). Basin #13 to #16

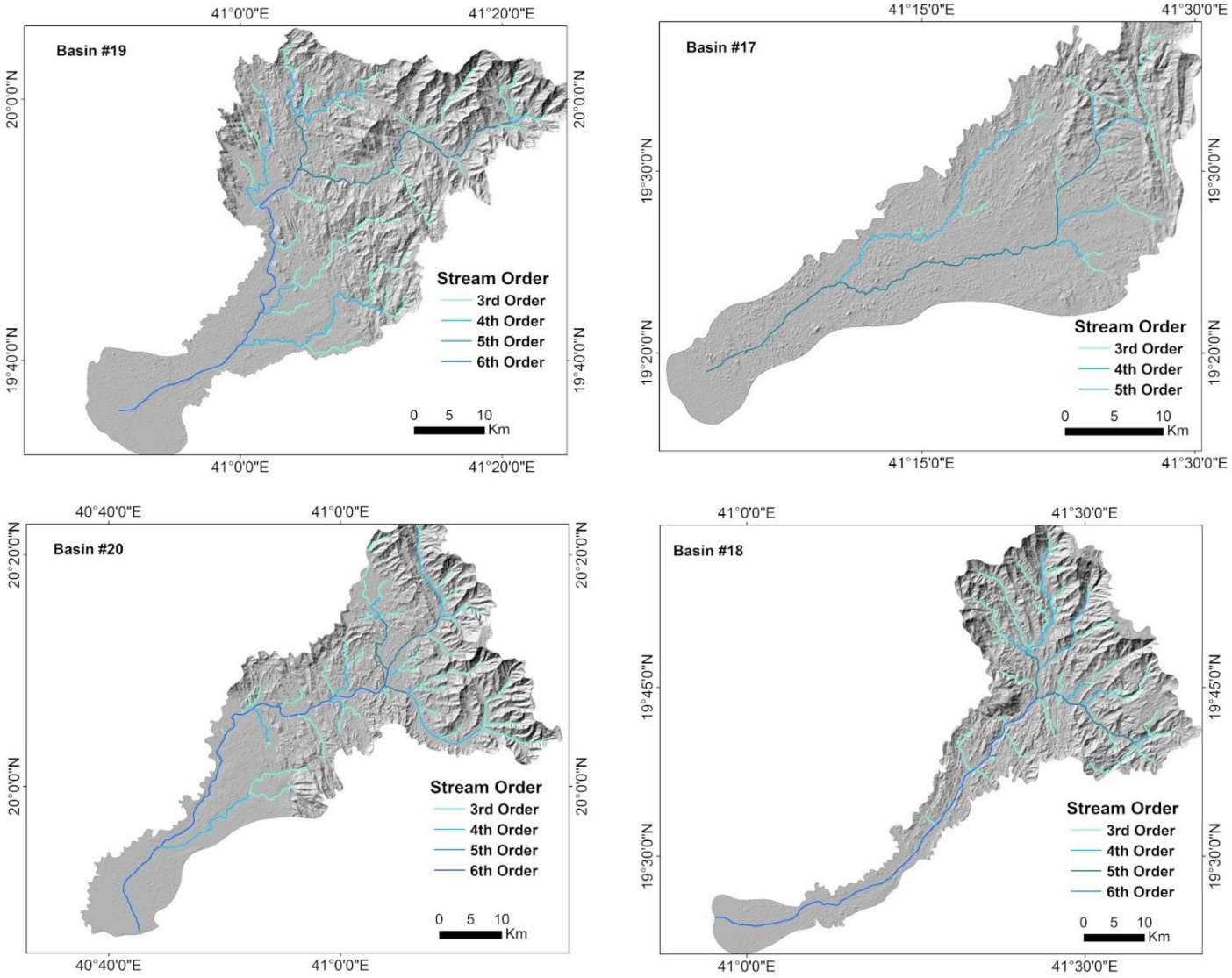

Figure 4-4 (continued). Basin #17 to #20

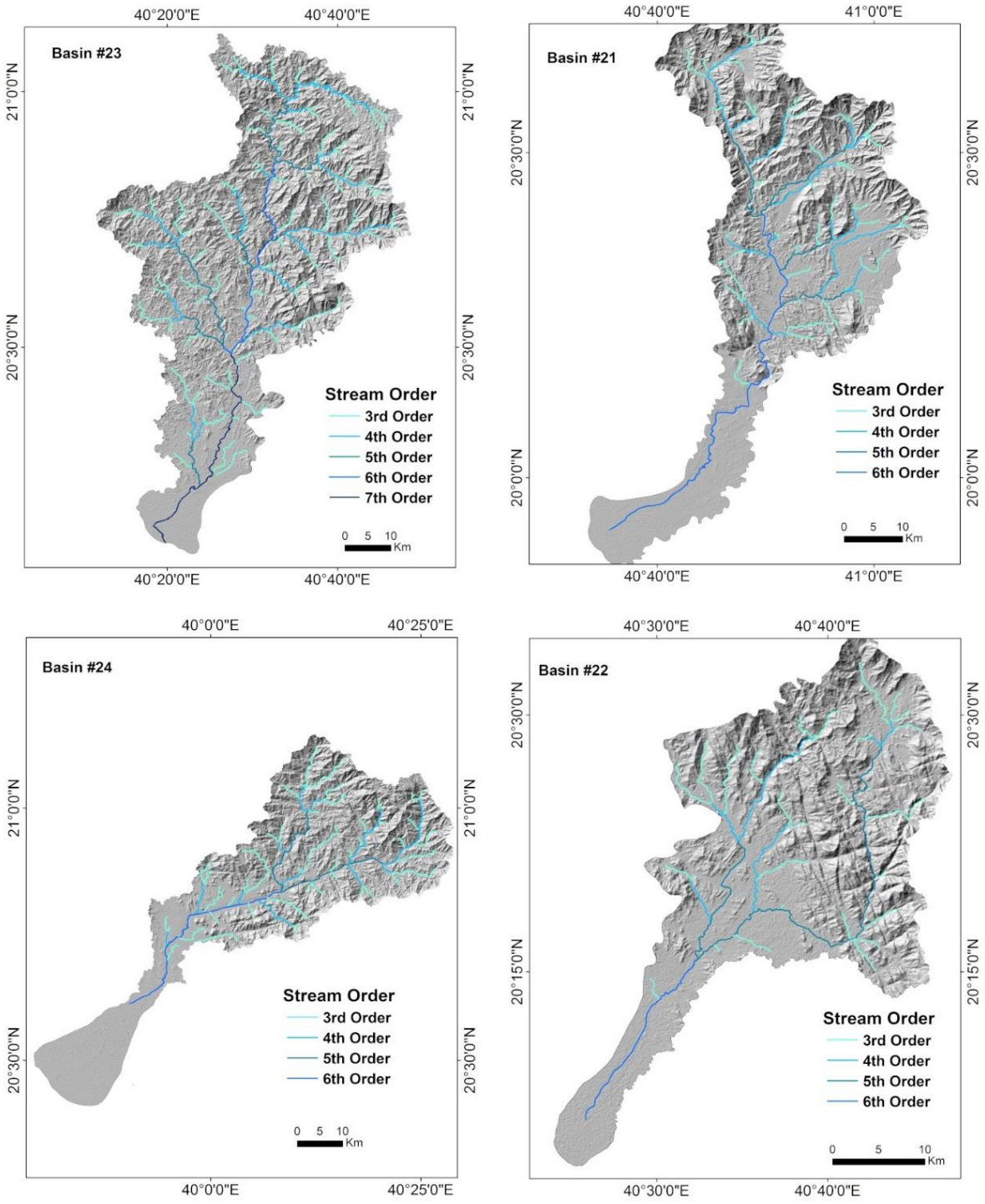

Figure 4-4 (continued). Basin #21 to #24

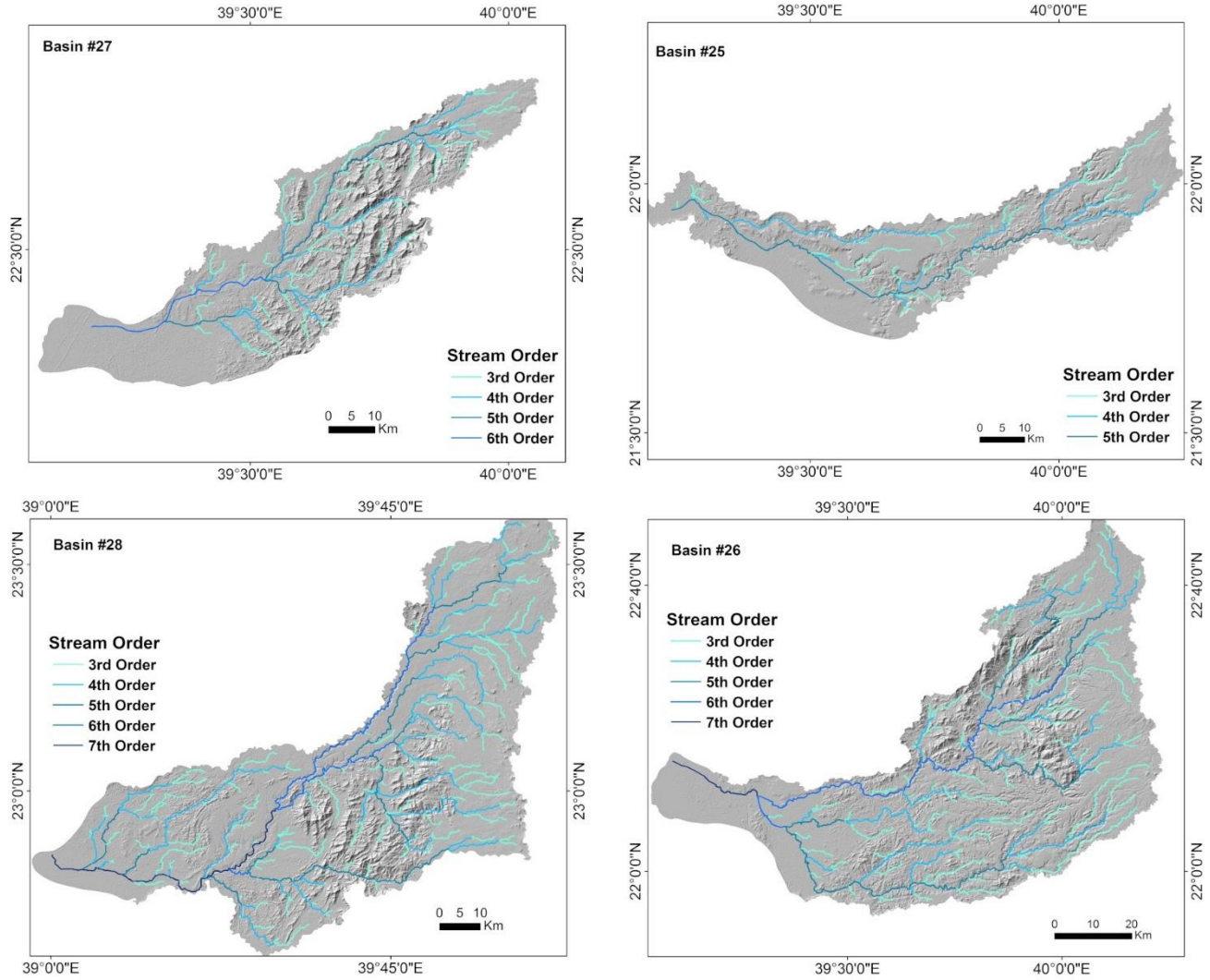

Figure 4-4 (continued). Basin #25 to #28

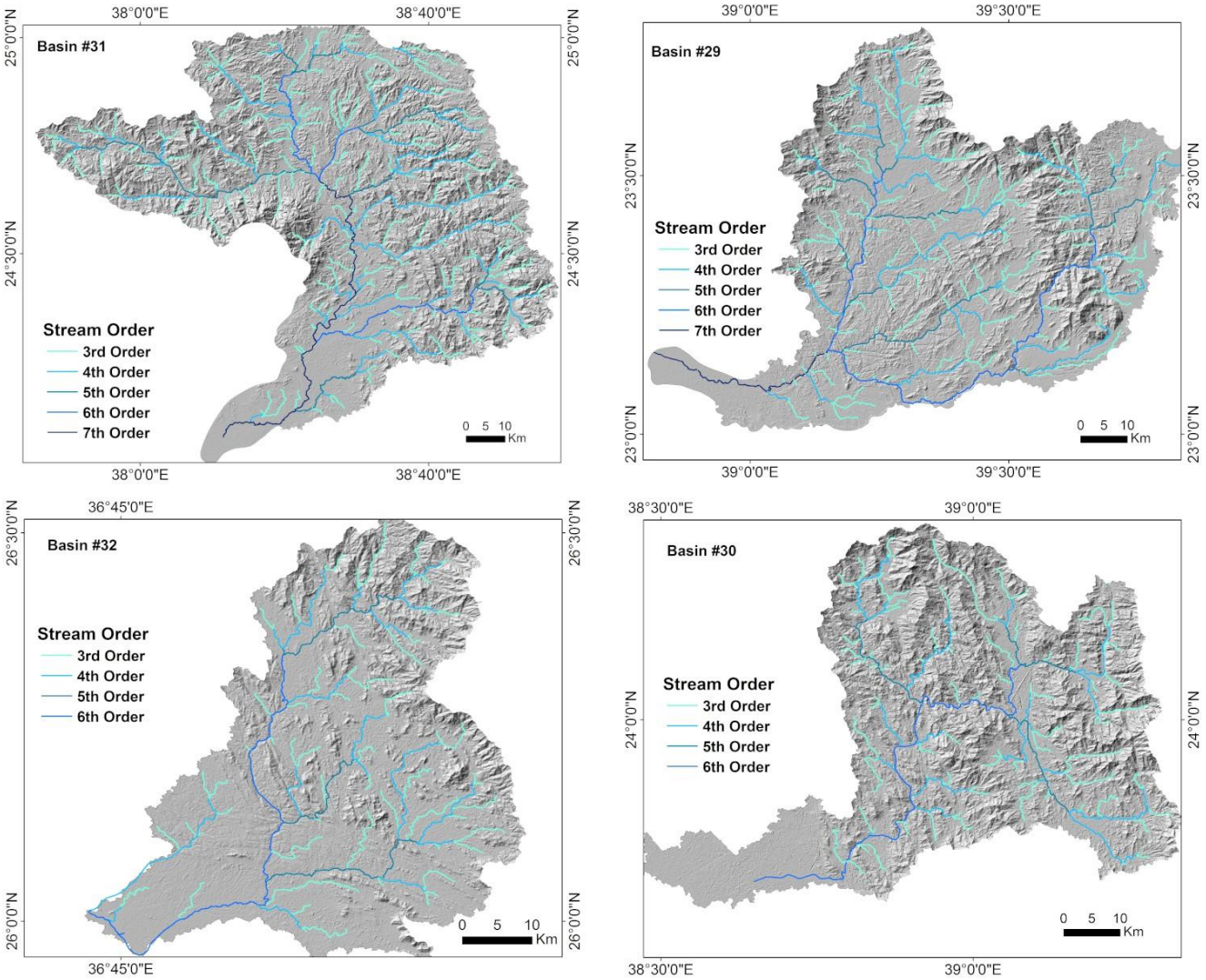

Figure 4-4 (continued). Basin #29 to #32

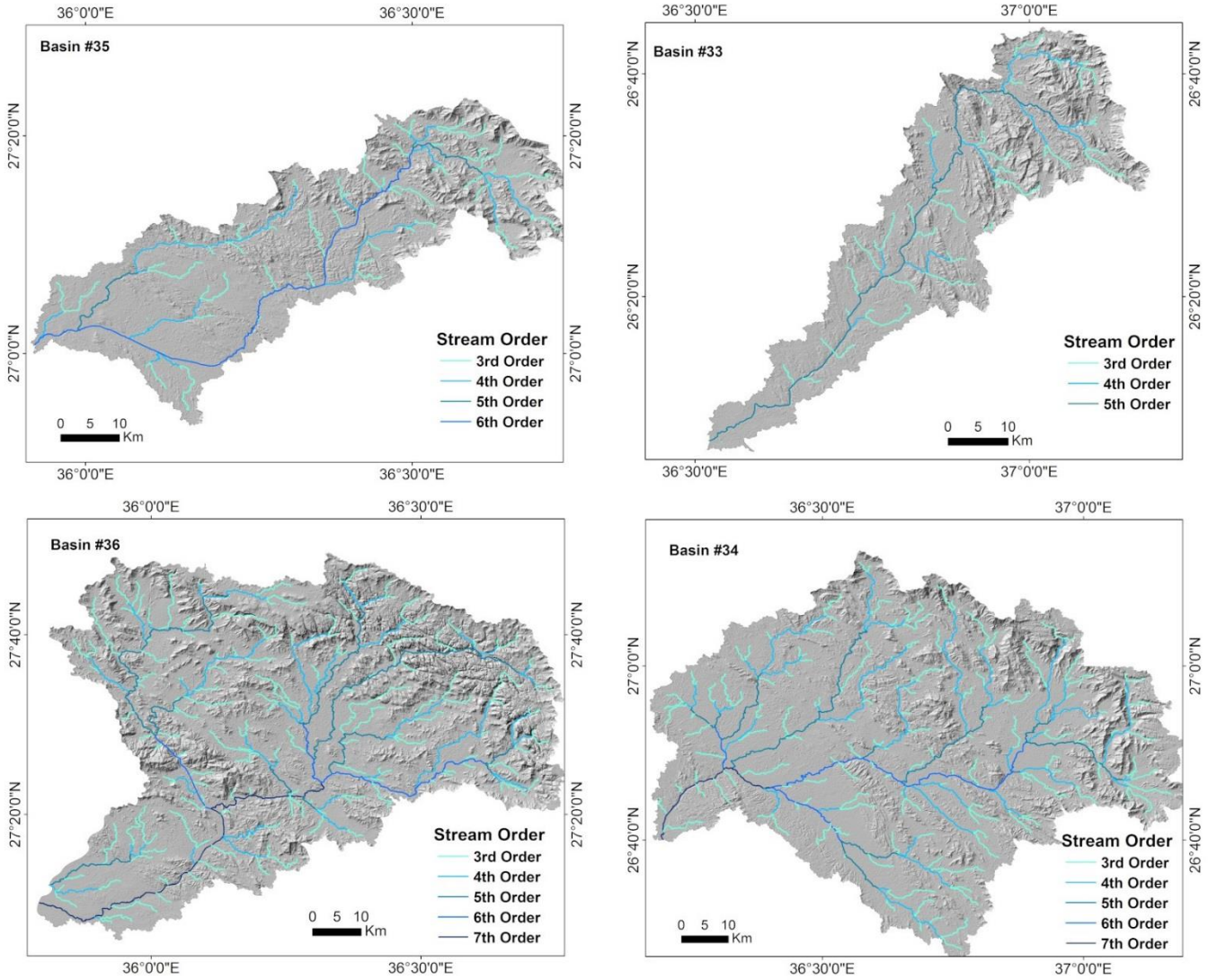

Figure 4-4 (continued). Basin #33 to #36

Table 4-1 Description and symbols for morphological parameters used in this study

Variable	Symbol	Description
Basin area*	*A*	
Basin perimeter*	*P*	
Basin length*	*Lb*	
Total number of streams	*Nu*	
Total stream length*	*Lu*	
Mean stream length	*Ls*	Total stream length / Total number of stream segments
Bifurcation ratio	*Rb*	Ratio of number of stream segments of one order to the number of the next higher order
Stream frequency	*Fs*	Total number of streams / Basin area
First order stream frequency	Fs_1	Number of first order streams / Basin area
Average length of first order stream	L_1	Total length of first order stream/ Number of first order streams
Ratio between average lengths of first to second order streams	R_{12}	Average length of first order streams / Average length of second order streams
Ratio of first order stream number to perimeter	R_{P1}	Number of first order streams / Perimeter
Drainage density*	*Dd*	Total stream length / Basin area
Maintenance coefficient*	*Mc*	1/ Drainage density
Form factor*	*Ff*	Basin area / Basin length^2
Circularity ratio*	*C*	$(4\pi \times$ basin area$)$ / Perimeter^2
Elongation ratio*	*Re*	$2/Lb \times \sqrt{(\text{basin area}/\pi)}$
Relief ratio*	*Rr*	Basin relief / Basin length
Relative relief*	*Rl*	Basin relief / (Perimeter × 100)
Ruggedness number*	*Rn*	Basin relief × Drainage density
Hypsometric Integral*	*HI*	(*Hmean – Hmin*) / (*Hmax – Hmin*)

* Variables also used for PC analysis of the 1046 sub-basins

4.3.1 Basin area

The basin area (*A*), also known as the drainage area, expresses the size of a basin and is the most fundamental characteristics for hydrologic analysis. In various hydrological applications including runoff and erosion rate estimation, drainage area is required as input. Once the drainage basin has been delineated, the area, usually measured in km^2, can be determined easily with the help of GIS.

4.3.2 Perimeter length

Perimeter of a drainage basin is defined as the horizontal projection of its water divide (Zavoianu, 1985). One can delineate drainage basin using a topographic map by manually tracing their perimeters or by using GIS and a DEM. Perimeter length (*P*) is the linear length of a drainage basin perimeter; it depends upon the total basin area and the shape. The length is generally measured in km and can be easily determined in a GIS environment.

4.3.3 Basin length

Basin length (*Lb*) is defined as the straight line distance from a basin's mouth to the head water divide measured through the direction of a main stream (Horton, 1932). Schumm (1956) pointed out that the maximum length of drainage basin should be measured parallel to the main stream.

4.3.4 Total number of streams

The stream order hierarchy proposed by Strahler (1964) has been used to calculate the total number of streams (*Nu*). In the Strahler stream order system, head waters of streams are designated as the first order. The confluences of two stream of order *n* forms a stream order of *n* + 1. For example, a second order stream is formed at the junction of two first order streams, and a third order stream is formed at the junction of two second order streams. *Nu* is the summed count of all the Strahler orders of stream in a drainage basin.

4.3.5 Total Stream length

Total stream length (*Lu*) is the sum of the lengths of all streams within a drainage basin. Fitzpatrick et al. (1998) described that the summed stream length determines the stream habitat and the availability of sediment transport. Stream length increases exponentially with increasing stream order and it depends upon the underlying rock characteristics and the degree of drainage development.

4.3.6 Mean stream length

There exist a geometric relationship between the numbers of stream segments in successive stream orders (Horton, 1945). Mean stream length (*Ls*) is the total stream length in a drainage basin divided by the total number of stream segments. It is a dimensional property that expresses the characteristic size of components of a drainage network and its contributing basin surface (Strahler, 1964).

4.3.7 Bifurcation ratio

Bifurcation ratio (*Rb*) is expressed as the ratio of the number of streams of an order *n* (Nu_n) to the number in the next higher order (Nu_{n+1}) (Horton, 1932). Mathematically it is expressed as:

$$Rb = Nu_n / Nu_{n+1}$$

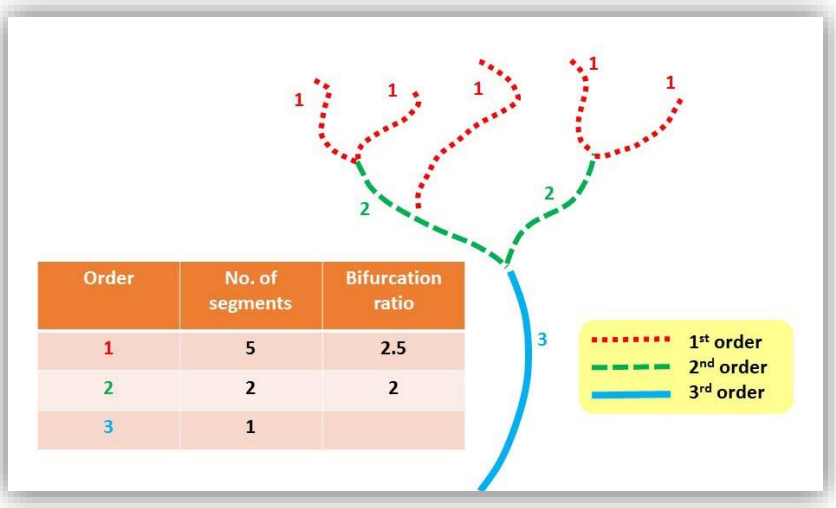

Order	No. of segments	Bifurcation ratio
1	5	2.5
2	2	2
3	1	

Figure 4-5 Example of stream ordering and the calculation of the bifurcation ratio.

Strahler, (1952) noted that *Rb* values remain fairly stable except for geologically disturbed areas. Sarangi (2003) pointed out that, if the value of *Rb* is small, the basin produces a sharp peak discharge; whereas if *Rb* is large, the basin produces an extended low peak flow. Schematic diagram showing bifurcation ratio calculation are shown in **Figure 4-5**.

4.3.8 Stream frequency

Stream frequency (*Fs*), an index to quantify the density of drainages in a basin, is derived by counting the total number of stream segments for all Strahler orders within a basin and dividing it by basin area (Horton, 1945). It is expressed as:

$$Fs = \frac{Nu}{A}$$

4.3.9 First order stream frequency

The drainage basins of the first-order tributaries are the last developed on a given area, and they often have steep sided V-shaped valleys and incised channels adjoined by belts of no erosion (Horton, 1945). In such cases, the runoff volume is adequate to produce erosion, and this part of valley will be cut down to stream level. Thus, first order streams are important in hydrological studies. First order stream frequency (Fs_1) is defined as the ratio of

total number of first order streams in a drainage basin to the area of the basin. First order streams are also sensitive to uplift and are a good indicator of tectonics (Keller and Pinter, 2002).

4.3.10 Average length of first order stream

Average length of first order streams (L_1) is expressed as the ratio of the total length of first order stream to the total number of first order streams (Miller et al., 1990).

$$L_1 = \frac{Lu_1}{Nu_1}$$

where Lu_1 and Nu_1 are the total length of first order streams and total number of first order streams, respectively. **Figure 4-6** shows the schematic diagram explaining L_1 variable.

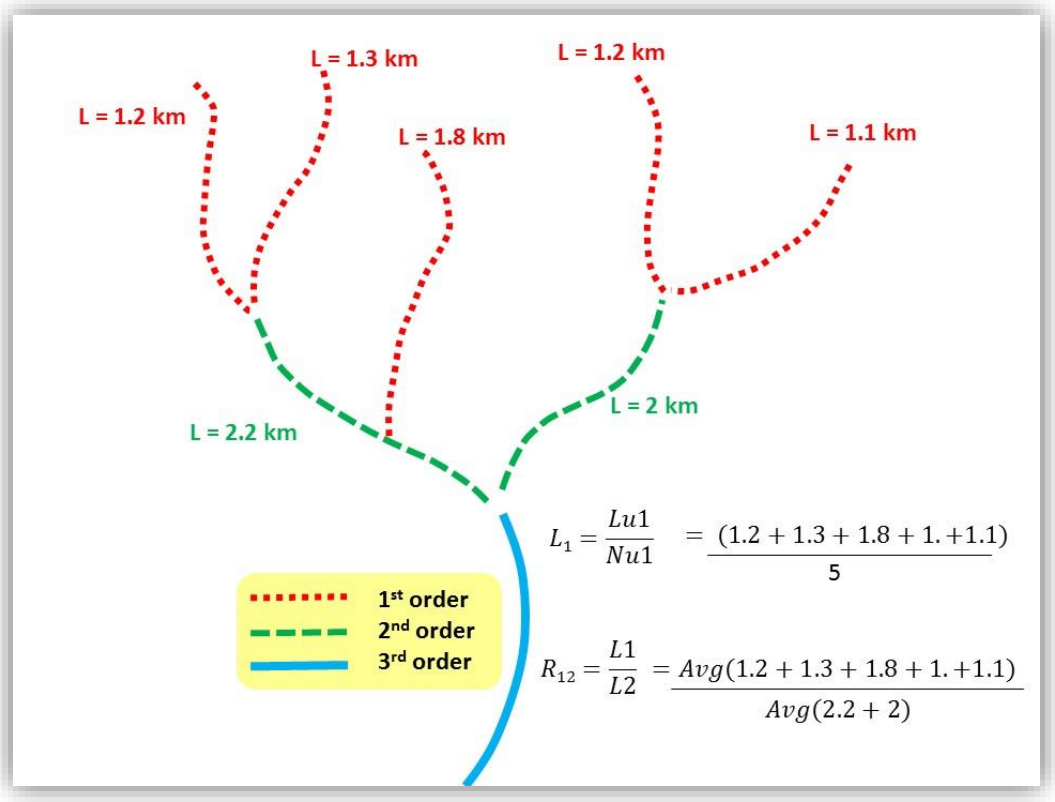

Figure 4-6 Schematic diagram explaining the average length of first order streams and ratio between average lengths of first to second order streams.

4.3.11 Ratio between the average lengths of first to second order streams

Miller et al. (1990) acknowledged the importance of lower order streams in drainage morphometric studies and expressed the ratio between the average lengths of first to second order streams (R_{12}) as:

$$R_{12} = \frac{L_1}{L_2}$$

where L_1 is the average length of first order streams and L_2 is the average length of second order streams. **Figure 4-6** shows the schematic diagram explaining R_{12} variable.

4.3.12 Ratio of first order stream number to perimeter.

The ratio of first order stream number to perimeter (R_{p1}) is expressed as the ratio of the total length of first order stream streams to the perimeter of the basin. It is calculated by dividing the total number of first order streams by the basin perimeter.

$$R_{p1} = \frac{Nu_1}{P}$$

4.3.13 Drainage density

Drainage density (*Dd*), total stream length per unit area, has often been used to express the degree of fluvial dissection (Oguchi, 1997). Drainage density is calculated by dividing drainage area by the total stream length (Horton, 1932) and is expressed as:

$$Dd = \frac{Lu}{A}$$

It is observed that smaller drainage density corresponds to smaller surface runoff (Sen, 2008). Numerous studies have related *Dd* to climate, vegetation, bedrock geology, and relief (e.g., Schumm, 1956; Melton, 1957; Wilson, 1971; Gregory and Gardner, 1975). Sketches of drainage density variations are depicted in **Figure 4-7**.

4.3.14 Maintenance coefficient

Maintenance coefficient (*Mc*), also known as constant of channel maintenance (Schumm, 1956) is defined as the inverse of drainage density and is expressed as:

$$Mc = \frac{1}{Dd}$$

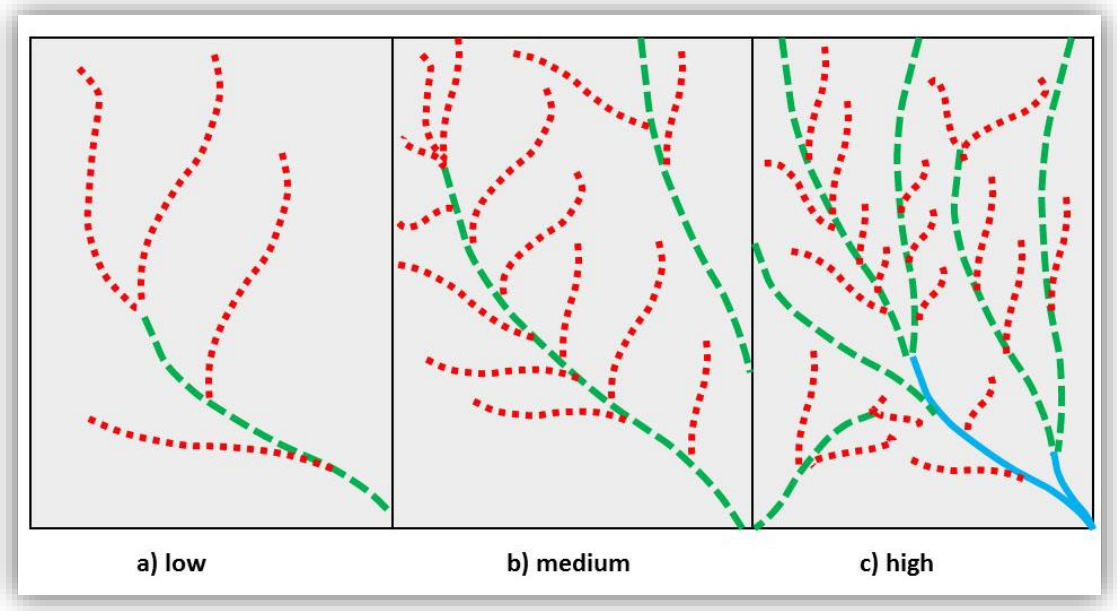

Figure 4-7 Schematic diagram showing drainage density variations a) low drainage density, b) medium drainage density and c) high drainage density.

4.3.15 Form factor

Form factor (*Ff*), an index of drainage basin outline, is defined as the dimensionless ratio of basin area to the square of basin length:

$$Ff = \frac{A}{Lb^2}$$

Gregory and Walling (1968) noted that if two basins have the same area, the more elongated one will tend to have smaller peaks but longer period of flood flows.

4.3.16 Circularity ratio

Miller (1953) defined the circularity ratio (*C*) as the ratio of the area of a basin to the area of a circle having the same circumference as the basin perimeter. The value of circularity ratio varies from 0 to 1. It is expressed as:

$$C = \frac{4\pi A}{P^2}$$

If the value of *C* is close to 1, it indicates that the basin is more circular and vice versa.

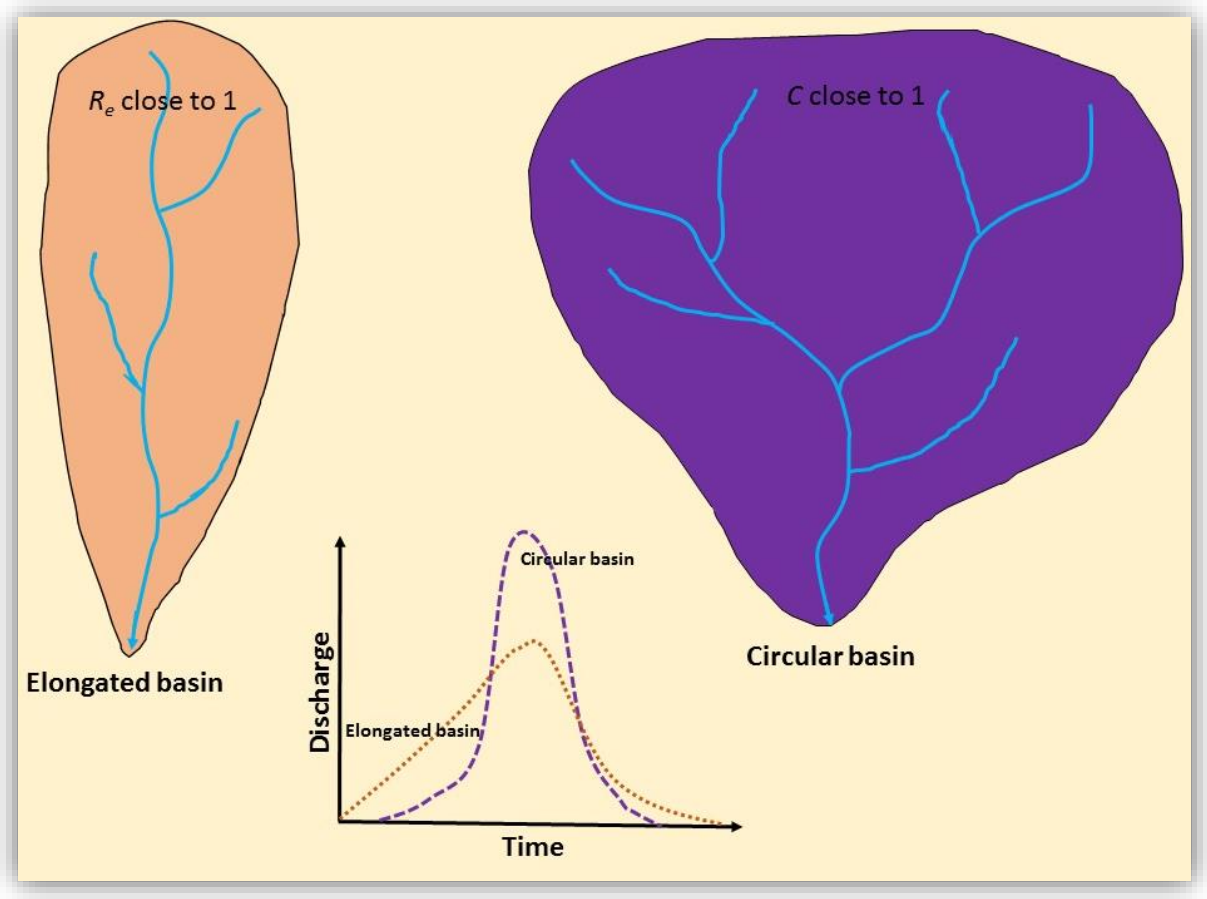

Figure 4-8 Sketch showing examples of circular and elongated basins and their relationship with discharge.

4.3.17 Elongation ratio

Similar to the circularity ratio, the elongation ratio (*Re*) also provides the measure of basin shape. **Figure 4-8** shows the schematic example of circular and elongated basins and their relationship with discharge rates. Elongation ratio is defined as the ratio of the diameter of a circle having the same drainage area as that of the circle to the maximum length of the basin (Schumm, 1956):

$$Re = \frac{2}{lb} \times \sqrt{(A/\pi)}$$

If the value of *Re* is close to 1, the basin is more elongated and vice versa. Both the values of *Re* and *C* are affected by the underlying lithological characteristics (Sreedevi et al., 2005).

4.3.18 Relief ratio

The relief ratio (*Rr*) is defined as the ratio of basin relief to the basin length (Schumm, 1956). Basin relief is calculated from the difference in elevation between the highest (*H*) and lowest (*h*) points in the basin. Therefore, *Rr* is expressed as:

$$Rr = \frac{H - h}{Lb}$$

Because *Rr* standardizes the change in elevation over distance, it is useful when comparing basins of different sizes.

4.3.19 Relative relief

Relative relief (*Rl*) is defined as the ratio of maximum drainage basin relief to the perimeter of the basin. It is expressed as:

$$Rl = \left(\frac{H}{P}\right) \times 100$$

Numerous researchers have indicated the strong relation between relative relief and the drainage density in different climatic locations around the globe (Yatsu, 1950; Schumm, 1956; Oguchi, 1997).

4.3.20 Ruggedness number

The ruggedness number (*Rn*) is the product of basin relief and drainage density. It increases when topography becomes more convoluted. It is expressed as:

$$Rn = (H - h) \times Dd$$

4.3.21 Hypsometric integral (*HI*) and hypsometric curves

Hypsometric analysis has been conducted to discuss the geomorphic form of the basins. The shape of the hypsometric curve and the value of the hypsometric integral (*HI*) provide valuable information particularly for geomorphological studies in relation to hydrology (e.g., Howard, 1990), climate (e.g., Masek et al., 1994), tectonics (e.g., Ohmori, 1993; Chen et al., 2003), and lithology (e.g., Lifton and Chase, 1992).

The hypsometric integral (*HI*) represents the relative proportion of the basin area below a given height (Strahler, 1952). Approximate *HI* values for drainage basins can be obtained by Pike and Wilson's (1971) formula:

$$HI \cong \frac{Hmean - Hmin}{Hmax - Hmin}$$

where $Hmean$ = mean elevation, $Hmin$ = minimum elevation, and $Hmax$ = maximum elevation of the drainage basins.

The hypsometric curve represents the relative proportion of the watershed area below or above a given height (Strahler, 1952). A convex curve represents relatively young, less eroded basins, an S-shaped curve represents moderately eroded basins and a concave curve indicates relatively old or more eroded basins (**Figure 4-9**) (Strahler, 1952; Keller and Pinter, 2002). This study uses MICRODEM software to plot the hypsometric curves for the 36 drainage basins.

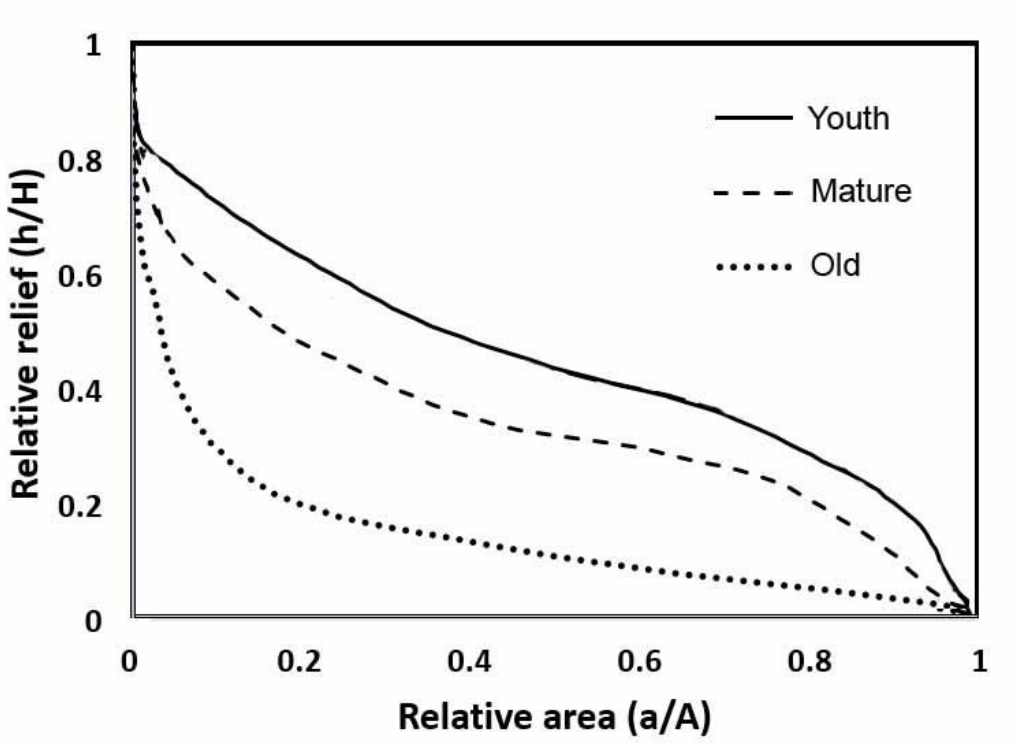

Figure 4-9 Changes in hypsometric curves (modified from Strahler 1952). Convex curves are typical for youthful stages, S-shaped curves for middle or mature stages and concave for old developmental stages of drainage basins.

4.4 Statistical analysis

Using the above parameters and the MYSTAT and STATISTICA software, statistical analyses were performed. Multivariate analyses such as principal component analysis (PCA), canonical correspondence analysis (CCA), redundancy analysis (RDA), cluster analysis (CA) and discriminant function analysis (DFA) have often been applied to geoscientific studies. One of the main advantages of these techniques is the ability to analyse large and complex datasets containing many variables and spatial units. Among these, this study performs PCA and CA because they are most basic and thus have been used intensively and successfully in various environmental and geoscientific studies (Aruga et al., 1995; Fournier et al., 2008). These two techniques are simple and enable the identification of structures within a data set, and reveal relationships between data components, so that important information can be retained, while noise is discarded.

4.4.1 Principal component analysis

PCA is mainly used in geomorphology for data reduction (Singh et al., 2009; Prima and Yoshida, 2010), and in many cases only a few principal components are needed to describe the essential data characteristics (Alberto et al., 2001). PCA calculates the correlation matrix, the principal component loading matrix and respective Eigen values to explain the structure of the parameters. This study employs PCA to examine the structural relationships of the 21 morphometric parameters for the 36 basins and the 13 morphometric parameters for the 1046 sub-basins as well as to classify the basins using the obtained component values.

4.4.2 Cluster analysis

In previous studies, CA has been used for grouping geomorphological units such as drainage basins based on morphology (de Andrade et al., 2008; Raux et al., 2011). The results of CA are usually shown in the dendrogram, whose horizontal axis corresponds to the linkage distance. Among the available approaches, this study chose the Euclidean (geometric) distance method because it utilizes more information about the cluster contents and has previously been successfully applied to the grouping of drainage basins (Raux et al., 2011). The present study applies CA to the objective classification of the 36 basins based on the 21 parameters.

4.5 Alluvial fans morphometry

Alluvial fans in the study area were identified and delineated by visual interpretation of satellite images (Landsat TM 4 and TM 5 30 m mosaiced UTM data downloaded from http://gis.ess.washington.edu/data/raster/GlobalData/GeoCover1990/) and from the DEMs. Areal and linear parameters of fans was measured from the delineated outline polygons of each fans using the GIS. The fan slope, altitude and relief parameters were measured from the ASTER GDEM.

The general relationship between fan area and contributing basin area is expressed as an exponential "power" function of the form:

$$A_f = c(A_d)^n$$

where A_f = fan area, A_d = drainage area, and c and n are empirical coefficients and exponents, respectively.

The relationship between fan slope and contributing basin area is expressed as:

$$S_f = c(A_d)^n$$

where S_f = fan slope.

4.6 Longitudinal profile analysis

4.6.1 Profile extraction

Most of the river longitudinal profile analyses are based on the relationship between stream gradient and erosion rate, which is governed by rock uplift, climate, and/or lithology (e.g., Wobus et al., 2006; DiBiase and Whipple, 2011). For the present study, longitudinal river profiles for the main channels of the 36 drainage basins were extracted utilizing the Stream Profiler Tools along with ArcGIS v.10 and MATLAB codes (available at: http://geomorphtools.org/). This tool set helps to extract river profiles from a DEM to generate the log-log plots of slope versus area and to calculate the steepness index and concavity of the channels. It is based on the methodology developed by Wobus et al. (2006) and Whipple et al. (2007). The main channels of the 36 drainage basins were first identified with the help of flow length tool in ArcGIS. Stream channels were then sampled in the tools at a 60 m interval and a 250 m smoothing window was applied (Whipple et al., 2007). Smoothing eliminates step like features found in a longitudinal profile due to intermittent elevation sampling in a DEM or internal error

while generating the DEM (Wobus et al., 2006). The extracted river profiles were also used to identify the knickzones in the study area.

4.6.2 Steepness and concavity indices

The steepness index (K_s) and the concavity index (θ) are derived from a generalized version of Hack's stream-length gradient index (*SL*), which is a proxy for stream power. *SL* is expressed as (Hack, 1973):

$$SL = \frac{dh}{dl} \times L$$

where $\frac{dh}{dl}$ is the local stream gradient and *L* is the upstream distance from the river head.

Values of K_s for a channel can be numerically linked to the stream power model using the following equation:

$$\frac{\partial z}{\partial t} = U - kS^m A^n$$

where $\frac{\partial z}{\partial t}$ is the change of channel bed elevation with time, *U* is rock uplift, *k* is coefficient of erosional efficiency that depends upon factors such as rock strength, climate, hydraulics, and erosional process, *S* is channel gradient, *A* is the upstream drainage area and *m* and *n* are positive exponents (Whipple and Tucker, 1999; Pederson and Tressler, 2012).

Assuming the river profile is in a steady state with respect to climate and uplift conditions, such that $\frac{\partial z}{\partial t} = 0$ and *U* and *k* are constant, the above expression can be simplified to a power-law expression as follows (Flint, 1974):

$$S = K_s A^{-\theta}$$

The steepness index, K_s, and concavity index, $\theta = \frac{m}{n}$, are calculated through slope of the regression line in a log-log, Slope-Area plot, where θ is the slope of the regression line and K_s is the slope intercept. To facilitate comparison among streams, this study follows the practice to calculate a normalized steepness index, K_{sn}, using 0.45 as fixed reference concavity θ_{ref} (e.g. Snyder et al., 2000; Kirby and Whipple, 2001, Miller et al., 2013). The smaller drainage areas represent debris flow dominated bedrock channels whereas large drainage areas represent fluvial processes dominated bedrock channels (Sklar and Dietrich, 1998). This study focused on the fluvial dominated part of the longitudinal profiles.

4.6.3 Identification of knickzones

The analysis of knickzones follows the methods described by Hayakawa and Oguchi (2006). At first, the sampling points along the extracted longitudinal river profile were set with an interval of 60 m that is larger than the diagonal length of an ASTER GDEM cell. Stream gradients of the rivers were then computed with varying measurement lengths, *d* (120–7440 m). The stream gradient, G_d (m/m) at each measuring point is calculated by the formula:

$$G_{\mathrm{d}} = \frac{e1 - e2}{d}$$

where $e1$ and $e2$ are elevations obtained from the DEM (m), upstream and downstream points $\frac{d}{2}$ away from the measurement point, respectively.

After the G_d calculation for each sampling point with varying *d*, a threshold value of relative steepness index, R_d is derived by fitting a regression line to G_d–*d* relation. As mentioned by Hayakawa and Oguchi (2006), a threshold value of R_d allows an objective and reproducible identification of knickzones. The regression equation to the G_d–*d* relation is:

$$G_{\mathrm{d}} = ad + b$$

where *a* and *b* are regression coefficients. R_d, the rate of gradient change with increasing *d* and an indicator of relative steepness, is the negative slope of regression line:

$$R_{\mathrm{d}} = -a$$

G_d changes as a function of *d* and it usually represents a local feature of river gradient when *d* is small, but a trend feature when *d* is large (Hayakawa and Oguchi, 2009). Here, G_d with a *d* range of 240 to 1320 m is considered for calculating the R_d value for all the streams. G_d for 120 m was found to be negative for some measurement points indicating unrealistic values inherited from DEM artifacts and errors. An example of G_d for different *d*, R_d distribution, and G_d–*d* relation along a river is shown in **Figure 4-10**.

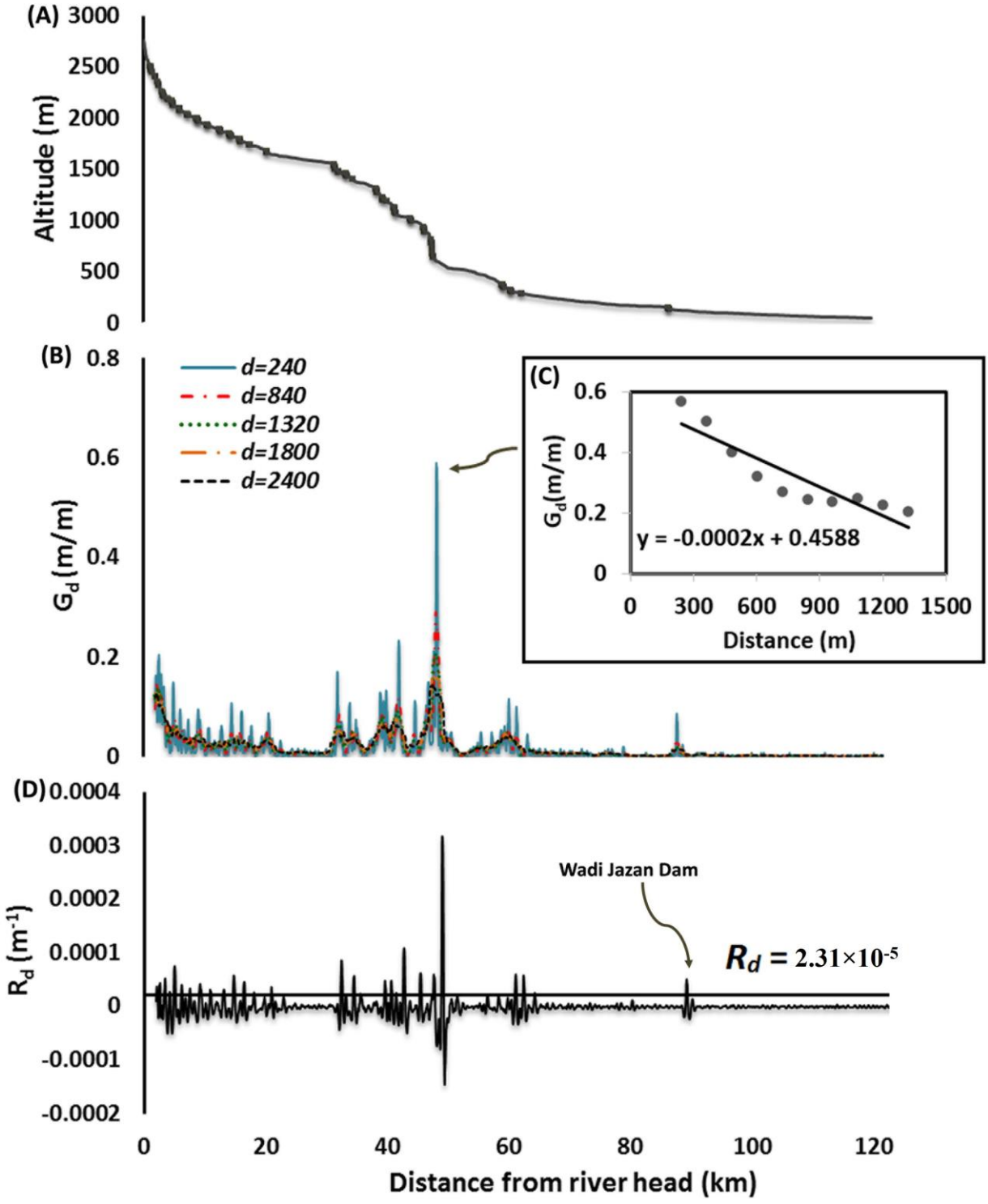

Figure 4-10 Longitudinal profile, Gd and Rd along river #7, Western Arabian Peninsula. A) Longitudinal profile of stream #7 (Wadi Jizan) and identified knickzones, B) G_d along the channel, C) G_d – d relation D) R_d profile for the same channel.

The uppermost and lowermost 660 m reaches of streams are not included in this calculation because R_d is calculated for points where G_d with d exists (Hayakawa and Oguchi, 2009). Based on the standard deviation of R_d for all the 36 streams in the Western Arabian Peninsula, the present study determined 2.31×10^{-5} m^{-1} as the threshold for knickzone extraction. In order to extract the well-defined knickzones the minimum length of knickzones to identify was set as 120 m, which is twice the length of sampling interval. Further, to reduce the ambiguity, minimum height to identify knickzones was set as 20 m, because the vertical accuracy of ASTER GDEM is 20 m. Hence, the margin of error in identifying the ambiguous knickzones was narrowed even if they have R_d values larger than 2.31×10^{-5} m^{-1}.

CHAPTER 5: Results

5.1 Evaluation of morphometric parameters

The results of the derivation of the 21 variables for the 36 major basins are shown in **Table 5-1 and Table 5-2**. **Table 5-3** summarizes the values of the minimum, maximum, mean, and standard deviation of the 13 morphometric parameters for the 1046 sub-basins. The area of the major basins ranges from 522 km^2 (basin #13) to 8292 km^2 (basin #6) with a mean of 3121 km^2. The average drainage area for the sub-basins of 4^{th} to 6^{th} orders is about 165 km^2. The perimeter of the major basins varies between 178 km (basin #17) and 830 km (basin #6) with a mean length of 431 km. The average perimeter of the sub-basins is 87 km. Basin length, which corresponds to the maximum length of the basins, ranges from 46 to 220 km with a mean of 105 km. The average basin length of sub-basins is about 20 km. Stream networks extracted from the DEM were classified according to Strahler's method; the order was found to vary between basins. Basins numbered 1, 6, 7, 8, 14, 15, 23, 26, 28, 29, 31, 34, and 35 were identified as seventh-order; basins 2, 3, 4, 5, 9, 10, 12, 16, 18, 19, 20, 21, 22, 24, 25, 27, 30, 32, and 36 were sixth-order; and four basins (11, 13, 17, and 33) were fifth-order (**Figure 4-4**). Basins numbered 1 to 6 and 25 to 29 are located in the terrain dominated by volcanic rocks while the remaining basins are found to be located in terrain dominated by crystalline lithologies (**Figure 3-3**). Stream number analysis shows that maximum number of streams are found to be located in basin #6, whereas the minimum number of streams are in basin #11. The length of all streams for different orders were measured from the vectorized stream networks using the DEM. Basins #6 and #11, with the maximum and minimum number of streams, also have the largest and smallest lengths of streams, respectively.

The correlation matrix of the 21 morphometric parameters is shown in **Table 5-4**. Strong correlations (R = 0.8–0.9) exist between some parameters that represent similar geomorphological characteristics: 1) *A*, *P*, *Lb*, *Lu*, and Nu; 2) *Fs*, *Dd*, and *Mc*; and 3) *C*, *Re*, and *Ff.* Good correlations (R = 0.7–0.8) exist between 1) *P* and *HI*, and 2) *Ff*, *Re*, and *C*. Moderate correlations (R = 0.5–0.7) include 1) *Re* and *Dd*, and 2) *HI* and *A*. Further, the correlation matrix of the 13 morphometric parameters for the 1046 sub-basins is shown in **Table 5-5**. Similar to the above results, *A*, *P*, *Lu*, and *Lb* have strong correlations (R= 0.8–0.9); *Ff*, *C*, and *Re* also have strong to good correlations (0.7–0.9); and moderate correlations are found between *C* and *Rr* or *Rl*. Considering such correlations, principal component analysis was conducted.

5.2 Principal component and cluster analyses

From the 21 parameters for the major basins, five principal components (PCs) were detected with eigenvalues greater than one (**Table** 5-6). These components account for around 87% of the total variance. All the parameters are well represented by these five PCs (**Table** 5-6). However, the contributions of the 4th and 5th components (PC4 and PC5) are smaller than those of the 1st to 3rd (PC1 to PC3). In addition, with PC4 and PC5, no parameter shows a loading value greater than 0.6. This study therefore focuses on the first three components. **Figure 5-1** shows the scree plot of eigenvalues associated with the five principal components. The results of PCA for the 13 parameters for the sub-basins is shown in **Table 5-7**. Four PCs were detected with eigenvalues greater than one that accounts about 82% of the total variance. **Figure 5-2** shows the scree plot of eigenvalues associated with the four principal components of 1046 sub-basins. The results are similar to those from the 21 parameters; therefore this study focuses on the latter.

Around 39% of the variance of the 21 parameters is described by PC1. The factor loadings indicate that PC1 represents parameters related to the dimensions of basins such as *A, P, Nu, Lu,* and *Lb,* and to the drainage texture as defined by *Fs, Fs_1, RP_1, Dd,* and *Mc* (**Table 5-6**). The sign of PC1 (**Table 5-8**) across the peninsula is mapped in **Figure 5-3a**. Negative PC1 scores correspond to smaller basin dimensions and coarser drainage texture. Such negative scores are mostly confined to the central part of the study area, particularly the Asir terrain, which extends from Yemen to the northern Jeddah region with altitudes greater than 3000 m. In contrast, a positive PC1 score indicates large basin dimensions and fine drainage textures. Most of the basins located in the Hijaz and Midyan terrains are associated with positive PC1 scores **(Figure 5-3a)**, having large values of *A*, *Dd*, *Fs*, Fs_1, and *Lb*. The drainage basins located in the Yemen Cenozoic volcanic terrain also tend to have positive PC1 scores.

Table 5-1 Morphometric parameters of the 36 major basins in the Western Arabian Peninsula

No	*Area (km)*	*Perimeter (km)*	*Number of streams*	*Length of streams (km)*	*Basin length (km)*	*Mean Elevation (m)*	*Maximum Elevation (m)*
1	5790	566	4192	6693	129	1374	3212
2	4713	743	3345	4893	150	1431	3226
3	2896	557	1879	2466	139	1464	2954
4	4086	619	2759	4053	147	1498	3658
5	2856	397	1900	2743	98	846	3587
6	8292	830	5818	8678	220	1413	3376
7	2748	497	1947	2919	125	795	2742
8	7078	514	4901	7509	130	1050	2991
9	1898	319	1195	1879	82	955	2988
10	1615	246	947	1550	65	383	2020
11	542	251	284	526	50	143	1035
12	976	197	626	1018	51	262	1396
13	522	249	368	566	46	301	906
14	5365	550	3781	5568	136	793	2995
15	3235	425	2087	3115	101	607	2714
16	2610	388	1627	2361	111	570	2399
17	801	178	375	582	62	174	1296
18	1374	314	879	1298	84	657	2491
19	1577	378	1005	1497	78	448	2485
20	1579	305	939	1401	85	438	2545
21	1849	331	1152	1785	95	672	2369
22	3245	450	2345	3353	109	818	2663
23	897	253	671	914	66	402	2210
24	1933	429	1275	1748	101	650	2609
25	2026	432	1083	1693	127	340	1292
26	5342	745	3496	5779	147	645	1674
27	2202	353	1345	2067	115	486	1658
28	5052	515	3652	6217	150	632	1769
29	4825	522	3676	5476	130	501	2137
30	2912	384	2172	3086	98	571	2331
31	6727	548	4976	7242	118	407	2284
32	2038	294	1552	2313	70	312	2036
33	1373	317	1098	1591	88	408	1657
34	4997	481	4134	6574	102	390	2004
35	1735	456	1292	2204	85	390	1749
36	4662	470	3924	5914	105	613	2120

- The minimum elevation is sea level

Table 5-2 Morphometric parameters of the 36 major basins in the Western Arabian Peninsula (Dimensionless parameters)

No	*Ls*	*Rb*	*Fs*	Fs_1	L_1	R_{12}	R_{P1}	*Dd*	*Mc*	*Ff*	*C*	*Re*	*Rr*	*Rl*	*Rn*	*HI*
1	1.6	3.9	0.72	0.57	1	2.09	5.84	1.15	0.87	0.34	0.22	0.66	0.02	0.0056	3.62	0.42
2	1.46	4.9	0.7	0.56	0.93	2.13	3.61	1.03	0.97	0.2	0.1	0.51	0.02	0.0043	3.32	0.44
3	1.31	4.39	0.64	0.51	0.79	1.95	2.66	0.85	1.18	0.14	0.11	0.43	0.02	0.0053	2.51	0.5
4	1.47	4.66	0.67	0.53	0.89	1.89	3.53	0.99	1.01	0.18	0.13	0.49	0.02	0.0059	3.62	0.41
5	1.44	4.35	0.66	0.52	0.9	2.1	3.79	0.96	1.04	0.29	0.22	0.61	0.04	0.009	3.44	0.24
6	1.49	4.21	0.7	0.56	0.93	2.04	5.68	1.04	0.96	0.17	0.15	0.46	0.02	0.0041	3.51	0.42
7	1.5	4.08	0.7	0.56	0.56	1.91	3.14	1.06	0.94	0.17	0.13	0.47	0.02	0.0058	3.05	0.32
8	1.53	4.07	0.69	0.56	0.93	2.1	7.73	1.06	0.94	0.41	0.33	0.73	0.02	0.0058	3.17	0.35
9	1.57	4.23	0.62	0.52	0.89	1.88	3.1	0.99	1.01	0.28	0.23	0.59	0.04	0.0094	2.96	0.32
10	1.64	3.79	0.58	0.44	0.95	3.12	2.95	0.95	1.05	0.38	0.33	0.69	0.03	0.0082	1.92	0.19
11	1.85	3.85	0.52	0.39	1.06	1.67	0.85	0.96	1.04	0.21	0.1	0.52	0.02	0.0041	0.99	0.14
12	1.63	3.47	0.64	0.48	0.96	1.8	2.4	1.04	0.96	0.37	0.31	0.69	0.03	0.0071	1.45	0.19
13	1.54	4.12	0.7	0.53	0.99	1.89	1.11	1.08	0.93	0.24	0.1	0.56	0.02	0.0036	0.98	0.33
14	1.47	3.65	0.7	0.57	0.91	2.14	5.59	1.03	0.97	0.28	0.22	0.6	0.02	0.0054	3.08	0.26
15	1.49	3.49	0.64	0.51	0.94	2.05	3.92	0.96	1.04	0.31	0.22	0.63	0.03	0.0064	2.61	0.22
16	1.45	4.26	0.62	0.49	0.9	1.98	3.32	0.9	1.11	0.21	0.21	0.51	0.02	0.0062	2.16	0.24
17	1.55	4.27	0.46	0.36	0.88	1.7	1.63	0.72	1.39	0.2	0.31	0.51	0.02	0.0073	0.93	0.13
18	1.48	3.97	0.63	0.51	0.89	1.86	2.22	0.94	1.06	0.19	0.17	0.49	0.03	0.0079	2.34	0.26
19	1.49	3.99	0.63	0.51	0.92	2.02	2.12	0.94	1.06	0.25	0.13	0.57	0.03	0.0066	2.34	0.18
20	1.49	3.82	0.59	0.47	0.94	2.14	2.4	0.88	1.14	0.21	0.21	0.52	0.03	0.0083	2.24	0.17
21	1.55	3.95	0.62	0.49	0.96	1.9	2.74	0.96	1.04	0.2	0.21	0.51	0.02	0.0072	2.27	0.28
22	1.43	4.06	0.72	0.58	0.89	2	4.2	1.03	0.97	0.27	0.2	0.58	0.02	0.0059	2.74	0.31
23	1.36	3.68	0.74	0.58	0.85	2.12	2.06	1.01	0.99	0.2	0.17	0.51	0.03	0.0087	2.23	0.18
24	1.37	4.29	0.65	0.52	0.82	1.88	2.37	0.9	1.11	0.18	0.13	0.49	0.03	0.0061	2.35	0.25
25	1.56	5.88	0.53	0.43	0.92	1.86	2.05	0.83	1.2	0.12	0.13	0.4	0.01	0.003	1.07	0.26
26	1.65	3.95	0.65	0.52	0.98	1.91	3.78	1.08	0.93	0.24	0.12	0.56	0.01	0.0022	1.81	0.39
27	1.54	4.1	0.61	0.48	0.93	2.05	3	0.93	1.08	0.16	0.22	0.46	0.01	0.0047	1.54	0.29
28	1.7	3.97	0.72	0.58	1.02	1.98	5.75	1.23	0.81	0.22	0.23	0.53	0.01	0.0034	2.18	0.36
29	1.49	3.99	0.76	0.6	0.9	1.9	5.6	1.13	0.88	0.28	0.22	0.6	0.02	0.0041	2.41	0.23
30	1.42	4.47	0.74	0.59	0.9	1.99	4.48	1.05	0.95	0.3	0.24	0.62	0.02	0.0061	2.45	0.25
31	1.46	4.07	0.73	0.59	0.86	1.91	7.32	1.07	0.93	0.48	0.28	0.78	0.02	0.0042	2.44	0.18
32	1.49	4.28	0.76	0.6	0.91	2.03	4.2	1.13	0.88	0.41	0.29	0.72	0.03	0.0069	2.3	0.15
33	1.45	5.71	0.79	0.63	0.92	2.05	2.75	1.15	0.87	0.17	0.17	0.47	0.02	0.0052	1.91	0.25
34	1.59	3.92	0.82	0.65	1.01	1.95	6.85	1.31	0.76	0.48	0.27	0.78	0.02	0.0042	2.63	0.2
35	1.71	4.01	0.74	0.57	0.92	1.97	2.17	1.27	0.79	0.24	0.1	0.55	0.02	0.0038	2.22	0.22
36	1.51	3.9	0.84	0.67	0.94	2.07	6.66	1.26	0.79	0.42	0.26	0.73	0.02	0.0045	2.67	0.29

Table 5-3 Minimum, maximum, mean and standard deviation of the 13 morphometric variables for the 1046 sub-basins

	A	*P*	*Nu*	*Lb*	*Dd*	*Mc*	*Ff*	*C*	*Re*	*Rr*	*Rl*	*Rn*	*HI*
Min	2.35	12.93	0.45	3.40	0.01	0.35	0.08	0.06	0.32	0.001	0.000003	0.001	0.08
Max	3161.74	603.87	3568.67	117.21	2.89	147.82	0.54	0.41	0.83	0.24	0.000699	3.61	0.66
Mean	164.76	87.15	182.91	19.95	1.12	1.10	0.31	0.22	0.62	0.07	0.000163	1.10	0.34
Std. Dev	318.03	70.43	361.09	14.28	0.21	4.65	0.09	0.07	0.10	0.04	0.000119	0.60	0.11

Table 5-4 Pearson correlation coefficient matrix for the 21 parameters for the 36 major basins

	A	*P*	*Nu*	*Lu*	*Lb*	*Ls*	*Rb*	*Fs*	*Fs1*	*L1*	R_{12}	RP_1	*Dd*	*Mc*	*Ff*	*C*	*Re*	*Rr*	*Rl*	*Rn*	*HI*
A	1.00																				
P	0.84	1.00																			
Nu	0.99	0.82	1.00																		
Lu	0.99	0.81	1.00	1.00																	
Lb	0.83	0.92	0.78	0.77	1.00																
Ls	-0.07	-0.14	-0.07	0.00	-0.21	1.00															
Rb	-0.07	0.13	-0.08	-0.10	0.21	-0.23	1.00														
Fs	0.44	0.35	0.53	0.53	0.23	-0.24	-0.04	1.00													
Fs1	0.50	0.41	0.59	0.58	0.31	-0.30	0.01	0.99	1.00												
L1	0.08	-0.07	0.08	0.13	-0.13	0.56	-0.13	-0.04	-0.08	1.00											
R_{12}	0.08	-0.01	0.08	0.08	0.00	-0.05	-0.13	0.09	0.07	0.07	1.00										
RP_1	0.88	0.56	0.92	0.91	0.55	-0.09	-0.16	0.61	0.66	0.10	0.15	1.00									
Dd	0.41	0.29	0.50	0.53	0.14	0.28	-0.16	0.86	0.82	0.24	0.06	0.56	1.00								
Mc	-0.42	-0.32	-0.50	-0.53	-0.16	-0.24	0.18	-0.87	-0.83	-0.22	-0.10	-0.56	-0.98	1.00							
Ff	0.35	-0.05	0.41	0.42	-0.19	0.15	-0.41	0.44	0.42	0.26	0.26	0.65	0.51	-0.51	1.00						
C	0.17	-0.32	0.19	0.20	-0.20	0.06	-0.31	0.06	0.07	0.16	0.32	0.49	0.09	-0.06	0.71	1.00					
Re	0.33	-0.06	0.39	0.40	-0.22	0.16	-0.45	0.44	0.41	0.28	0.26	0.63	0.51	-0.51	1.00	0.70	1.00				
Rr	-0.40	-0.46	-0.39	-0.41	-0.51	-0.27	-0.31	-0.09	-0.09	-0.19	0.27	-0.24	-0.23	0.16	0.20	0.21	0.23	1.00			
Rl	-0.44	-0.55	-0.45	-0.47	-0.46	-0.31	-0.24	-0.26	-0.24	-0.24	0.26	-0.26	-0.42	0.38	0.06	0.37	0.08	0.91	1.00		
Rn	0.63	0.62	0.63	0.61	0.59	-0.38	-0.08	0.46	0.53	-0.26	0.21	0.58	0.28	-0.34	0.19	0.02	0.19	0.29	0.18	1.00	
HI	0.50	0.71	0.46	0.46	0.71	-0.18	0.22	0.19	0.24	-0.10	-0.01	0.24	0.12	-0.15	-0.30	-0.38	-0.30	-0.31	-0.34	0.50	1.00

Table 5-5 Pearson correlation coefficient matrix for the 13 parameters for the 1046 sub-basins

	A	*P*	*Nu*	*Lb*	*Dd*	*Mc*	*Ff*	*C*	*Re*	*Rr*	*Rl*	*Rn*	*HI*
A	1.00												
P	0.90	1.00											
Nu	0.98	0.90	1.00										
Lb	0.87	0.99	0.86	1.00									
Dd	-0.03	-0.01	0.06	-0.02	1.00								
Mc	-0.01	-0.01	-0.02	-0.01	-0.24	1.00							
Ff	0.00	-0.19	-0.01	-0.27	-0.16	-0.01	1.00						
C	-0.24	-0.49	-0.26	-0.50	-0.22	-0.03	0.75	1.00					
Re	0.00	-0.20	-0.01	-0.28	-0.16	-0.01	0.99	0.76	1.00				
Rr	-0.32	-0.49	-0.32	-0.49	-0.24	-0.04	0.34	0.66	0.34	1.00			
Rl	-0.32	-0.49	-0.33	-0.48	-0.23	-0.03	0.26	0.65	0.26	0.99	1.00		
Rn	0.14	0.14	0.15	0.17	0.04	-0.07	0.06	0.15	0.06	0.49	0.47	1.00	
HI	-0.09	-0.08	-0.10	-0.07	-0.15	-0.02	0.01	0.07	0.00	0.13	0.13	-0.02	1.00

Table 5-6 Loadings of the 21 morphometric parameters for the first five components of PCA

	Factor Loadings				
Parameter	**PC1**	**PC2**	**PC3**	**PC4**	**PC5**
A	0.911763	-0.17273	0.08098	0.342669	-0.03329
P	0.764186	-0.55657	0.089115	0.128756	0.142031
Nu	0.946974	-0.10644	0.057263	0.26575	-0.06108
Lu	0.94996	-0.09205	0.001147	0.274075	-0.02755
Lb	0.683328	-0.63711	0.167616	0.241936	0.031288
Ls	-0.05116	0.190109	-0.77229	0.248946	0.384528
Rb	-0.08387	-0.53205	-0.02025	-0.22626	-0.40006
Fs	0.748015	0.232055	0.047212	-0.59679	-0.07459
Fs_1	0.781462	0.177351	0.115885	-0.55787	-0.11089
L_1	0.097148	0.260336	-0.62145	0.2713	0.291586
R_{12}	0.1121	0.324192	0.295407	0.17923	0.344227
RP_1	0.907522	0.214539	0.098206	0.231816	-0.20348
Dd	0.722438	0.318535	-0.34645	-0.46007	0.138791
Mc	-0.72995	-0.30898	0.283821	0.474825	-0.2067
Ff	0.480384	0.805752	-0.04334	0.150512	-0.13892
Re	0.467213	0.820957	-0.04185	0.145588	-0.10085
C	0.153426	0.722995	0.127097	0.442997	-0.3238
Rr	-0.35327	0.528468	0.644333	-0.11527	0.304962
Rl	-0.4733	0.45548	0.684161	0.046296	0.146238
Rn	0.638797	-0.06565	0.645218	-0.0266	0.281952
HI	0.453778	-0.63909	0.169415	-2.8E-05	0.308461
Eigen Value	8.197	4.331082	2.690094	1.971644	1.082773
% Total	39.03333	20.6242	12.80997	9.38878	5.15606
Cumulative %	39.0333	59.6575	72.4675	81.8563	87.0123

PC2, which explains around 21% of the total variance, represents parameters *HI*, *C*, *Re* and *Ff* (**Table** 5-6), which reflect the general shape of a basin. Positive PC2 scores often correspond to low *HI* and nearly circular basins, according to the values of *C*, *Re* and *Ff*. Basins with positive PC2 scores tend to be located in the southern Asir, northern Hijaz, and Midyan terrains (**Figure 5-3b**). In contrast, negative PC2 scores are found in the Yemen, northern Asir and southern Hijaz regions (**Figure 5-3b**).

PC3 explains 13% of the total variance, and represent variances in *Ls*, L_1, *Rr*, *Rl*, and *Rn* (**Table** 5-6). This component therefore represents relief characteristics: basins with high relief and shorter streams have positive PC3 scores, and negative scores indicate low relief and longer streams. The spatial variation in PC3 scores (**Table**

5-8) is plotted in **Figure 5-3c**. The PC3 scores tend to be positive in the Asir and Yemen terrains, while most of the basins located in the Hijaz and Midyan regions have negative PC3 scores.

From the dendrogram obtained from the cluster analysis (**Figure 5-4**), two major clusters, A with 24 basins and B with 12 basins, can be identified. Cluster A is subdivided into Clusters I and II, with 17 and 7 basins, respectively. Cluster B can also be subdivided into Clusters III and IV, with nine and three basins, respectively. The relationships between the clusters and the PCA scores (**Figure 5-5**) show that the clusters well correspond to the values of PC1. In general, the PC1 scores of basins in each of the clusters tend to increase in the following order: I, II, III and IV. Correlations between the clusters and the PC2 or PC3 scores are less clear. However, clusters II and IV have consistently positive PC3 scores, while clusters I and III are characterized by a wider range of PC3 scores, including some negative values.

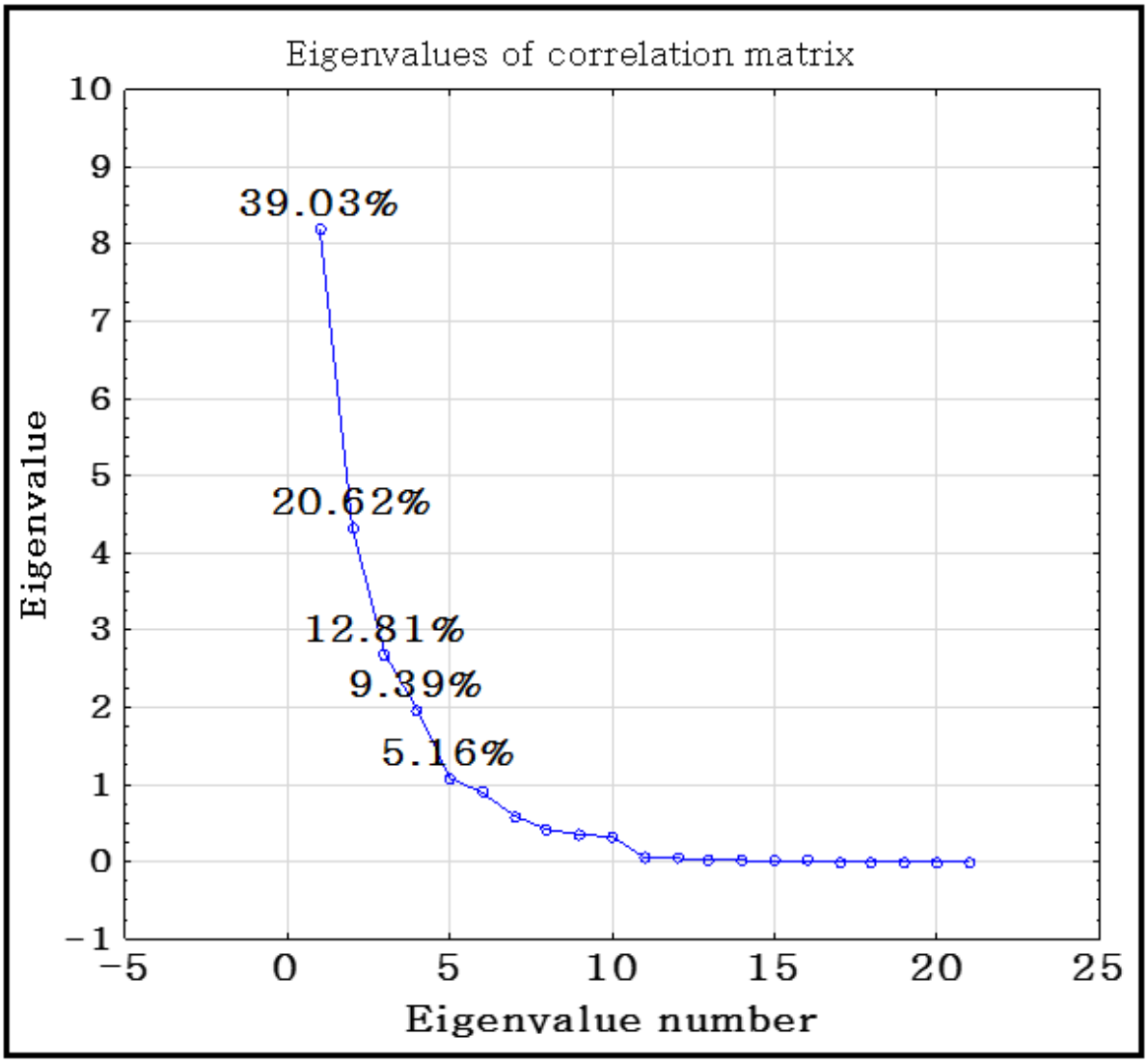

Figure 5-1 Scree plot of Eigen values associated with the principal components for the 36 main basins.

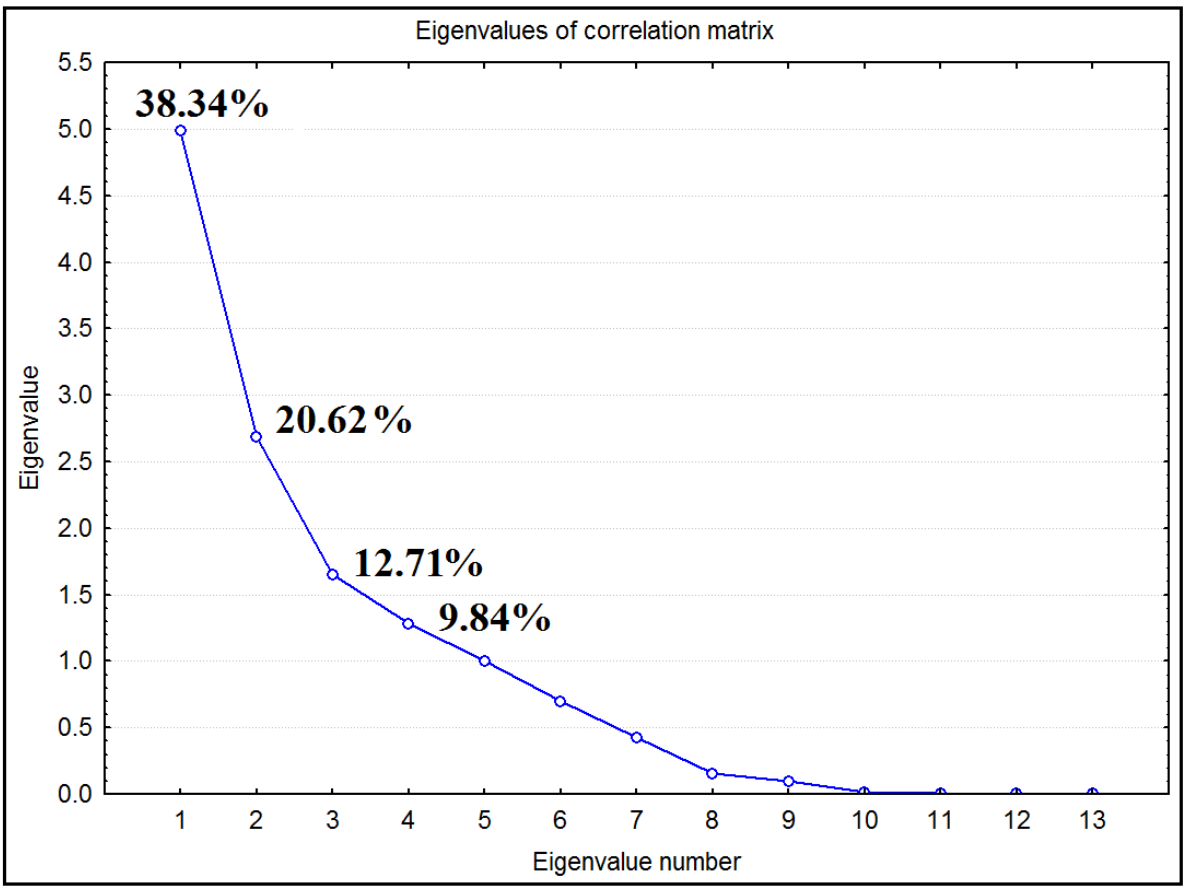

Figure 5-2 Scree plot of Eigen values associated with the principal components for the 1046 sub-basins.

Table 5-7 Loadings of the 13 morphometric parameters for the four components of PCA

	Factor loadings			
Parameter	**PC1**	**PC2**	**PC3**	**PC4**
A	-0.967668	-0.061741	-0.065639	0.012556
P	-0.957182	0.171318	-0.165556	0.011099
Nu	-0.960086	-0.047357	-0.064725	-0.057403
Lb	-0.938311	0.243178	-0.134654	0.019255
Dd	0.043092	0.149437	-0.164243	-0.797572
Mc	0.016536	0.033362	-0.134244	0.683171
Ff	0.025791	-0.977753	0.080242	0.025398
C	0.293726	-0.778274	0.418295	0.075221
Re	0.030950	-0.979846	0.081968	0.024520
Rr	0.314508	-0.271366	0.875000	0.102108
Rl	0.325440	-0.210432	0.877968	0.109708
Rn	-0.280240	0.052780	0.796094	-0.175198
HI	0.095496	0.072686	0.147246	0.386731
Eigen value	4.985344	2.680754	1.653131	1.279309
% Total	38.34880	20.62119	12.71639	9.84084
Cumulative %	38.34880	58.96998	71.68638	81.52722

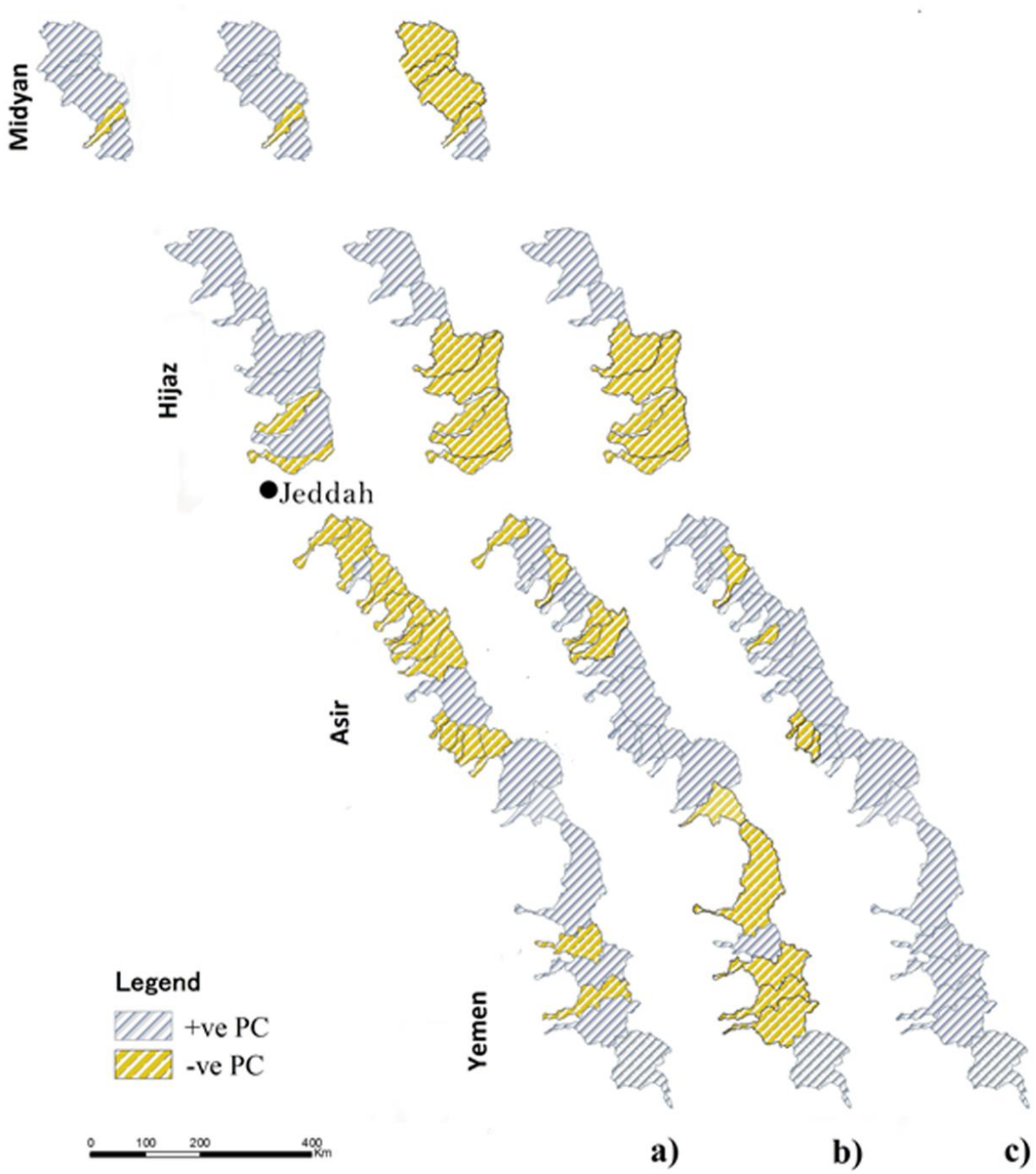

Figure 5-3 Maps showing the spatial distributions of: a) PC1 scores, b) PC2 scores, and c) PC3 scores of the major basins within the study area.

Table 5-8 Factor loading values for the first three principal components for the 36 drainage basins.

Basin No	***PC1 score***	***PC2 score***	***PC3 score***
1	1.36	0.25	0.10
2	0.79	-1.49	0.46
3	-0.33	-1.89	1.32
4	0.35	-1.28	0.90
5	-0.26	0.60	1.65
6	1.76	-1.91	0.44
7	0.03	-0.96	1.24
8	1.47	0.70	0.51
9	-0.59	0.63	1.03
10	-0.83	1.92	0.49
11	-1.56	0.03	-2.68
12	-0.84	1.64	-0.79
13	-0.79	0.00	-1.59
14	0.86	0.05	0.54
15	-0.12	0.57	0.38
16	-0.56	-0.38	0.32
17	-2.11	-0.02	-0.23
18	-0.93	-0.04	0.64
19	-0.82	0.26	0.39
20	-1.12	0.37	0.68
21	-0.71	0.00	-0.01
22	0.27	0.02	0.57
23	-0.83	0.68	1.24
24	-0.70	-0.70	0.87
25	-1.09	-2.05	-1.28
26	0.84	-1.21	-1.61
27	-0.62	-0.67	-0.67
28	1.19	-0.38	-1.66
29	1.00	-0.01	-0.40
30	0.22	0.42	0.38
31	1.45	0.86	0.04
32	0.09	1.67	0.15
33	-0.16	-0.41	-0.47
34	1.67	1.52	-1.08
35	0.08	0.11	-1.53
36	1.56	1.11	-0.35

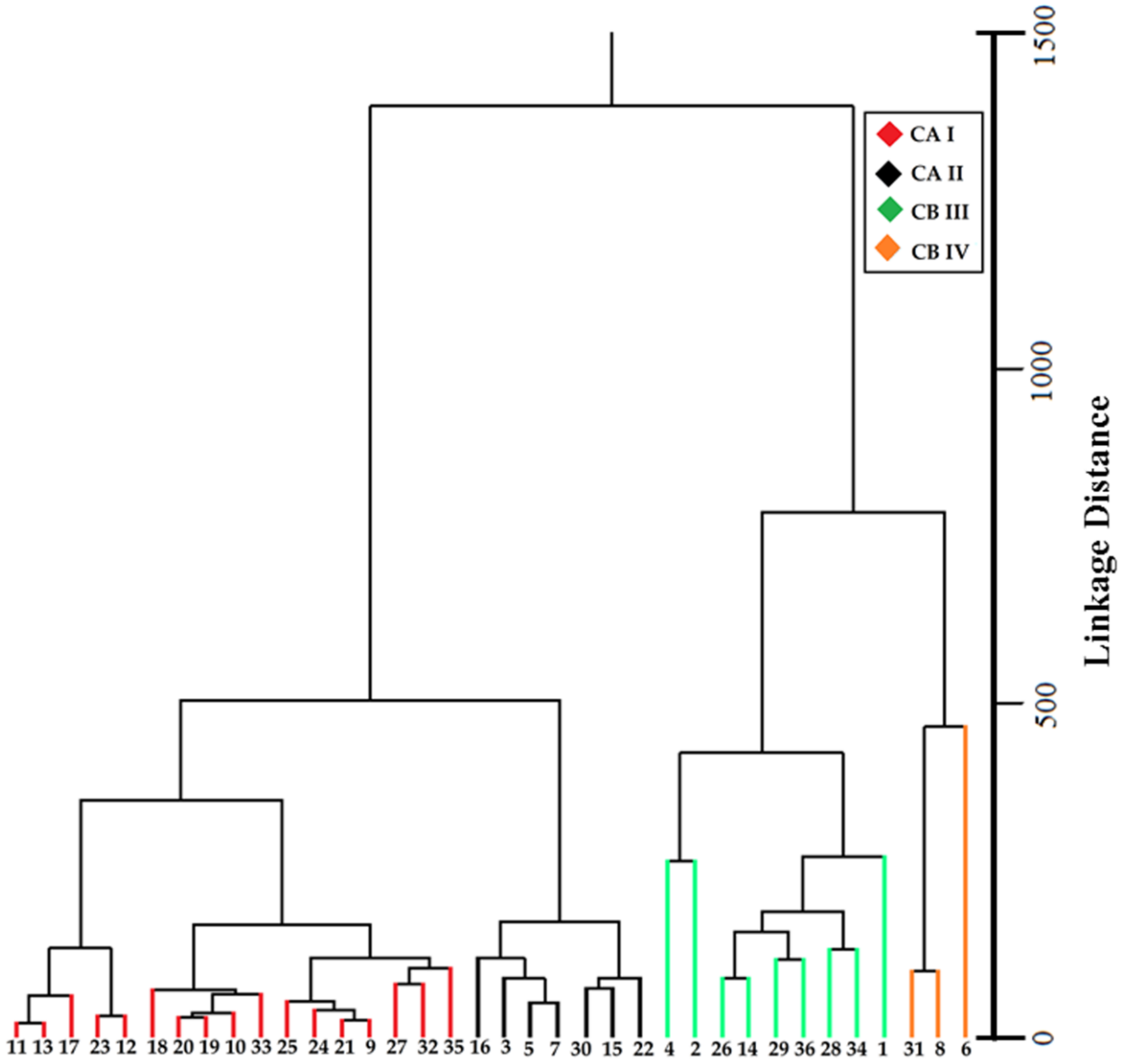

Figure 5-4 Dendrogram obtained by CA for the 36 major drainage basins in the Western Arabian Peninsula. The Y-axis indicates the relative similarity of different cluster groups; the smaller the linkage distance, the greater the similarity between basins or cluster.

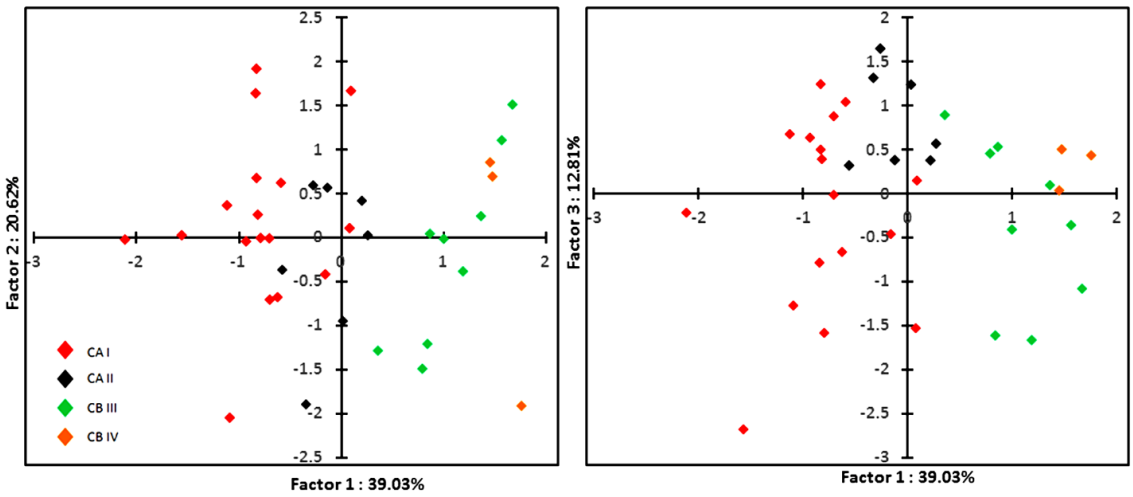

Figure 5-5 Principal component analysis loading plots for basin clusters. a) PC1–PC2 axis. b) PC1–PC3 axis.

5.3 Hypsometric analysis

As noted in section 4.3, hypsometric integral is thought to reflect tectonics, basin geometry such as basin area or circularity, climate and/or lithology. Since a wide variety of different topography can produce the same hypsometric values; in conjunction with the PCA, this study also performed an independent analysis of basin hypsometry. The aim of this particular analysis is to investigate whether basin hypsometry is inherently dependent on the scale, shape, lithology or tectonics of drainage basins. To demonstrate this, mean *HI* value for different Strahler orders were plotted against the central distance of each basins, starting from the basin #1 in southern Yemen towards the northern Saudi Arabia (**Figure 5-6**). Hypsometric analysis was applied to all the 36 major basins and 1046 sub-basins. The *HI* values for the major basins range from 0.13–0.50 and those for the 1046 sub-basins range from 0.08–0.66 (**Table 5-2 and Table 5-3**). The *HI* versus distance plots for the major basins and sub-basins of order 6, 5, and 4 show weak negative correlations with the distance from south-western tip of the peninsula (**Figure 5-6a-d**). It is noted that the average *HI* values increases to some extent from 0.27 for the major basins to 0.33 for the sub-basins. However, this difference is found to be statistically insignificant. Because Strahler orders represent the basin dimension, the *HI* values of these basins were compared with the basin area. For clarity this study also plotted *HI* versus basin area and basin circularity (**Figure 5-6e-f)**. As noted in Section 5.1, the average basin area for the 1046 sub-basins is 165 km^2. From **Figure 5-6,** it is clear that the *HI* values of basins in the Western Arabian Peninsula do not correlate with either basin area or circularity, which represents the horizontal geometry of basins.

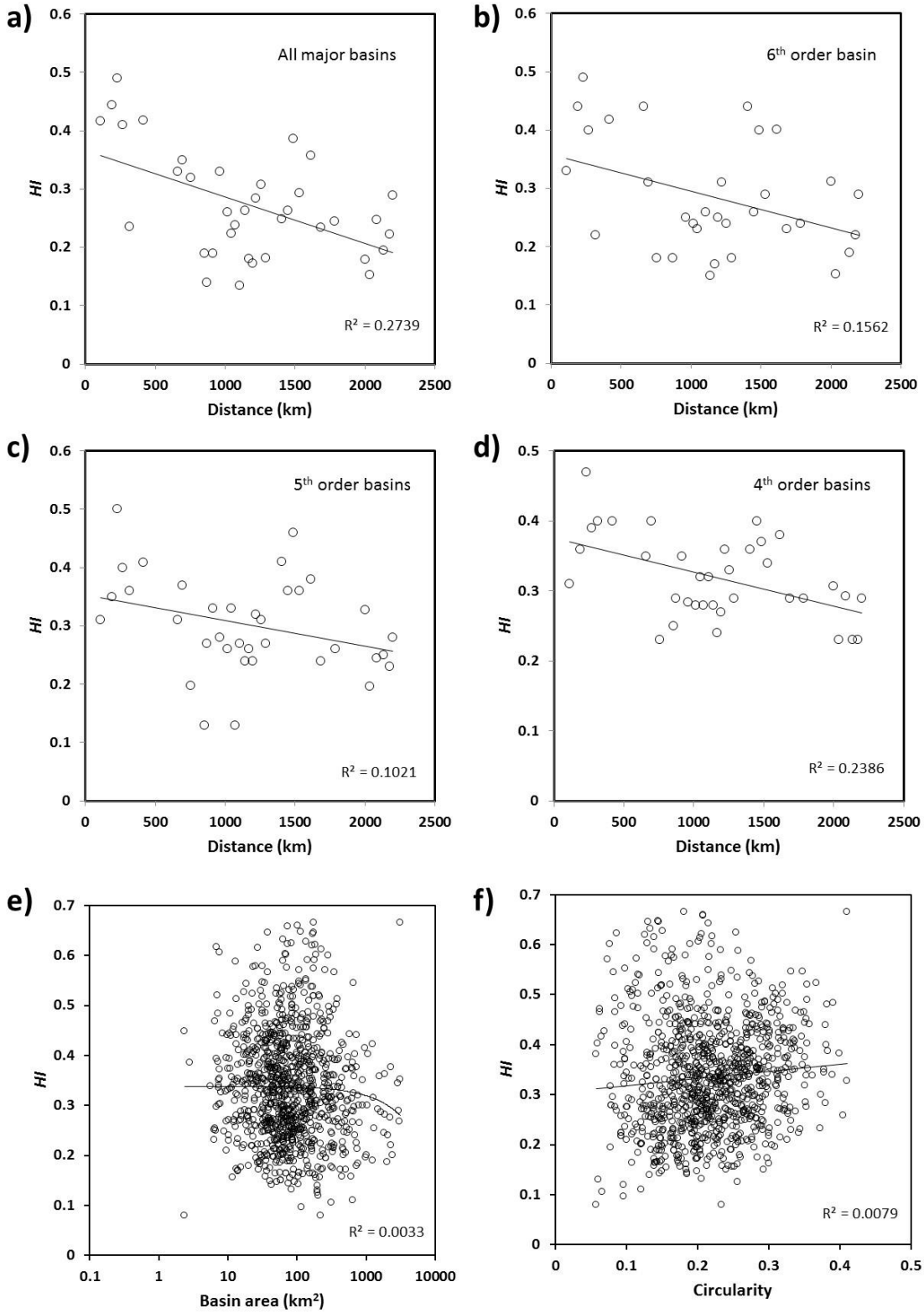

Figure 5-6 Spatial and scale dependency of hypsometric integral. a-d) Plots of mean HI vs. N–S distance for basins with different orders. Distance of the basin center from the southern tip of Yemen is plotted. e) HI vs basin area. f) HI vs circularity ratio.

Further, the hypsometric curves of the 36 basins in the Western Arabian Peninsula were plotted (**Figure 5-7)**. As mentioned in section 4.3, a convex curve with high integral indicates youthful, less eroded basin; S-shaped curve indicates mature or moderately eroded basin; and a concave curve with low integral indicates relatively old or highly eroded basin **(Figure 4-9)**. The results of hypsometric curves in the study area revealed similar kind of variations between the basins (**Figure 5-7**). The topographic comparisons of curves indicate that such variations were caused due to lithological differences. As noted in Section 5.1, basins #1 to #6 and #25 to #29 are located in volcanic domain while the other basins are located in the crystalline rocks. **Figure 5-7** indicates that the hypsometric curves of basins in the terrains dominated by volcanic rock are generally convex and S-shaped; whereas, the hypsometric curves of basins dominated by crystalline rocks are concave. However, outliers from these trends were observed for basins #5, #9, #13 and #25. To demonstrate such differences according to rock types, a whisker plot of *HI versus* lithology was provided (**Figure 5-8**). The average *HI* value for the basins with volcanic rocks is higher (0.36), compared to that with crystalline rocks (0.23). The Mann-Whitney U-test found that the difference is highly significant ($P < 0.01$).

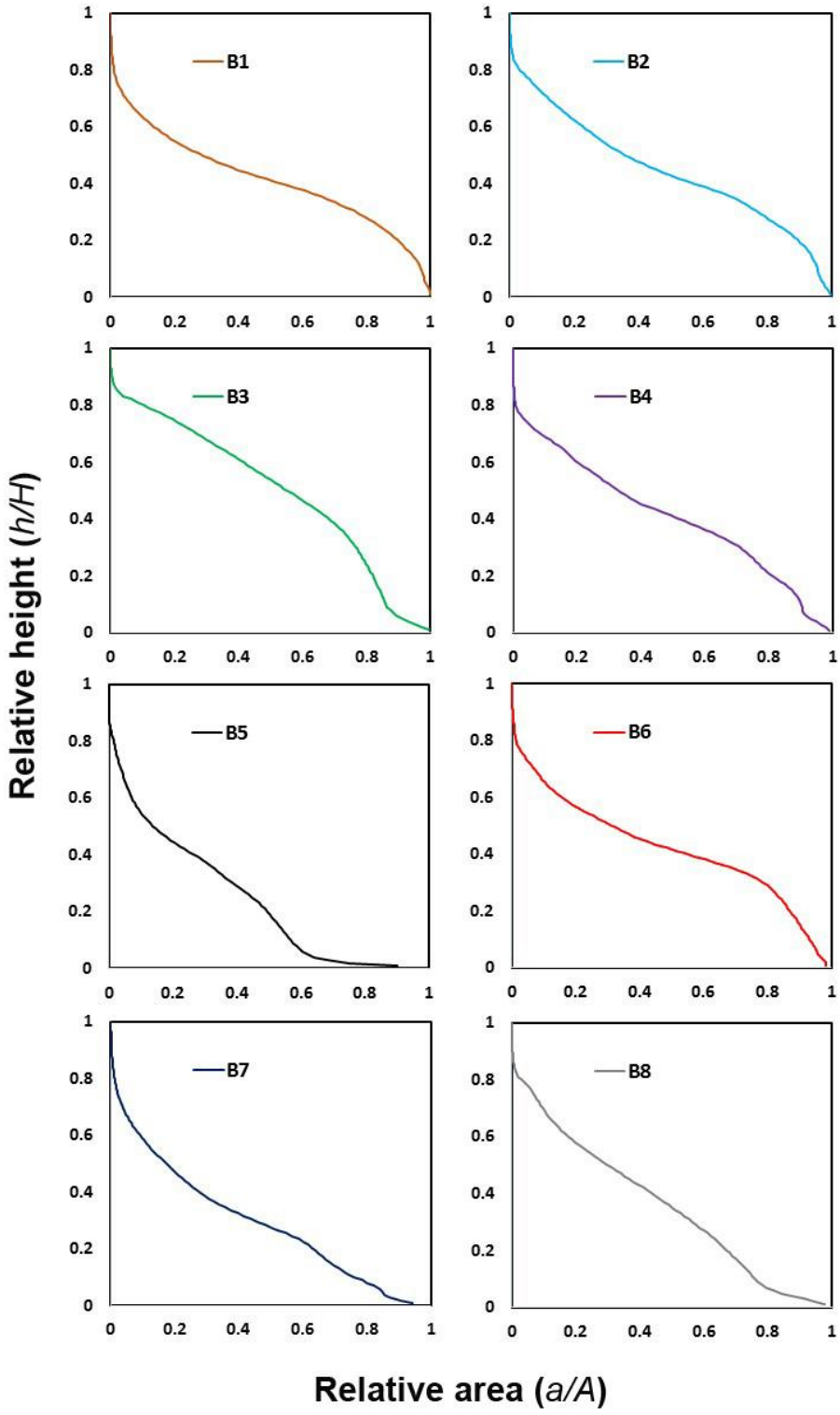

Figure 5-7 Hypsometric curves for the 36 basins

(basins #1 to #8).

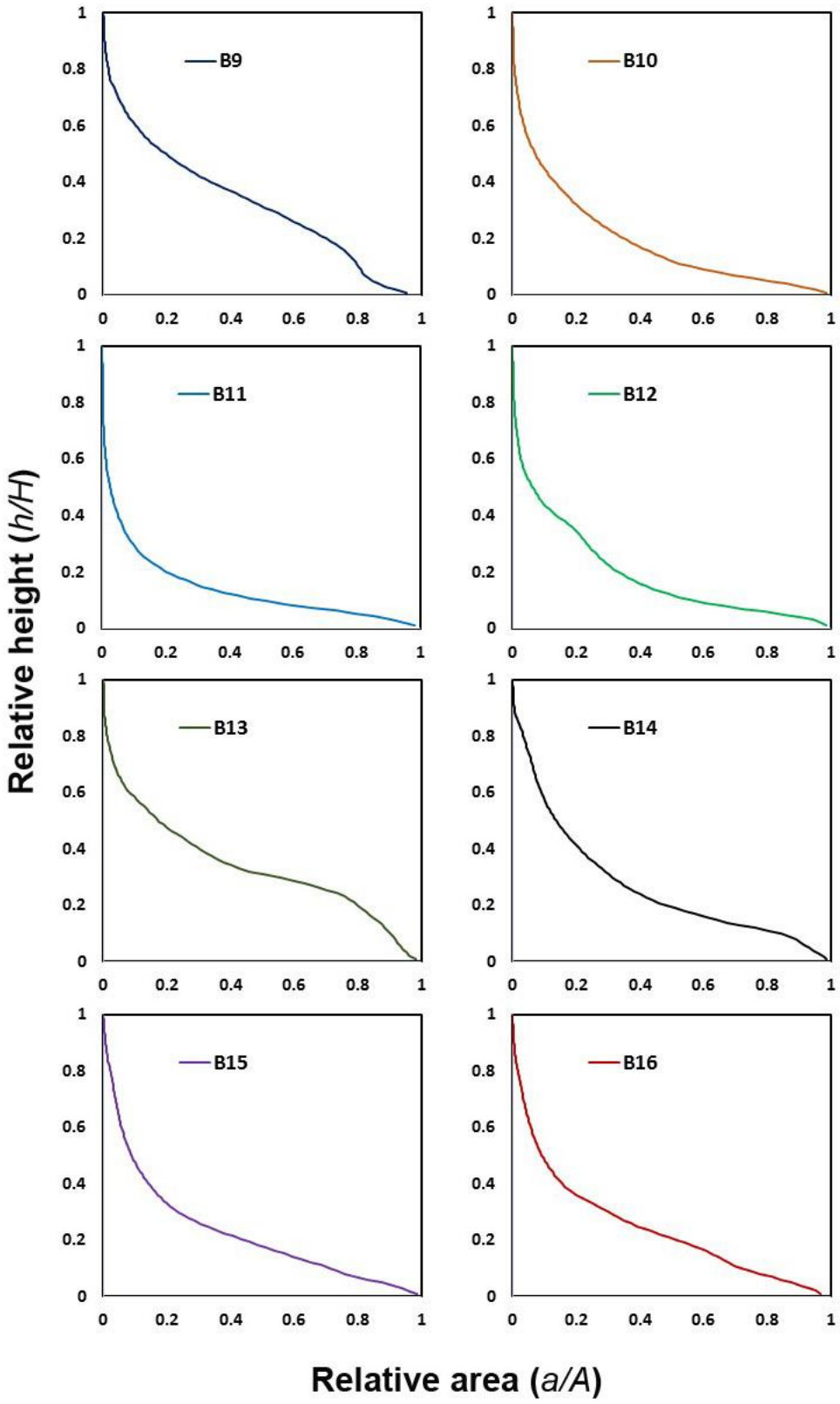

Error! Reference source not found.. Continued (basins #9 to #16).

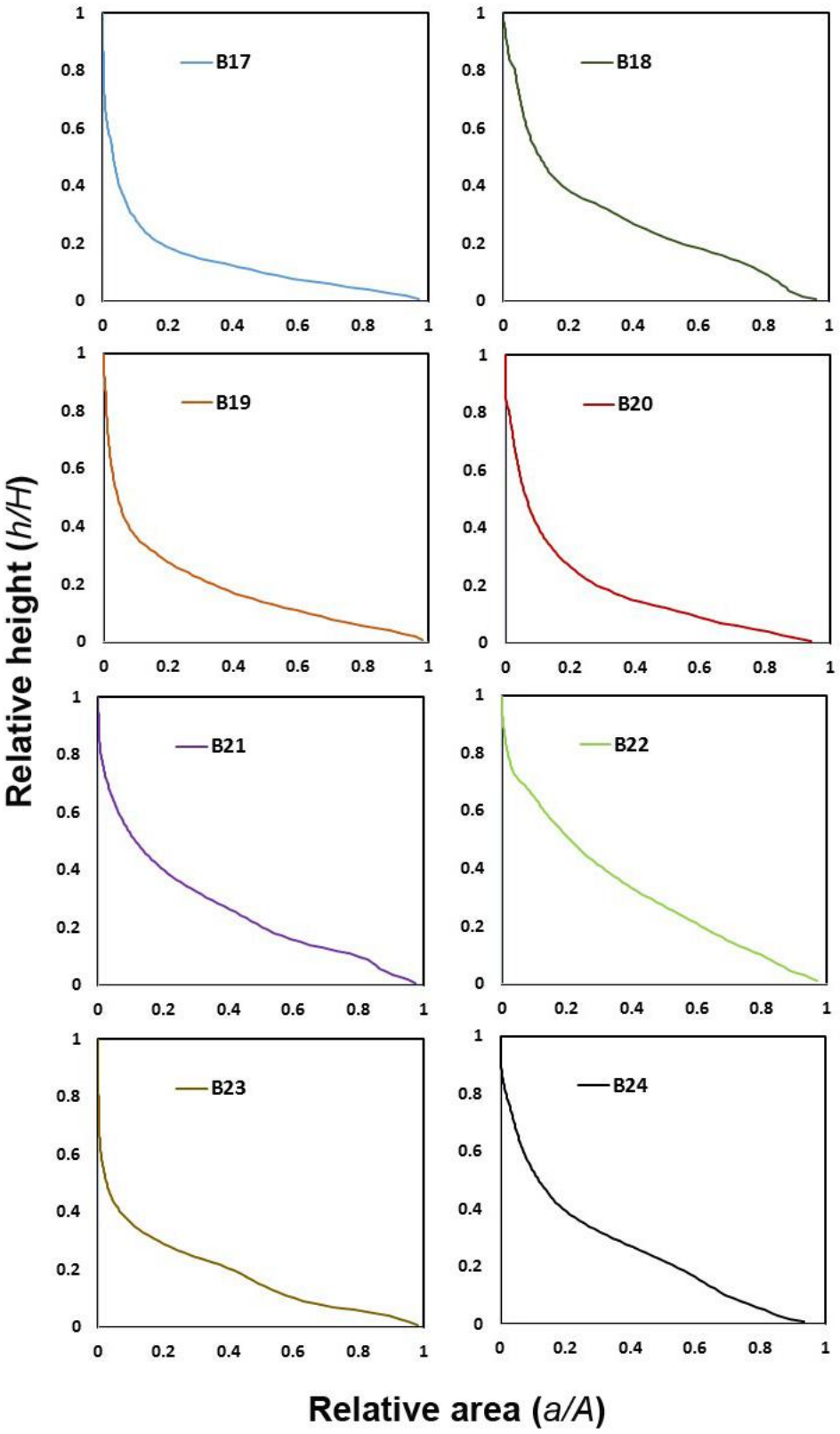

Error! Reference source not found. Continued (basins #17 to #24).

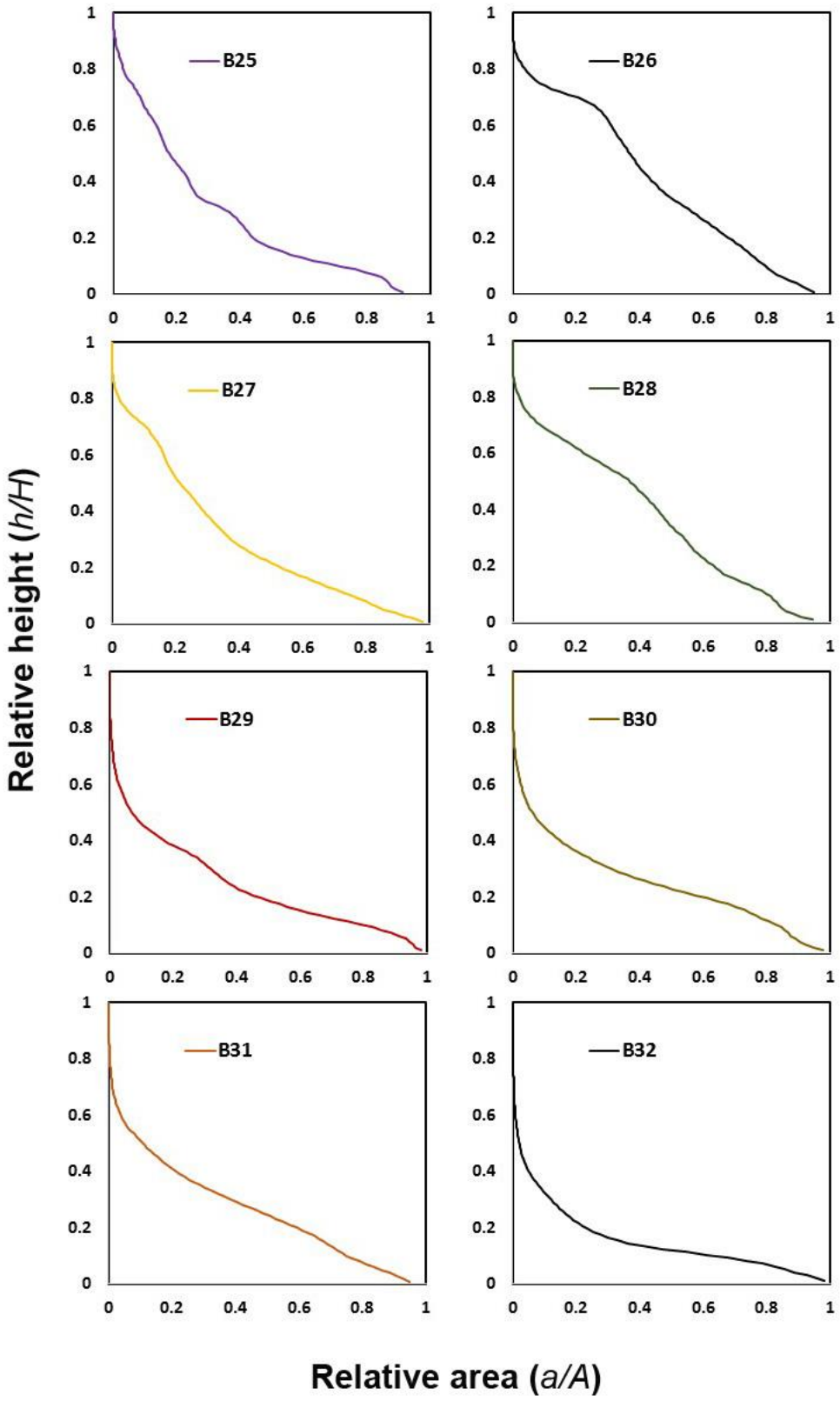

Figure 5-7. Continued (basins #25 to #32).

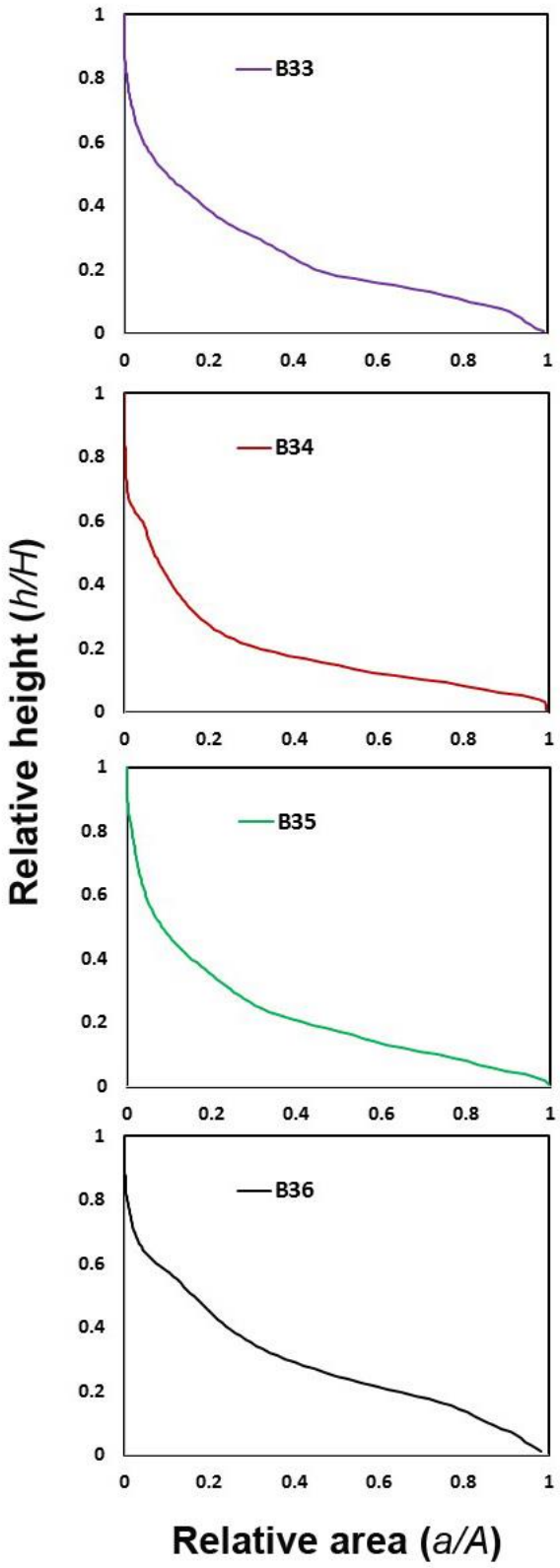

Figure 5-7. Continued (basins #33 to #36).

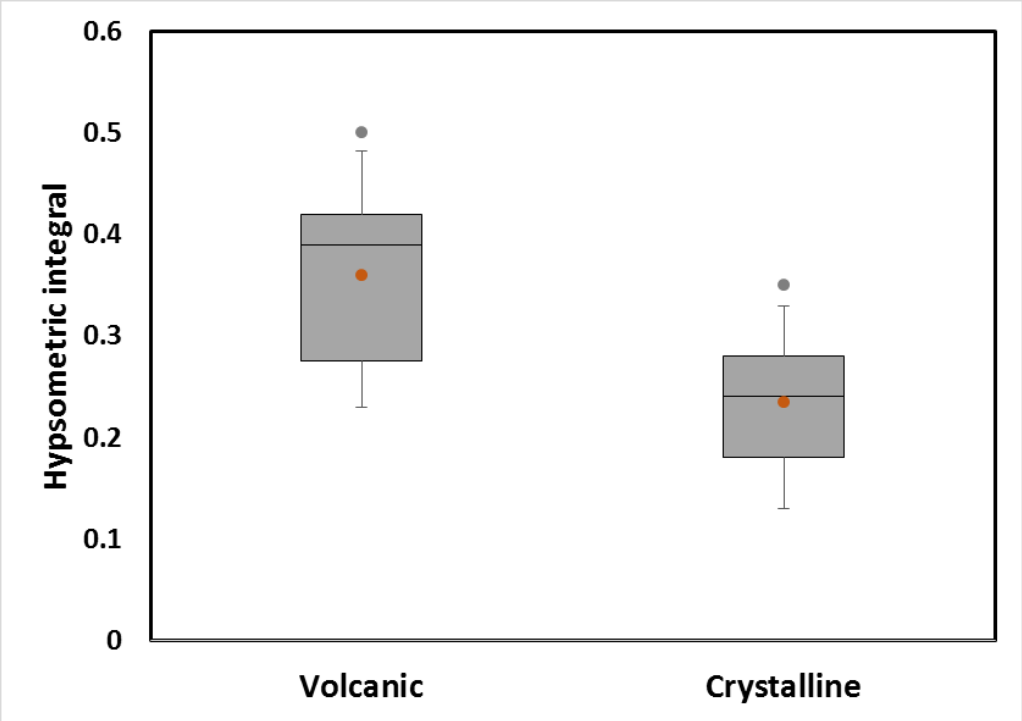

Figure 5-8 Hypsometric integral versus lithology. Line inside the box: median, upper hinge of the box: upper quartile, lower hinge of the box: lower quartile, ends of the vertical lines: maximum and minimum values except for outliers exceeding 1.5 times the inter-quartile range, grey dots: outliers, orange dots; mean. The differences shown in the graph is statistically significant ($P < 0.01$)

5.4 Alluvial Fans

Alluvial fans of several kilometer long were observed in the mouth of many studied drainage basins (**Figure 5-9**). Boundaries of 23 well developed alluvial fans shown by subtle changes in terrain gradient and vegetation were delineated based on the visual interpretation of satellite images as well as shaded relief map derived from the DEM using GIS. For each of the 23 fans, several morphometric variables commonly used in the literature were derived with the help of DEM and their relationships were examined (**Table 5-9**). The fan area ranges from a few tens to hundreds of square kilometer with an average value of about 300 km^2. The largest fans are mapped for basin #6 (1193 km^2) and basin #8 (980 km^2). The smallest fans are mapped for basin #12 and #13 with an area of 14 km^2 and 15 km^2 respectively. The fan length measured from apex to distal boundary ranges between 6 and 55 km.

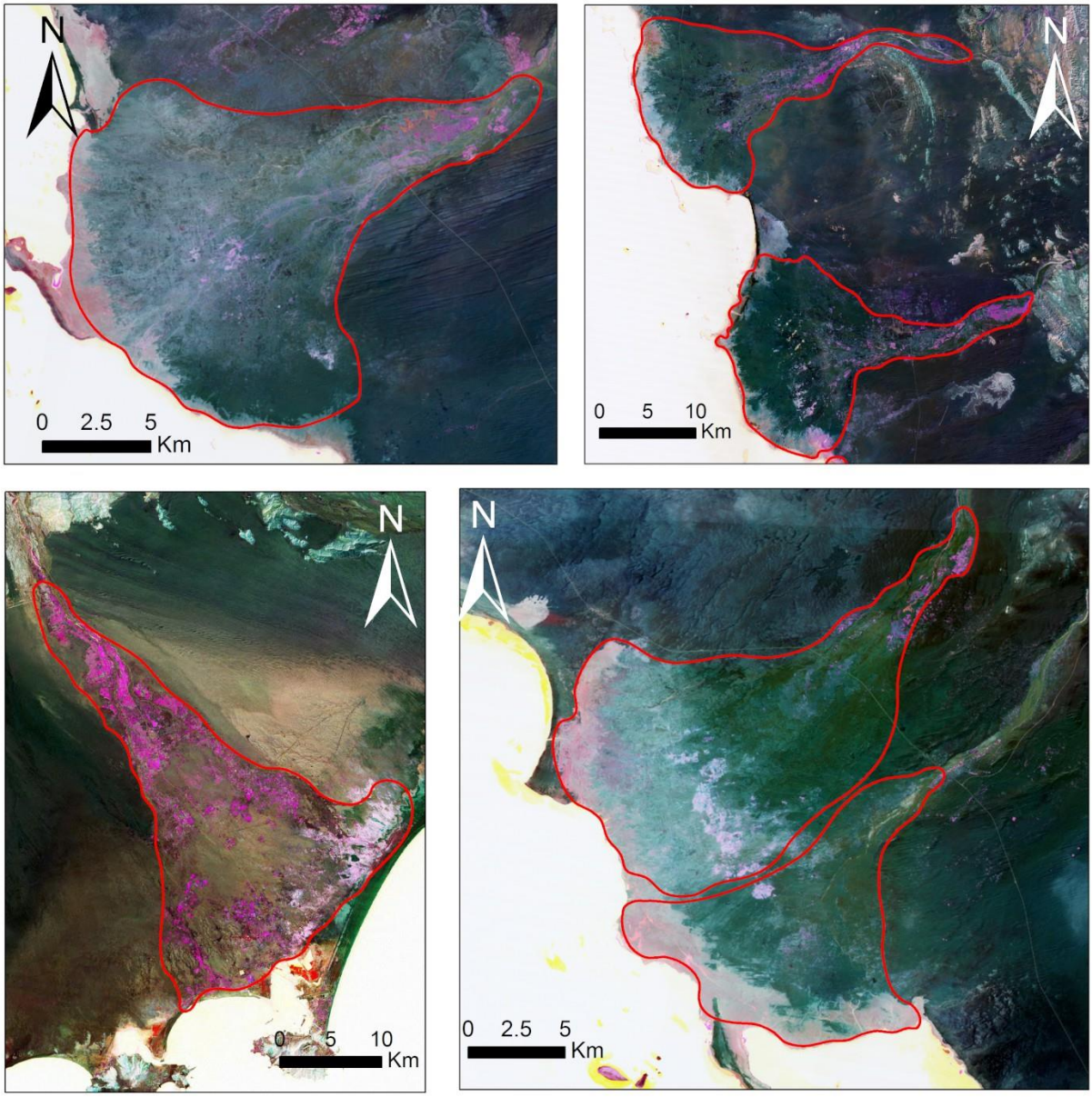

Figure 5-9 Examples of alluvial fans several kilometer long at the mouth of the large drainage basins in the Asir terrain.

The log-log power expression of fan area versus the contributing basin area shown in **Figure 5-10a**, and that of fan length versus contributing basin length shown in **Figure 5-10b** suggest a positive correlation. The arithmetic plot between mean fan slope and mean basin slope also shows a positive correlation (**Figure 5-10c).** However, no significant correlation is observed between mean fan slope and contributing basin area (**Figure 5-10d**), mean fan slope and fan area (**Figure 5-10e**), mean basin slope and contributing basin area (**Figure 5-10f**), between relief ratio of fan and relief ratio of contributing basins (**Figure 5-10g**), and relief ratio of fan and contributing basin area (**Figure 5-10h**).

Table 5-9 Morphometric parameter of alluvial fans in the study area

Id	Basin area (km^2)	Fan area (km^2)	Basin length (km)	Fan length (km)	mean basin slope (tan)	mean fan slope (tan)	Relief ratio of basin	Relief ratio of fan
1	5790	537	129	46	0.273	0.098	0.0244	0.0064
2	4713	481	150	44	0.317	0.071	0.0215	0.0067
3	2896	111	139	38	0.352	0.081	0.0213	0.0053
4	4086	335	147	42	0.310	0.091	0.0249	0.0060
5	8292	1193	220	55	0.288	0.056	0.0153	0.0035
6	2748	213	125	43	0.287	0.064	0.023	0.0029
7	7078	980	130	49	0.309	0.07	0.023	0.0027
8	1898	70	82	14	0.335	0.033	0.0364	0.0034
9	1615	168	65	23	0.221	0.089	0.0311	0.0052
10	976	14	51	6	0.192	0.061	0.0274	0.013
11	522	15	46	6	0.159	0.041	0.0197	0.0048
12	5365	389	136	39	0.236	0.04	0.022	0.0027
13	3235	290	101	33	0.241	0.059	0.0269	0.0030
14	2610	267	111	35	0.230	0.083	0.0216	0.0032
15	1374	173	84	30	0.309	0.073	0.0297	0.0042
16	1577	200	78	23	0.245	0.074	0.0319	0.004
17	1579	110	85	18	0.252	0.055	0.0299	0.0030
18	1849	186	95	25	0.289	0.065	0.0249	0.0043
19	3245	297	109	30	0.270	0.082	0.0244	0.0043
20	1933	442	101	35	0.293	0.073	0.0258	0.0034
21	2026	355	127	31	0.120	0.053	0.0102	0.0040
22	5052	88	150	15	0.143	0.033	0.0118	0.0022
23	4825	125	130	27	0.223	0.059	0.0164	0.0033

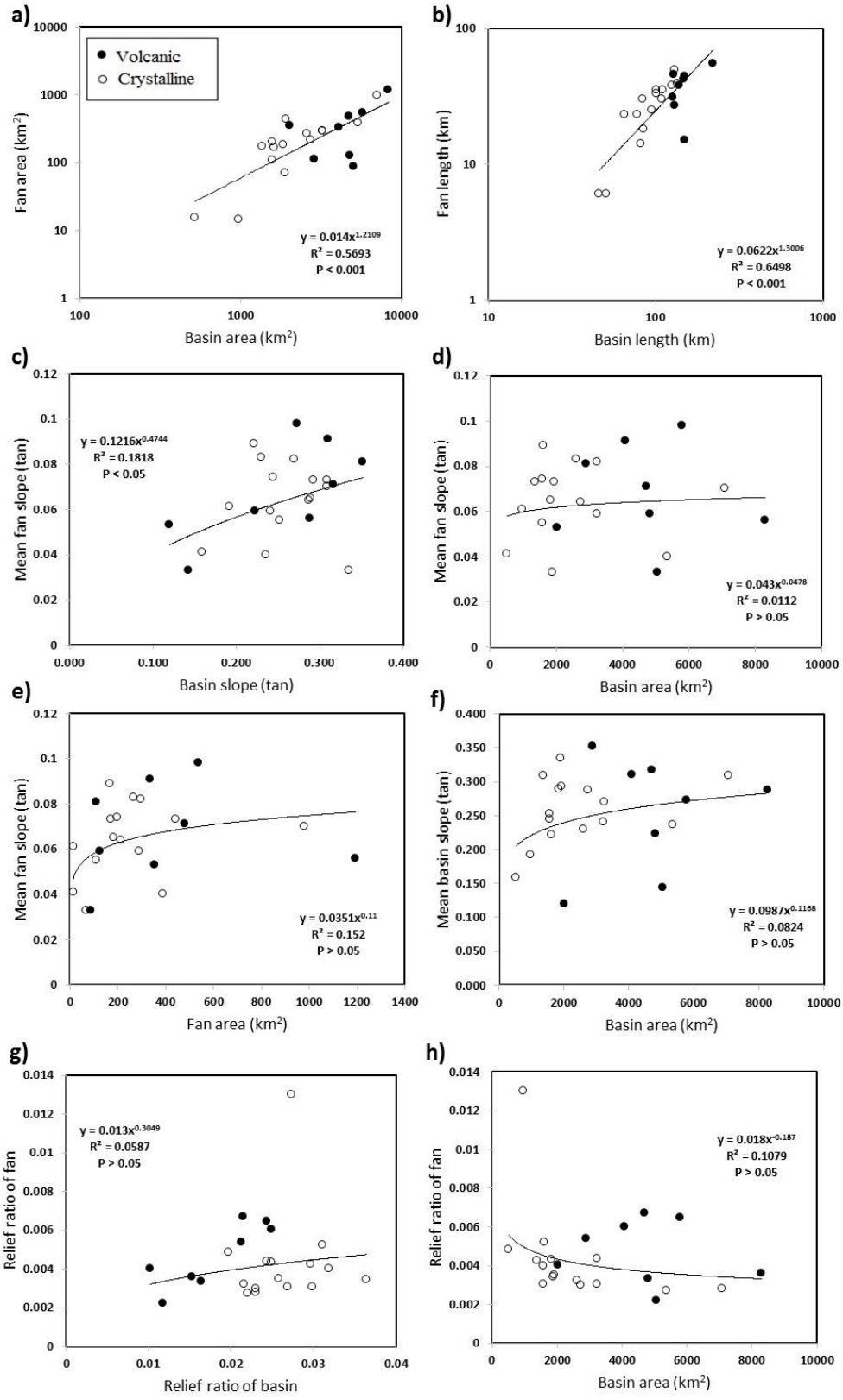

Figure 5-10 Morphometric relationship between alluvial fans and contributing basin area. a) log-log fan area–basin area relation, b) log-log fan length–basin length relation, c) fan slope–basin slope, d) fan slope–basin area, e) fan slope–fan area, f) basin slope–basin area, g) relief ratio of fan–relief ratio of basin, h) relief ratio of fan–basin area.

.

5.5 Steepness and concavity of river longitudinal profiles

Table 5-10 summarizes the steepness index and concavity values for the main channels of each 36 drainage basins. The results displayed in **Figure 5-11** show pronounced variations in the steepness and concavity depending on the location of the channel. The steepness index (K_{sn}) ranges from 24 to 199 with a mean and a standard deviation of 81 and 47 respectively. Concavity values (θ) vary from 0.21 to 1.6 with a mean of 0.59 and a standard deviation of 0.27. The anomalously high values of K_{sn} and θ appear in highly disturbed channels like #7 shown in **Figure 5-11**.

The profile steepness and concavity can be interpreted in terms of lithology if no correlation is observed with tectonic elements. Since the western margin of the Arabian plate is believed to be passive and no significant active tectonism is reported, this study attempted to relate the steepness and concavity indices with lithological variations. As noted in Section 5.1, basins #1 to #6 and #25 to #29 are located in the terrain dominant with volcanic lithology while the other basins are located in the Precambrian crystalline lithologies. The results show that the mean values of the steepness index for the channels underlined by volcanic rocks are larger than those in the crystalline domains; whereas the concavity index is larger for the channels dominated by crystalline lithologies than those by the volcanic domains. **Figure 5-12a** shows the whisker plots of K_{sn} values for the channels with the two major lithologic types. The mean value of K_{sn} for the channels with volcanics is 108 and that for the crystalline lithology is 70. The Mann-Whitney U-test has found that the difference is statistically significant ($P < 0.05$). **Figure 5-12b** shows the whisker plots of θ values for the channels with the volcanic and crystalline lithologies. The mean value of θ for the channels for the volcanics is 0.43 and that for the crystalline lithology is 0.66. The difference is statistically significant ($P < 0.05$).

Table 5-10 Summary of steepness and concavity index for the 36 major streams in the study area

River no	Steepness index	Concavity index	River no	Steepness index	Concavity index
1	125	0.21	19	99.8	0.79
2	128	0.32	20	40.8	0.90
3	146	0.28	21	67.2	0.6
4	147	0.48	22	43.3	0.7
5	192	0.62	23	101	0.35
6	164	0.35	24	126	0.84
7	199	1.6	25	52.7	0.35
8	98.2	0.46	26	78.5	0.71
9	94.6	0.46	27	68.2	0.79
10	68.4	0.65	28	48.1	0.26
11	27.1	0.65	29	35.1	0.45
12	42.8	0.78	30	58	0.54
13	29	0.42	31	42.8	0.47
14	144	1.3	32	54.8	0.63
15	43.8	0.4	33	41.6	0.46
16	62.9	0.55	34	61	0.51
17	24.5	0.59	35	53.9	0.51
18	54.6	0.85	36	60	0.70

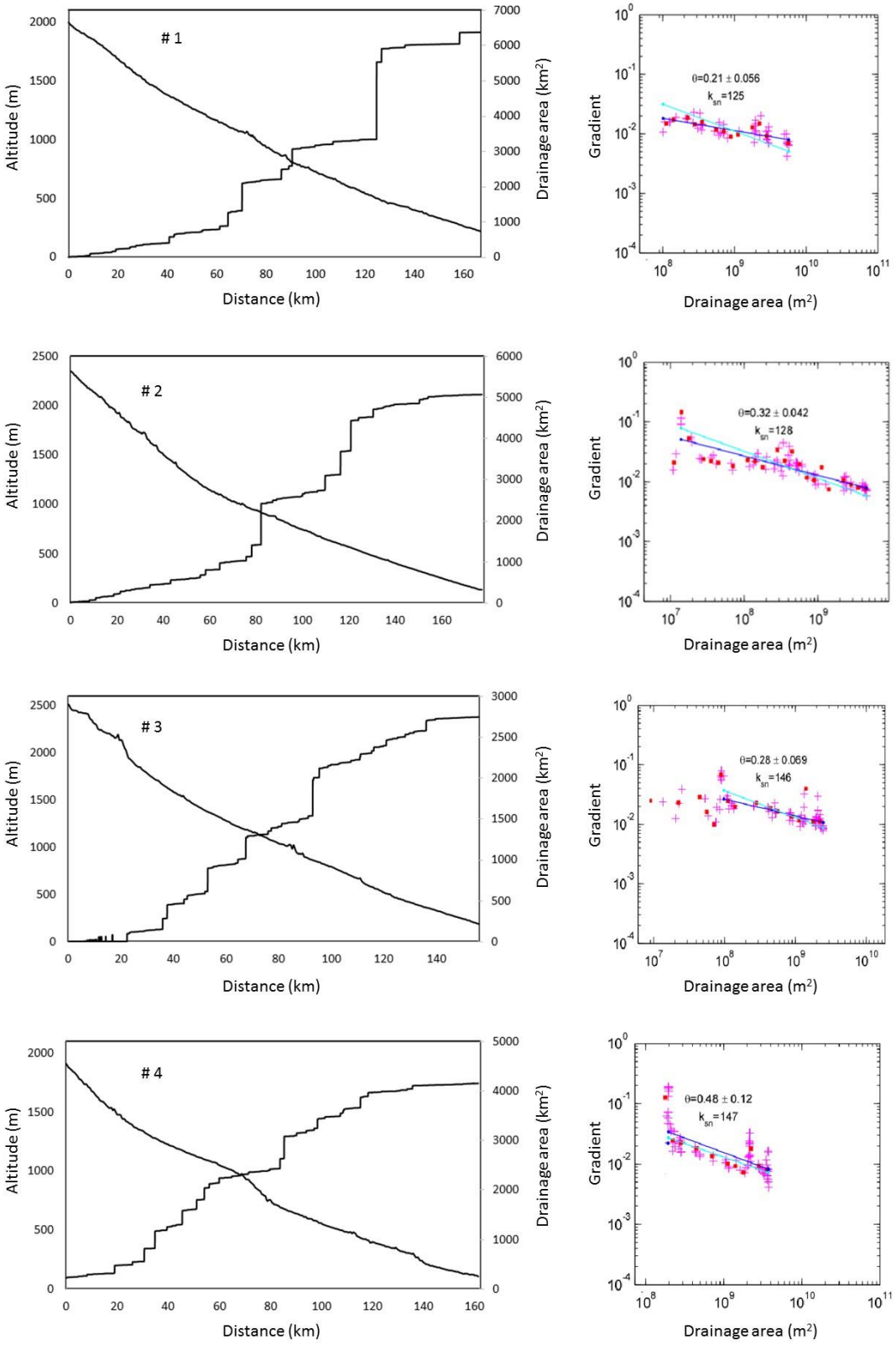

Figure 5-11 Channel longitudinal profile, drainage area, and the steepness and concavity indices for each major drainage basin. (basins #1 to #4)

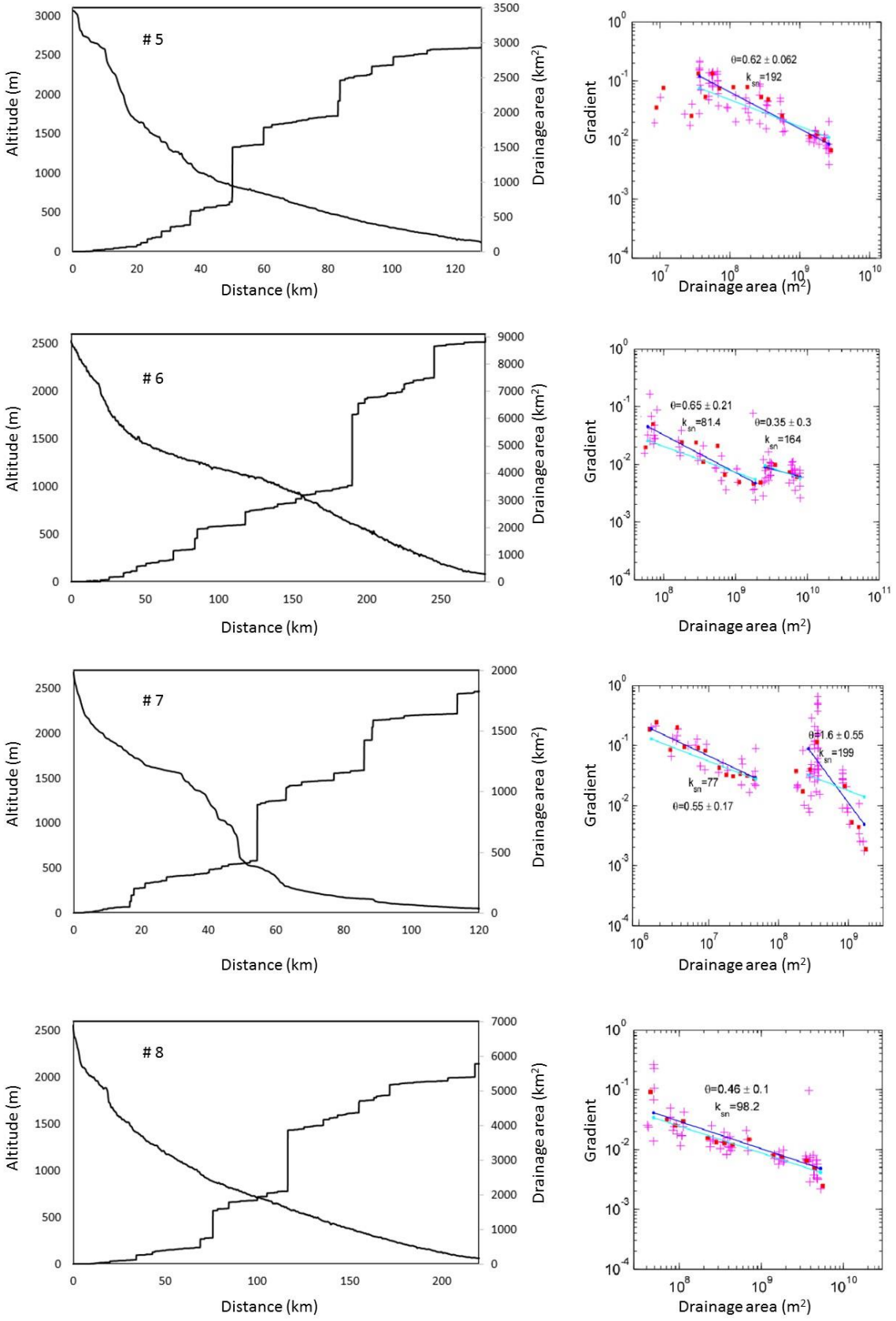

Figure 5-11. Continued (basin 5 to 8)

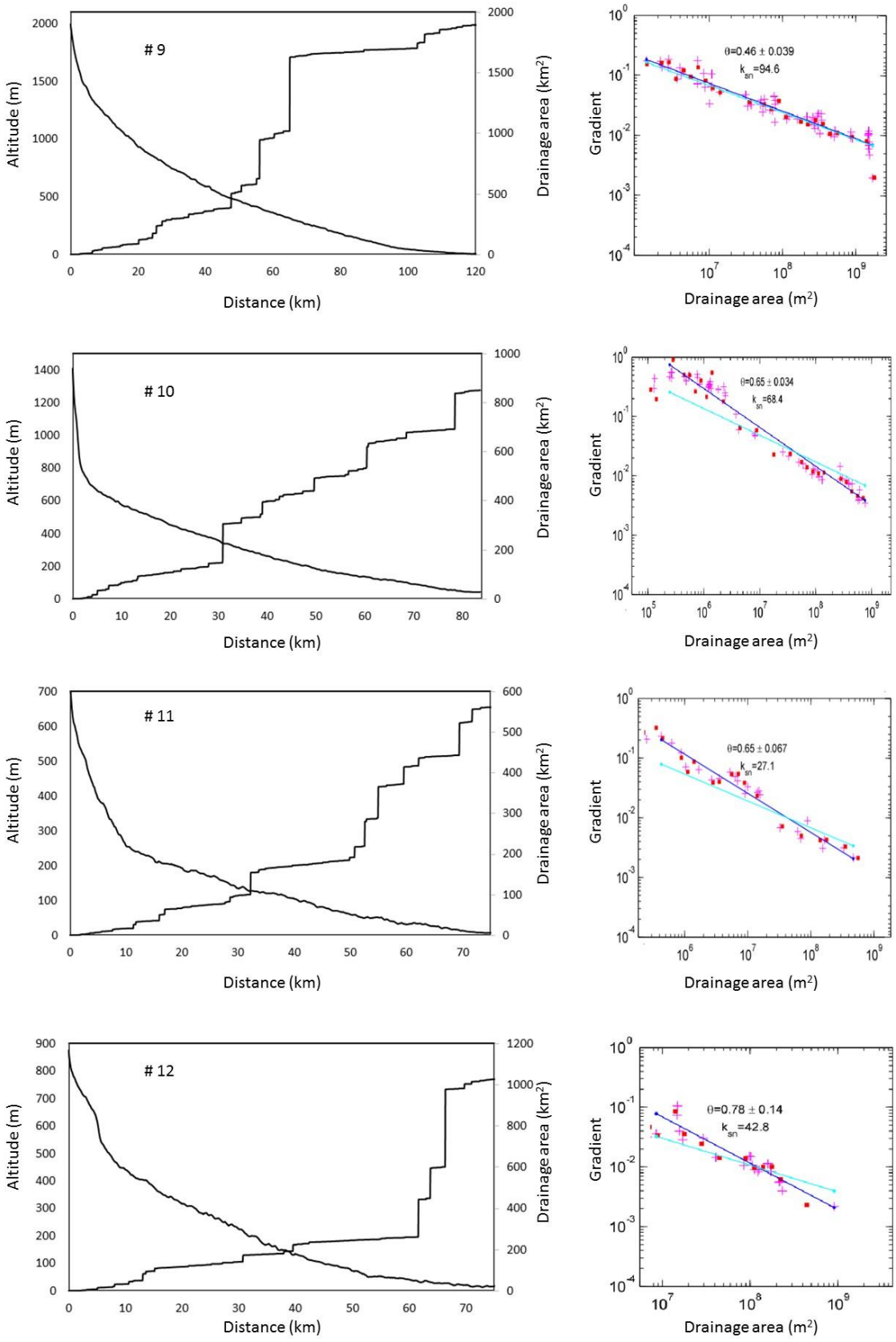

Figure 5-11. Continued (basin 9 to 12)

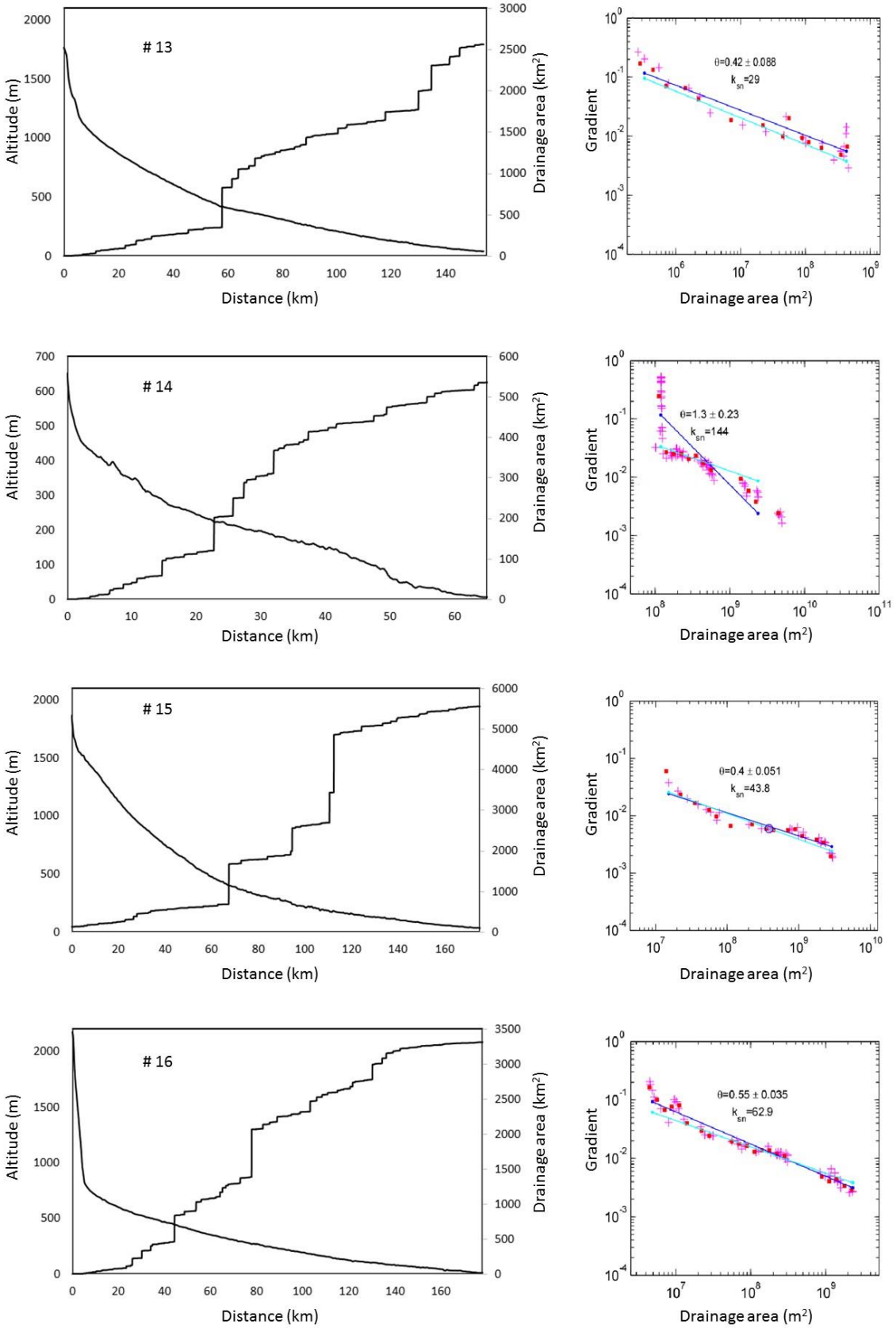

Figure 5-11. Continued (basins #13 to #16)

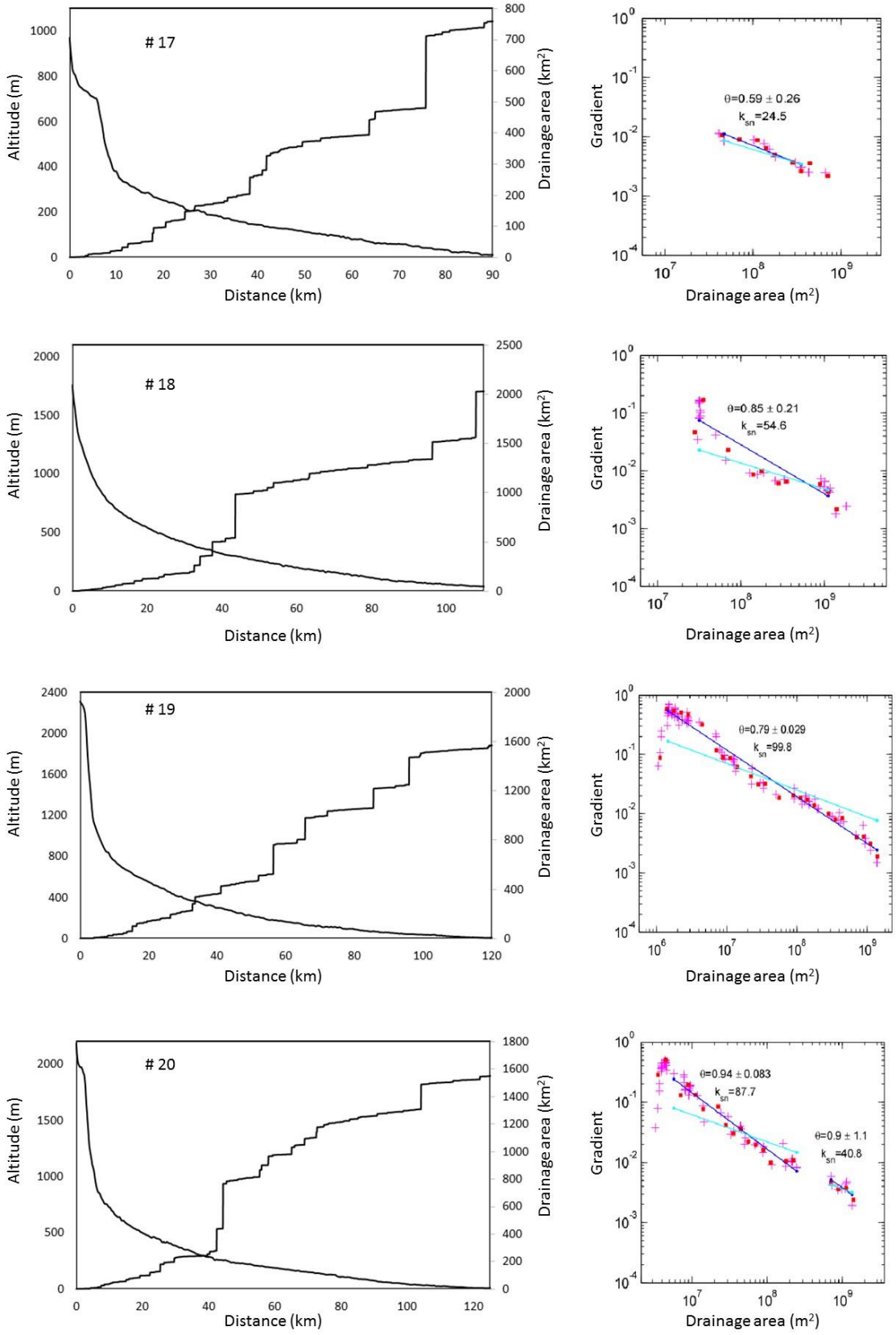

Figure 5-11. Continued (basins #17 to #20)

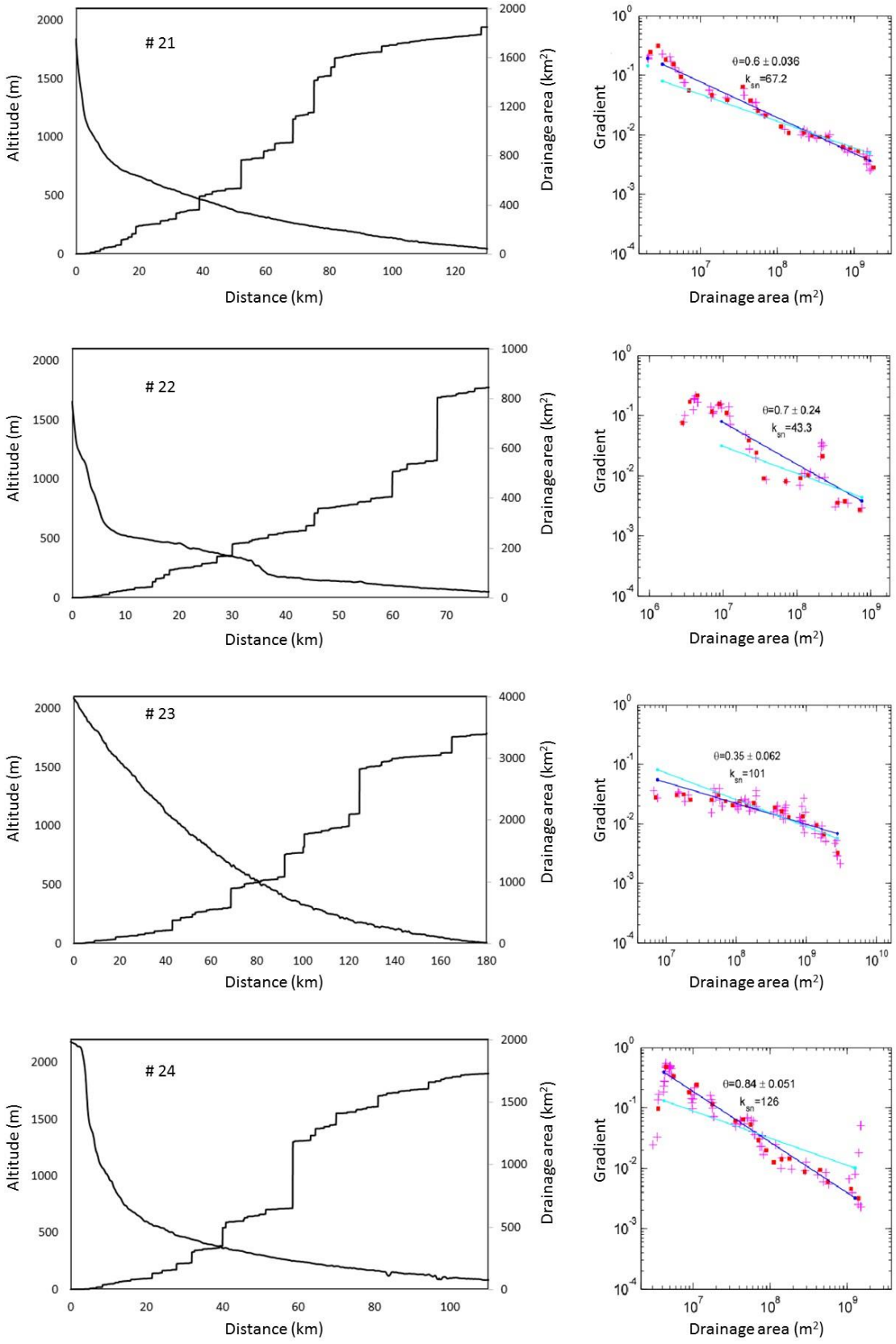

Figure 5-11. Continued (basins #21 to #24)

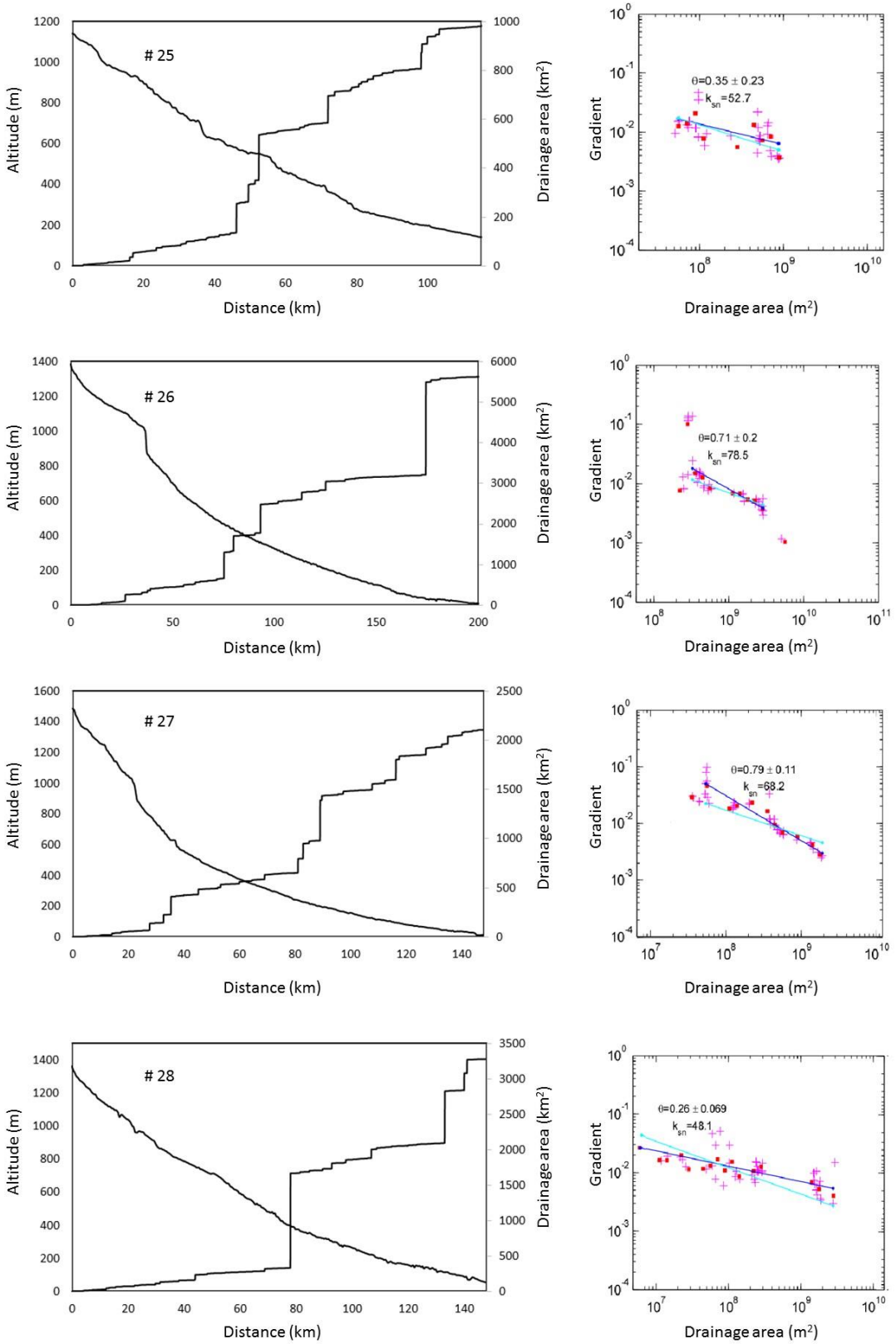

Figure 5-11. Continued (basins #25 to #28)

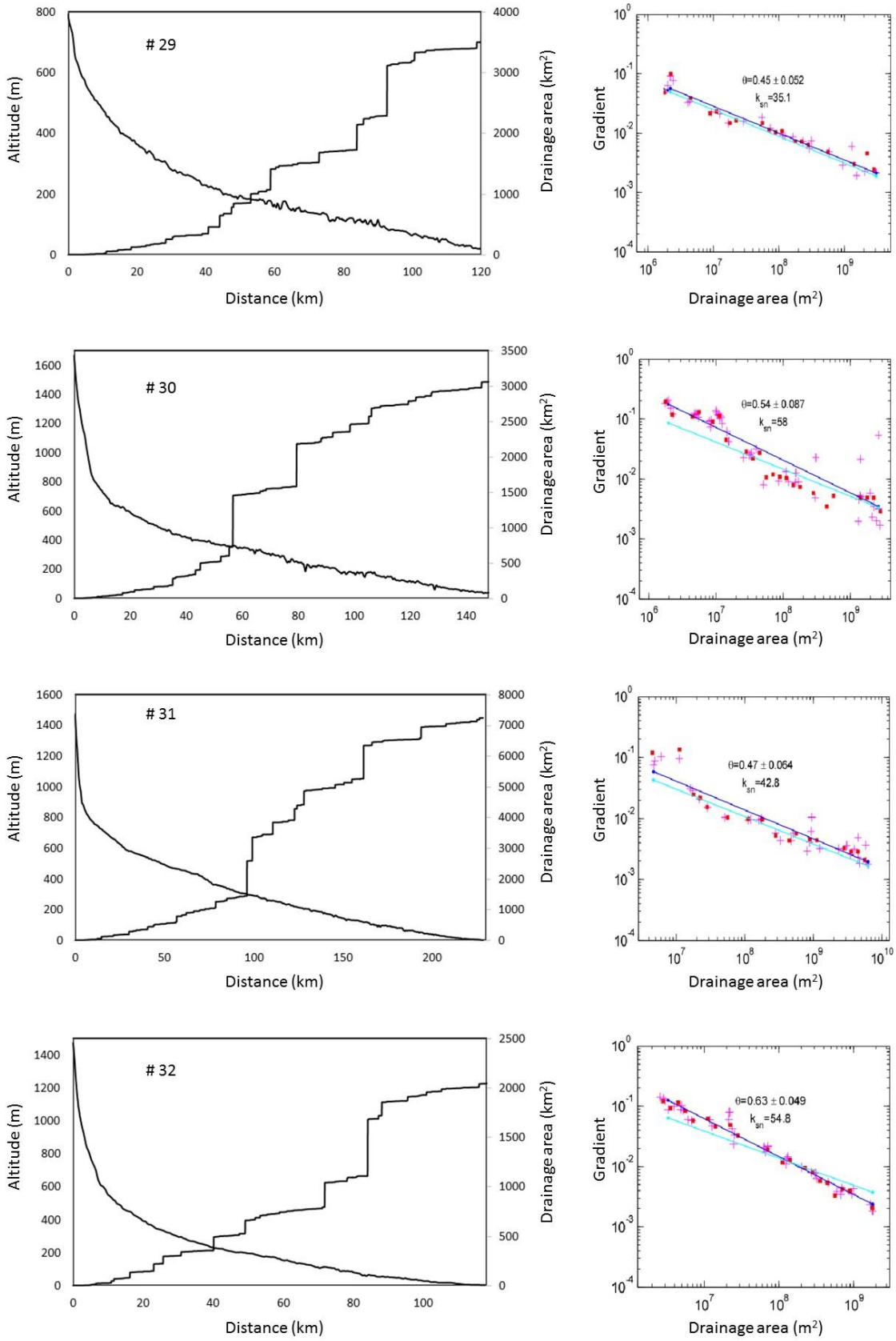

Figure 5-11. Continued (basins #29 to #32)

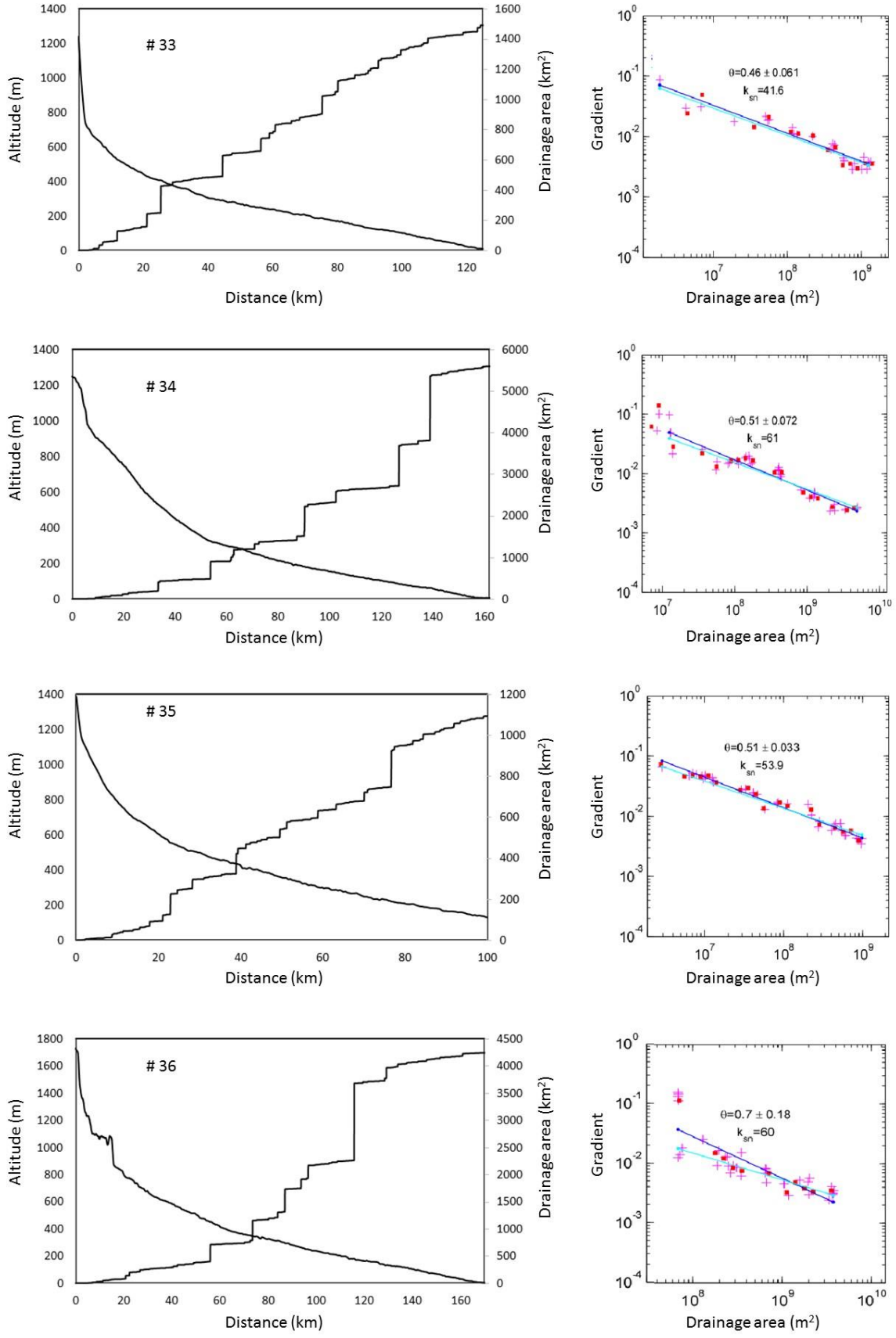

Figure 5-11. Continued (basins #33 to #36)

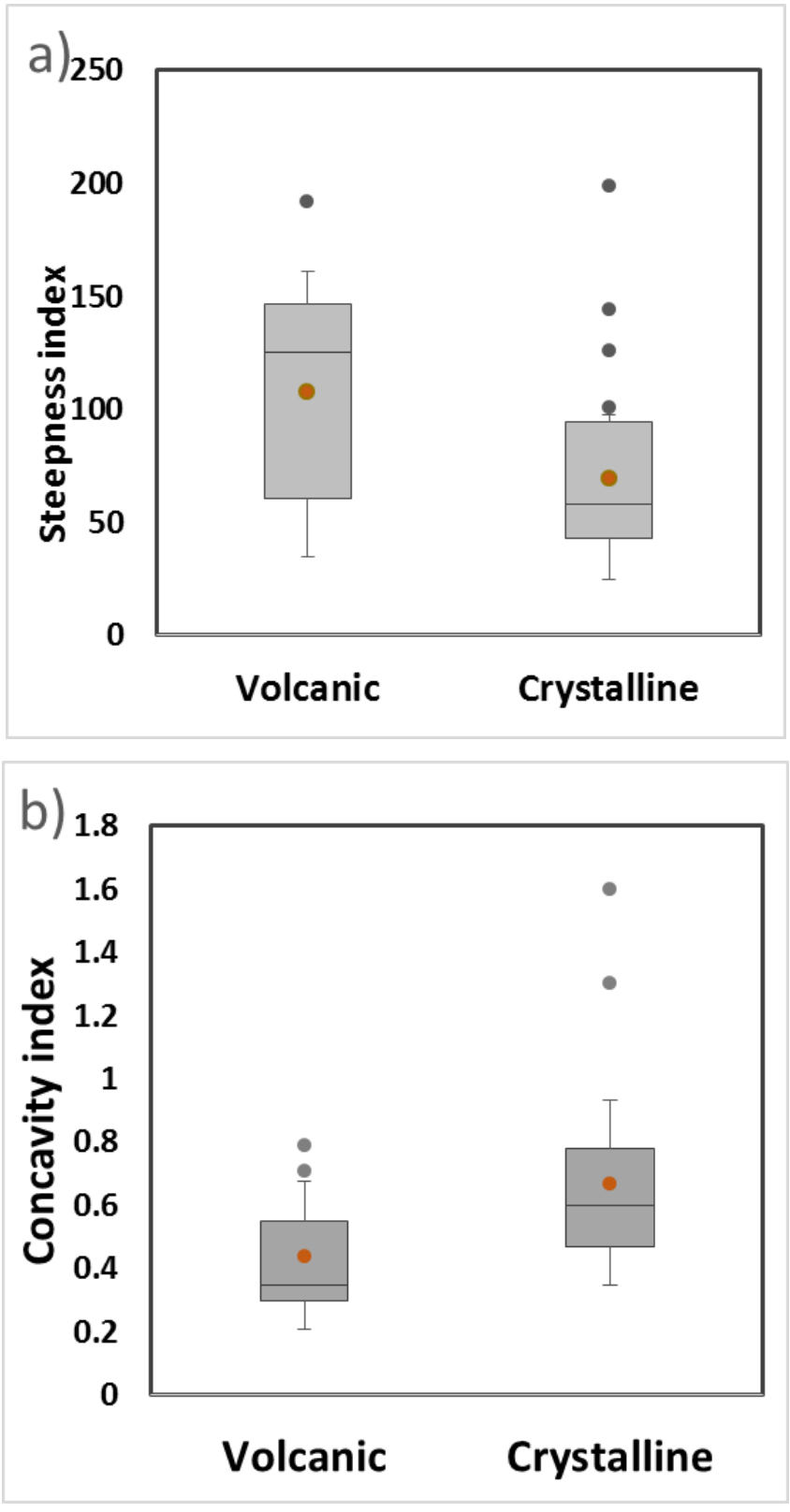

Figure 5-12 Comparison of a) the steepness index and b) the concavity index for channels located in two different lithologic types in the study area. The difference shown in the graph is statistically significant ($P < 0.05$). Line inside the box: median, upper hinge of the box: upper quartile, lower hinge of the box: lower quartile, ends of the vertical lines: maximum and minimum values except for outliers exceeding 1.5 times the inter-quartile range, grey dots: outliers, orange dots; mean.

5.6 Knickzone analysis

The analysis of streams with a total length of 5121 km in the Western Arabian Peninsula identified 325 knickzones. The total length of the identified knickzones is 83.76 km. Knickzone frequency, the number of knickzones per stream length, is 0.063 km^{-1}, and knickzone density, the percentage of knickzones reach length to total given stream length, is 1.63%. **Table 5-11** shows the summary of general statistical values of knickzones identified. The mean height is 36.36 m, the mean length is 257.72 m, the mean gradient is 0.14 m m^{-1}, and the mean relative steepness value is 6.44×10^{-5} m^{-1}. An example map showing the distribution of knickzones in Western Arabian Peninsula (Basin #7) is shown in **Figure 5-13**.

Table 5-11 General Knickzone statistics

	Height (m)	Length (m)	Gradient (m m^{-1})	R_d (m^{-1})
Mean	36.36	257.72	0.143	6.44E-05
Standard deviation	27.65	82.57	0.075	4.45E-05
Maximum	257	600	0.611	0.000411
Minimum	20	120	0.047	2.67E-05

Of the 325 knickzones identified, four are taller than 150 m. These four knickzones were confirmed from the high resolution satellite images of Google Earth and Bing Maps (**Figure 5-14**).

Scatter plots of knickzones between locational factors and form factors were provided to evaluate the systematic relationship between them (**Figure 5-15**). The comparisons between the measured knickzone factors showed no statistically significant correlations except for that between drainage area and distance from river head (**Figure 5-15a–j**). Distinct knickzones taller than 100 m in height, larger than 400 m length and gradient higher than 0.3 mm^{-1} are observed in the middle altitudes between 800 and 2000 m (**Figure 5-15a-c**). The correlation between distance from river head and form factors demonstrates that knickzones are located all along the longitudinal profiles of the streams (**Figure 5-15d-f**). However, very tall, large and steep knickzones are usually observed close to the river head except the few in the middle reaches as noted above. **Figure 5-15g-i** shows that steep gradients are observed in even large drainage areas. The correlation between knickzone's drainage area and distance from the divide shown in the **Figure 5-15j** is a consequence of Hack's (1957) relation which states that the distance from the divide is a power law function of drainage area.

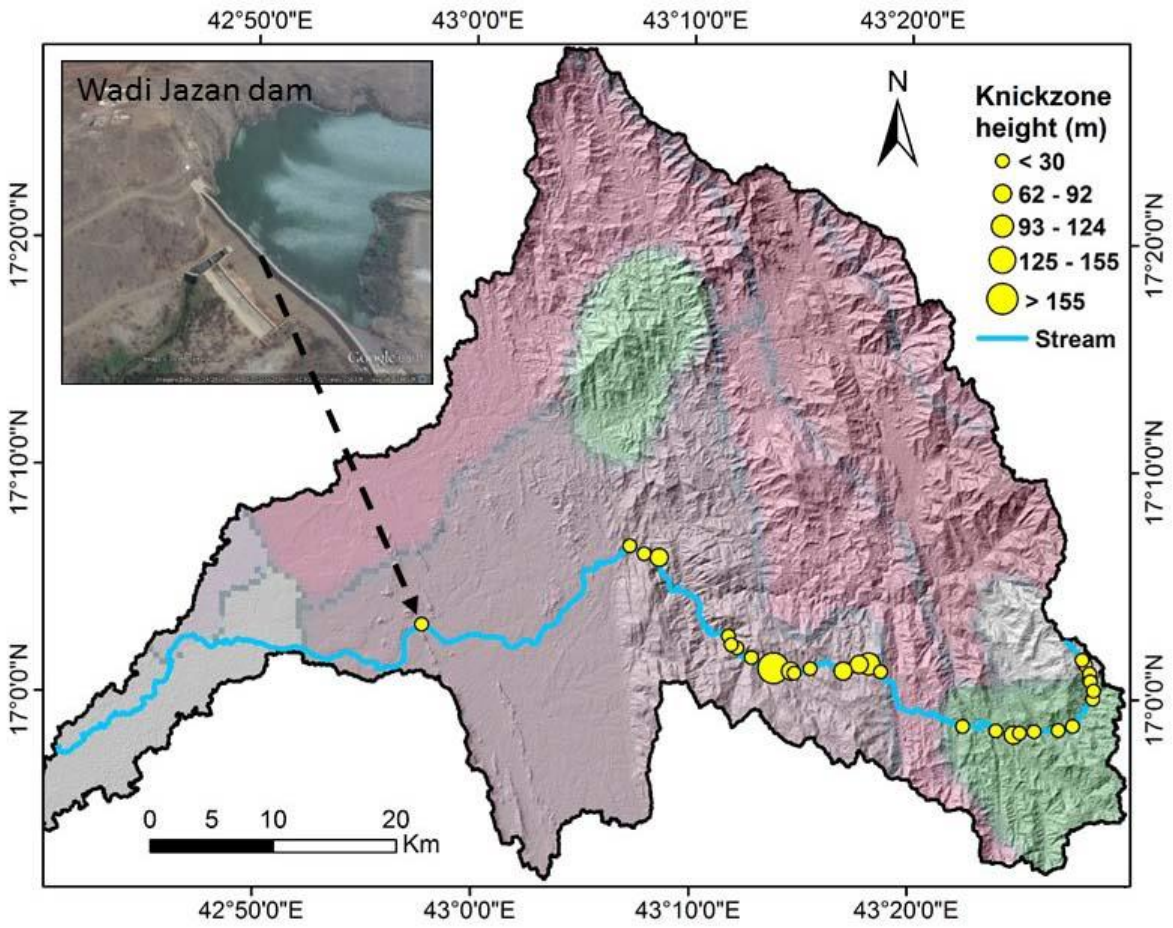

Figure 5-13. Map showing knickzone distribution in the main channel of Basin #7 (Western Arabian Peninsula).

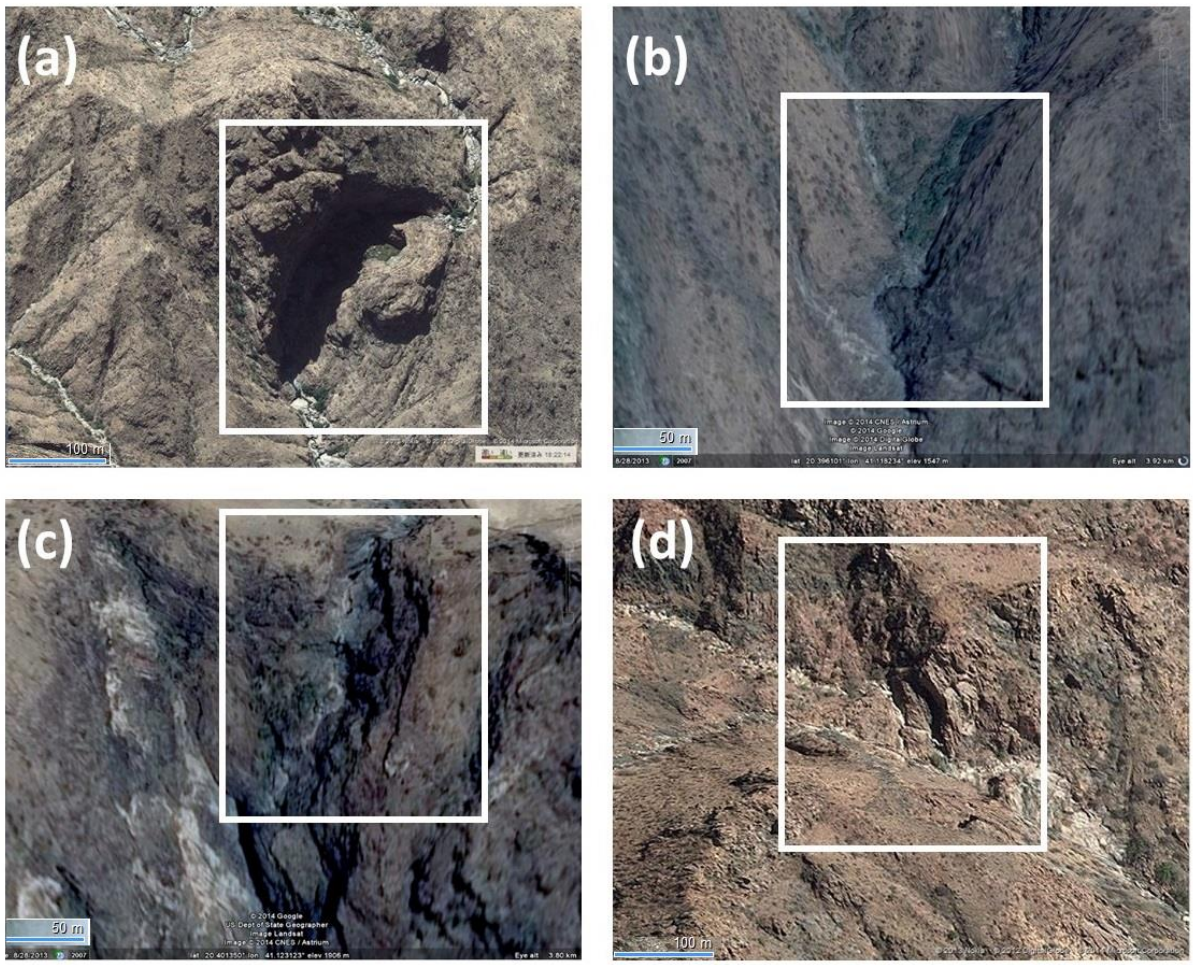

Figure 5-14 Identified knickzones observed from Google Earth and Bing Maps a) stream #7 (181 m height), b) and c) stream #20 (227 and 189 m height respectively), and d) stream #24 (257 m height)

To demonstrate the abundance of knickzone in each classes of locational parameter, knickzones frequency for altitude, distance from river head, drainage area, and trend gradient were examined (**Figure 5-16, column graphs**). Also examined are knickzone abundance for different classes of height to represent the form factor. The height classes were determined using the knickzone percentiles of 25th, 50th, 75th, and 90th. (**Figure 5-16, line graphs**). **Figure 5-16a** shows that the knickzones are more abundant between elevation 1400 and 2400 m. The three peaks of shorter knickzone occurrences and the three peaks of taller knickzone occurrences are shown in **Figure 5-16a**. The first peak at 800–1200 m is common to short and tall knickzones. The second and third peaks for shorter knickzones are at 1400–1600 m and 2000–2400 m respectively. Extremely tall knickzones (> 83 m) are frequent in 1800–2000 m and 2400–2600 m altitude ranges, but above 2600 m, no large knickzones exist. Shorter and taller knickzones are abundant at less than 20 km from river head, but three more peaks of shorter knickzone abundance occur in the middle and lower reaches (**Figure 5-16b**). Although smaller drainage areas (<

500 km^2) correspond to major abundance of both the shorter and taller knickzones, the larger drainage areas (1500–4000 km^2) also contain a large chunk of short knickzones occurrences (**Figure 5-16c**). As expected, large gradient rivers tend to have taller knickzones (**Figure 5-16d**).

Similar to the height factor, this study also examined the length of the knickzones by different percentiles (25th, 50th, 75th, and 100th) and in relation to the various location factors mentioned above (**Figure 5-17**). The graph shows that the relationship between the abundance of longer knickzones (>300 m) and altitude is not very clear. However, small-length knickzones (<240 m) are much more abundant in the higher altitudes (**Figure 5-17a**). Both long and small-length knickzone are more abundant in the reaches closer to the river head. A peak for small-length knickzones is also observed in the lower reaches (**Figure 5-17b**). As expected, small-length knickzones are frequent in reaches far away from the divide. However, no clear correlation is observed in between the drainage area and knickzone length except that longer knickzones are absent in drainage areas larger than 4000 km^2 (**Figure 5-17c**). Similar to the taller knickzone classes, the longer knickzones are dominant at higher gradients (**Figure 5-17d**).

To determine whether any particular lithologies favored the occurrence of knickpoints, this study examined the relationship between knickpoint frequency and the two dominant lithologic types: volcanic and crystalline. The knickzone frequencies for volcanic and crystalline rocks are 0.088 and 0.049 respectively (**Table 5-12**). Knickzone density is also higher in volcanic rocks (2.19%) than in the crystalline rocks (1.32%). The abundance of and properties of knickzones according to the lithologic types are shown in **Figure 5-18**. The figure shows that the abundance of knickzones for the two lithologies is almost similar for most of the altitude classes except that for 1000 to 1400 m, which is favorable for crystalline rocks and altitude above 2000 m, favorable for volcanics (**Figure 5-18a**). In relation to upstream distance, the favored location for knickzones with crystalline lithology is near the river head and their presence in the lower reaches is limited. In contrast, not much preference was found for volcanics, though the knickzones are still more abundant close to the river heads (**Figure 5-18**b). For 500–3500 km^2 in the upstream area, knickzone frequency for the crystalline rocks increases with the area; other than this, no clear trend is observed in relation to drainage area and lithology (**Figure 5-18c**). The trend gradient and the mean gradient for different rock types show that steeper gradients (> 0.4 mm^{-1}) are observed for crystalline rocks (**Figure 5-18d,f**). Similarly, taller knickzones are also associated with crystalline rocks and are located near the stream heads.

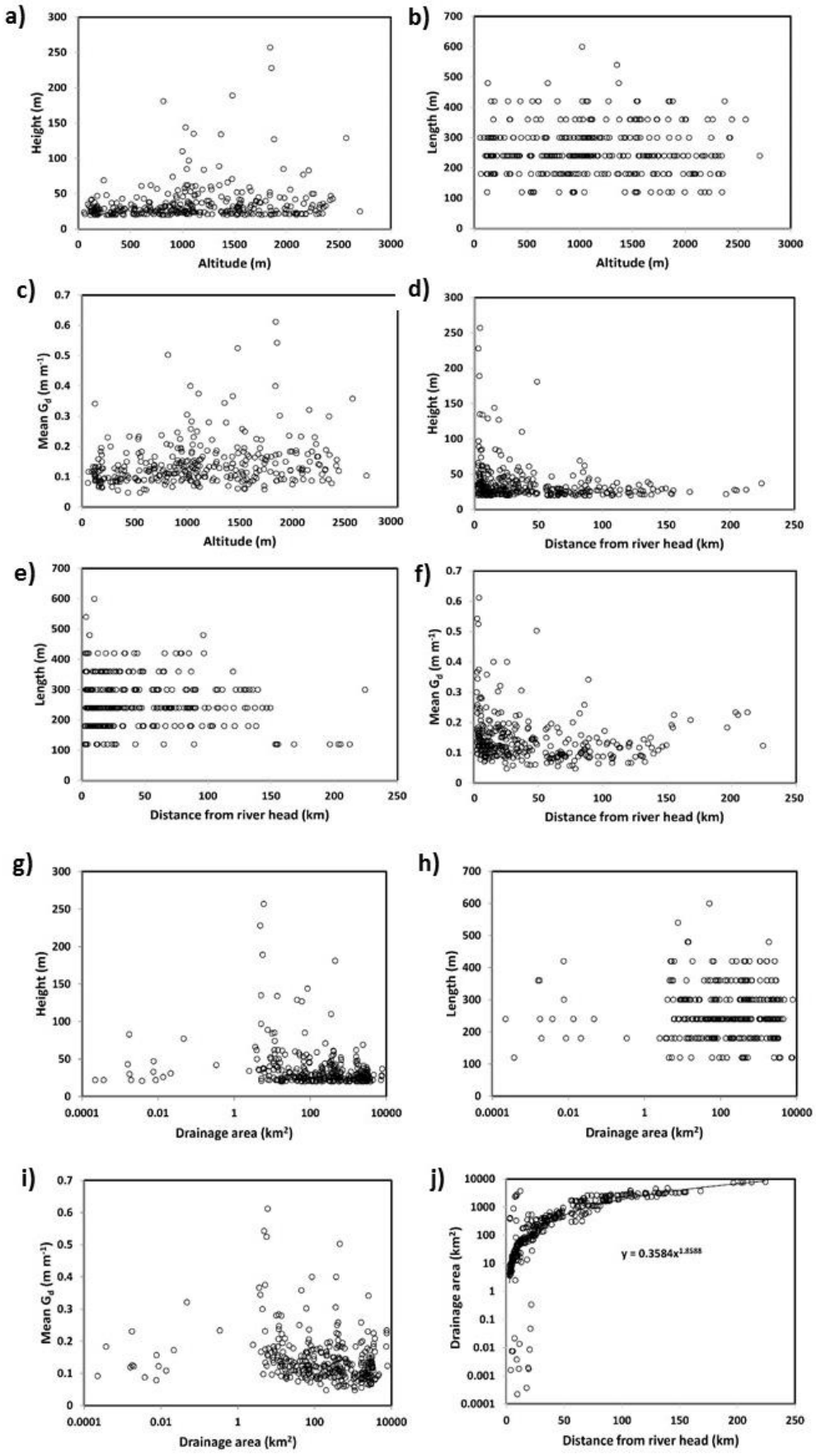

Figure 5-15 Relationships between form parameters of knickzones and locational factors

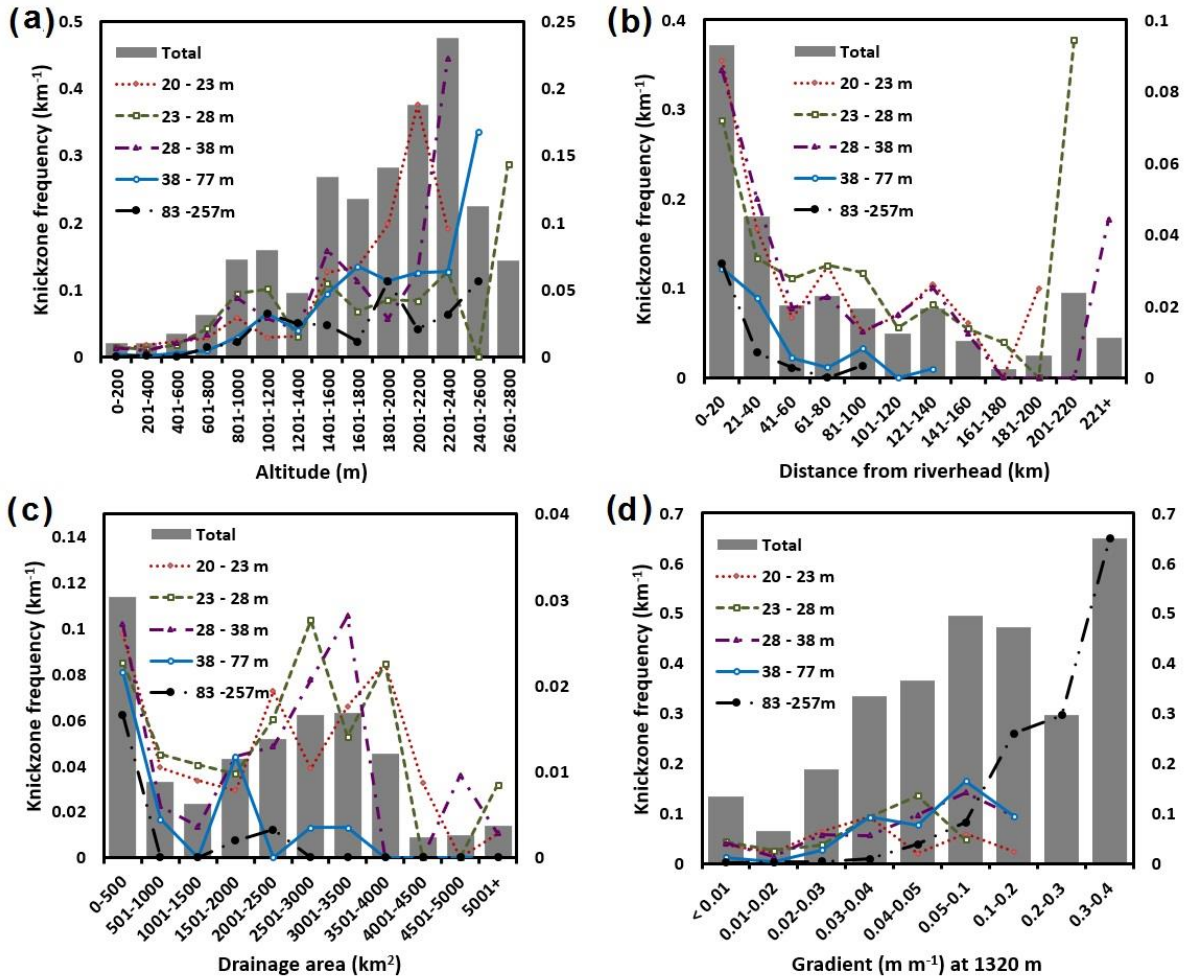

Figure 5-16 Graphs showing knickzone frequency and locational factors for different height classes: a) altitude, b) distance c) drainage area, and d) gradient at the measurement length of 1320 m. Lines show the frequency of knickzones for different height classes: 25, 50, 75 and 90 percentiles.

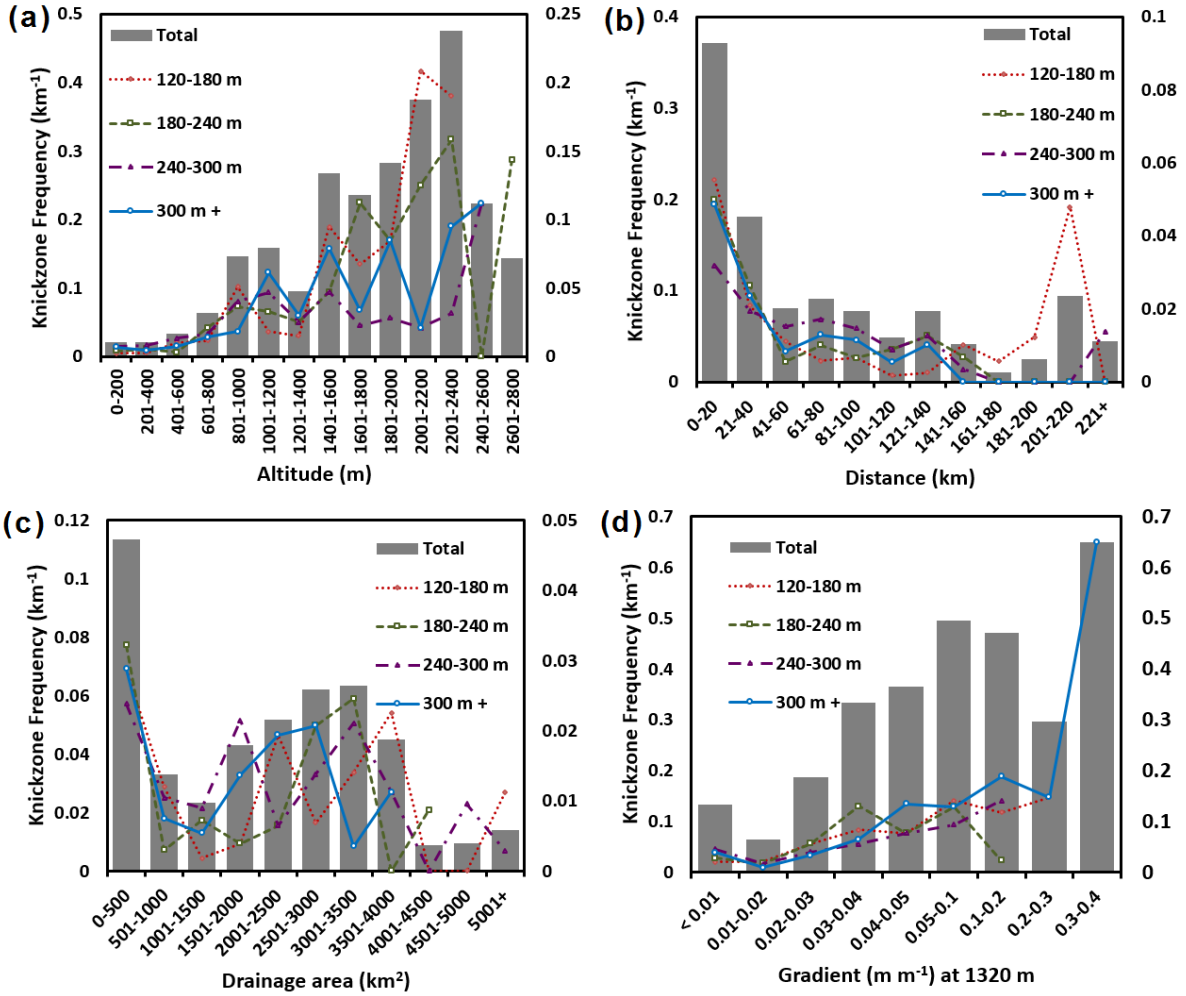

Figure 5-17 Graphs showing knickzone frequency and locational factors for different length classes. a) altitude, b) distance c) drainage area, and d) gradient at the measurement length of 1320 m. Lines show the frequency of knickzones for different length classes: 25, 50 and 75 percentiles.

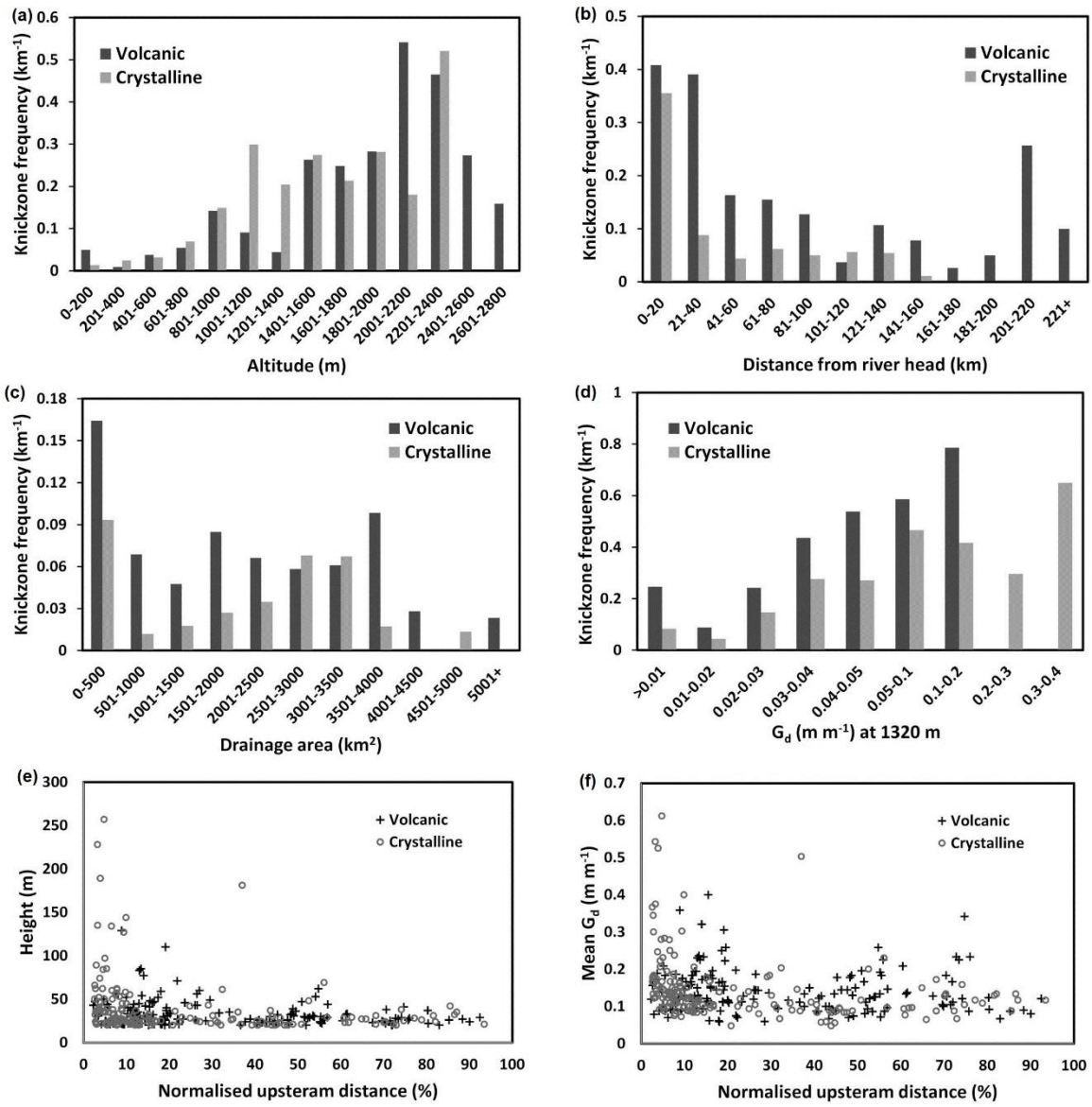

Figure 5-18 Knickzone frequency and locational factors for two dominant rock type: a) altitude, b) distance, c) drainage area, d) gradient at the measurement length of 1320 m. e) and f) Relationships between height and gradient of knickzones along normalized upstream distance of each rock types.

Table 5-12 Differences in knickzone frequency and knickzone density for two dominant lithologies, and those for channel segments with or without fault intersection

Type	Knickzone frequency	Knickzone density
Volcanic rocks	0.088	2.19
Crystalline rocks	0.049	1.32
Channels with fault intersection	0.060	--
Channels without fault intersection	0.069	--

Furthermore, distribution of major faults was analyzed in relation to knickzones. **Figure 4-1** show major faults described in the geological map of the Middle East (CGMW). The knickzone frequency for channels with or without fault intersection is 0.060 and 0.069 respectively (**Table 5-12)**.

As noted precipitation decreases from southern Yemen towards the north (**Figure 4-2**). **Figure 5-19** shows the relationship between knickzone frequencies for channels in different terrains and mean annual precipitation for each terrain in 1998–2013 TRMM data. The trend of precipitation is Yemen > Asir > Hijaz > Midyan, and the knickzone frequency shows a trend Yemen > Hijaz > Asir > Midyan. The Yemen and Hijaz terrains are dominated by volcanic rocks whereas the Asir and Midyan terrains are dominated by crystalline rocks (**Figure 3-3**). The results thus suggest that the knickzone frequency in terrains with an identical lithology is positively correlated with precipitation.

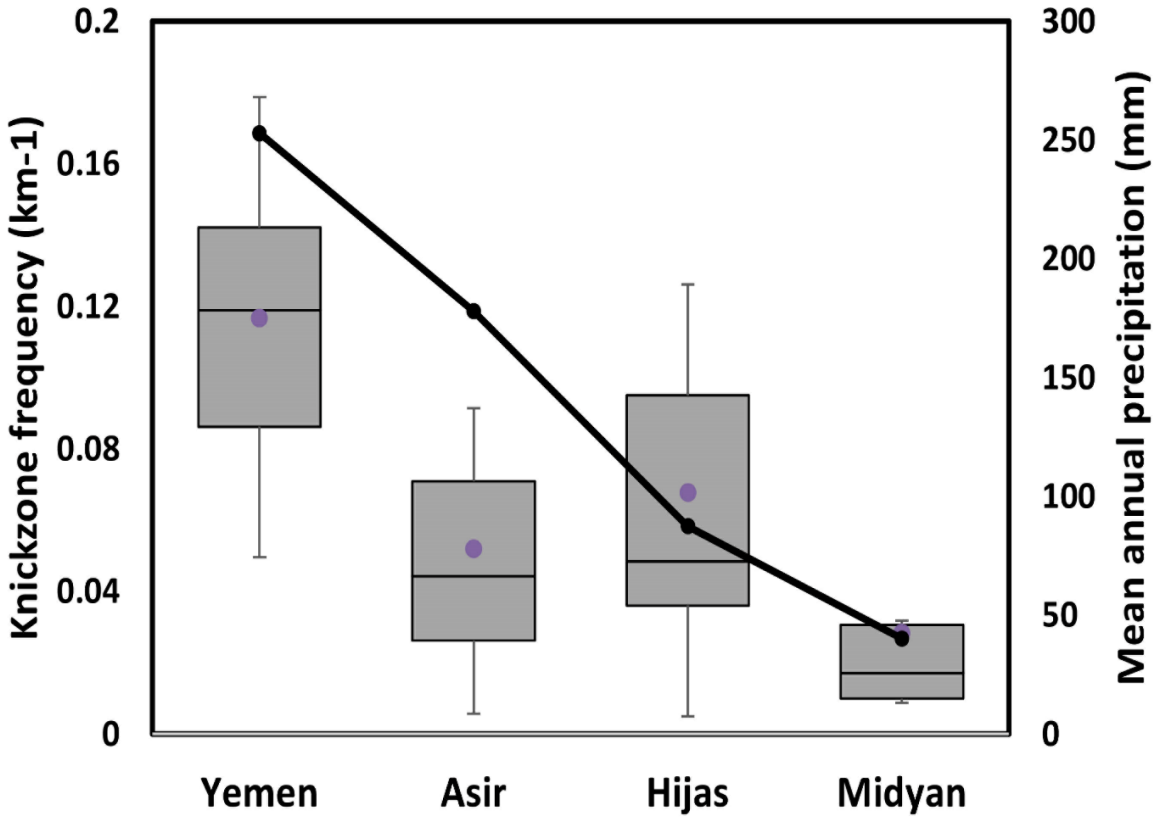

Figure 5-19 Relationship between knickzone frequency for channels in different terrains and mean annual precipitation for the corresponding terrains from 1998–2013 TRMM data. Note that Yemen and Hijaz are dominated by volcanic rocks whereas Asir and Midyan are dominated by crystalline rocks. Column graph: knickzone frequency, line graph: precipitation, line inside the box: median, upper hinge of the box: upper quartile, lower hinge of the box: lower quartile, ends of the vertical lines: maximum and minimum values except for outliers exceeding 1.5 times the inter-quartile range, blue dots; mean.

CHAPTER 6: Discussion

In the light of the results obtained from PCA concerning drainage basin morphometric variables, basin hypsometry, longitudinal profile characteristics, and alluvial-fan properties, this chapter discusses drainage basin characteristics and the driving factors of basin development in the Western Arabian Peninsula.

6.1 Principle component analysis

6.1.1 PC1

The importance of PC1 in classifying the drainage basins is made clear by the following two observations: 1) the component explains around 40% of the total variance of the morphometric parameters; and 2) it corresponds well to the classification of basins using CA. PC1 represents the basin dimensions and drainage texture, and they are positively correlated (**Table 5-6**), such that larger basins tend to have finer textures, giving larger values of *Dd*. It is well known that the relief ratio or basin slope generally tends to decrease with increasing basin size (Oguchi and Ohmori, 1994; Tucker and Bras, 1998), which also holds true for this study area (**Table 5-4**). Previous studies have also related *Dd* to the relative relief or slope of a terrain (Montgomery and Dietrich, 1992; Oguchi, 1997), and both positive and negative correlations have been observed, depending on the dominant hillslope processes (Tucker and Bras, 1998; Talling and Sowter, 1999). In the study area, the drainage texture parameters, such as *Dd*, have negative correlations with relief and slope parameters *Rr* and *Rl* (**Table 5-4**), indicating that mass wasting on steeper slopes is responsible for a reduced *Dd*. Indeed, steep areas in the study area are typically characterized by the occurrence of frequent landslides (Youssef et al., 2012; Alharbi et al., 2013). Therefore, the marked correlation between basin dimensions and drainage texture, as depicted in the main structure of PC1, seems to reflect the effects of relief and slope of a terrain.

It is clear that the effect of relief and slope is not the sole factor determining the main structure of PC1, because PC3, a component theoretically independent of PC1, more directly represents the relief and slope parameters. In other words, the effects of these parameters are not well reflected in PC1, and so there must be other mechanisms controlling the positive correlations between basin dimension and drainage texture. One possible factor is the hydrological characteristics of drainage basins, which are related to climate. In an arid climate, the production of marked channelization with large and relatively frequent flow requires a large upstream area. If such

channelization occurs along the trunk stream, it leads to channelization along tributaries due to a fall in the local base level; this brings about positive correlations between basin dimensions and drainage texture. Observations from the 1-m resolution imagery of the study area provided by Bing Maps reveal that, in the trunk streams of large drainage basins, lateral erosion has been occurring, resulting in the streams cutting into the valley-side slopes. This also leads to a fall in the local base level for the tributaries, more accelerated channelization, and a finer drainage texture. In contrast, such lateral erosion is limited in smaller basins.

Subyani et al. (2012) also conducted PCA for ten basins in the Hijaz terrain, and the PC1 found in that study is similar to this study, in that it represents basin dimensions and drainage density. However, they described these parameters simply as 'major morphometric parameters', and did not consider the relationships between basin dimensions, drainage texture, relief and slope parameters, and hydrological characteristics. This study has therefore not only confirmed the preliminary observations made by Subyani et al. (2012) from a smaller data set, but has also provided a geomorphological interpretation of the most important principal component.

6.1.2 PC2

PC2 represents the general shape of the basins, in terms of circularity and standardized hypsometry. PC2 is theoretically independent of PC1, and this is supported by the different parameters represented by the two components: basin dimensions such as area and basin shape such as circularity may be regarded as independent. One significant aspect of PC2 is its correlation with geology. **Figure 6-1** shows the scores of PC1 to PC3 for each drainage basin according to the two major lithological types: crystalline rocks and volcanic rocks. From this, it can be seen that PC1 and PC3 are basically unrelated to geology. In contrast, PC2 clearly correlates with geology, in that the PC2 values for basins underlain by crystalline rocks tend to be positive, while those for volcanic rocks tend to be negative. This observation indicates that, although lithology is not included as a parameter in the PCA, its effect on the general shape of river basins is reflected in a PC. Generally, those basins underlain by volcanic rocks are more elongated, and less eroded in terms of hypsometry. The correlation between lithology and basin elongation in part of this study area was also indicated by Subyani et al. (2012). However, in their analysis, the parameter relating to basin circularity was not regarded as a major parameter of any PC. Their PC2 is more related to basin slope and relief, and they did not discuss the effects of geology on their PCs. In statistical analyses of geomorphological units such as drainage basins, lithology is usually represented as a categorical variable, because its quantification as a continuous variable, including a representative index for rock strength or weathering

vulnerability, is difficult. Therefore, PCA and CA usually do not incorporate geological parameters. However, if geological differences are considered along with the results from PCA and CA, it may be possible to discuss the potential lithological influence on landforms, as demonstrated in this study.

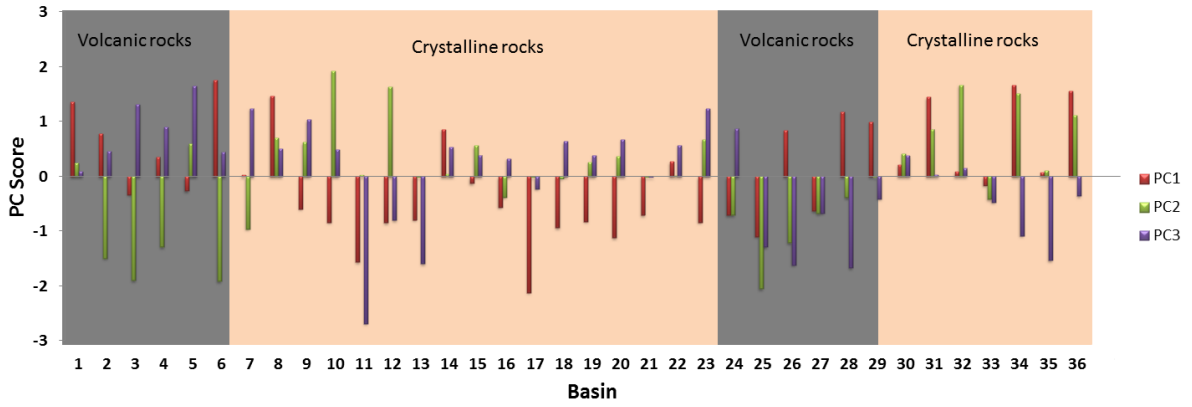

Figure 6-1 Scores of PC1, PC2, and PC3 for each drainage basin according to the two major lithology types in the study area

6.1.3 PC3

PC3 reflects relief components and the length of each stream segment. More specifically, steeper basins tend to have shorter stream segments. This corresponds to the negative correlation between *Dd* and relief and slope, as noted above. Although PC3 explains a smaller percentage of the total variance than PC2, it better explains the secondary level variation observed in the CA result, as noted in Section 5.2. Although both PCA and CA can be used to classify river basins, giving similar results in this study area as far as the most important component (PC1) is concerned, they also represent somewhat different features and processes, such as hydrological conditions that may affect formation of the first-order streams with different channel-head areas, or more frequent confluences, despite similar total stream lengths.

Where PCA has been previously applied to drainage basin parameters, those parameters that represent basin dimensions were not included, to focus on the standardized parameters (Miller et al., 1990; Singh et al., 2009). This approach is in line with the common use of standardized parameters, such as *Dd* and *HI*, and may be effective in avoiding complications in analyses and discussion. However, as indicated in this study, the absolute basin size does influence the standardized parameters of drainage texture in some cases, and may therefore be essential in classifying drainage basins. Thus, it will be important to include parameters that represent absolute basin size in statistical analyses of drainage basins, at least in the early stages of analysis. Following this, it will be possible to

focus on the standardized parameters only if the effect of absolute basin size is found to be minor.

6.2 Alluvial fan morphometry

The alluvial fans identified in the study area permit measurement of morphometric properties that are commonly used in the literature to analyse the erosion and deposition of drainage basins. Previous works have demonstrated the existence of statistical relationships between fan area or fan gradient and such factors as basin area, basin relief, and sediment grain size (e.g., Blair and McPherson, 1994; Harvey, 1997). Power law functions usually express geometric relationships between alluvial fans and contributing basins (e.g., Bull, 1964; Hooke, 1968; Harvey, 1990; Lin et al., 2009). The well-known fan area–basin area relationship also holds true for the study area (**Figure 5-10a**), indicating that the size of the drainage basin influences the volume of sediment discharged to the site of fan deposition, and hence they control the size of fans constructed over time. **Figure 5-10b** shows a similar phenomenon: the length of the contributing basin area is positively related to the fan length. Blair and McPherson (1994) pointed out that, to have an optimal fan development, relatively flat lowland areas are required. This condition is satisfied for Western Arabia by the presence of wide coastal plains, several tens of kilometres long, at the foot of the mountains. Hence, the large drainage basins may have large fans at their foot.

The mapped fans in the study area tend to be larger and longer than most of the fans described in the literature above. **Figure 6-2** shows the plot of fan area versus the contributing basin area from this study along with those from other studies with different climatic settings (Italian Po Plain – Guzzetti et al., 1997; Spain, Murcia fans, California coast and Death Valley – Harvey, 1997; Mars – Moore and Howard, 2005; Taiwan – Lin et al., 2009). The size of the fans in the Western Arabia tends to be larger than the others. However, the basin area for the Arabian fans is also larger, and the fans are located along the overall trend of the fan area–basin area relationship if the relationships for the other areas are extrapolated toward larger sizes (**Figure 6-2**).

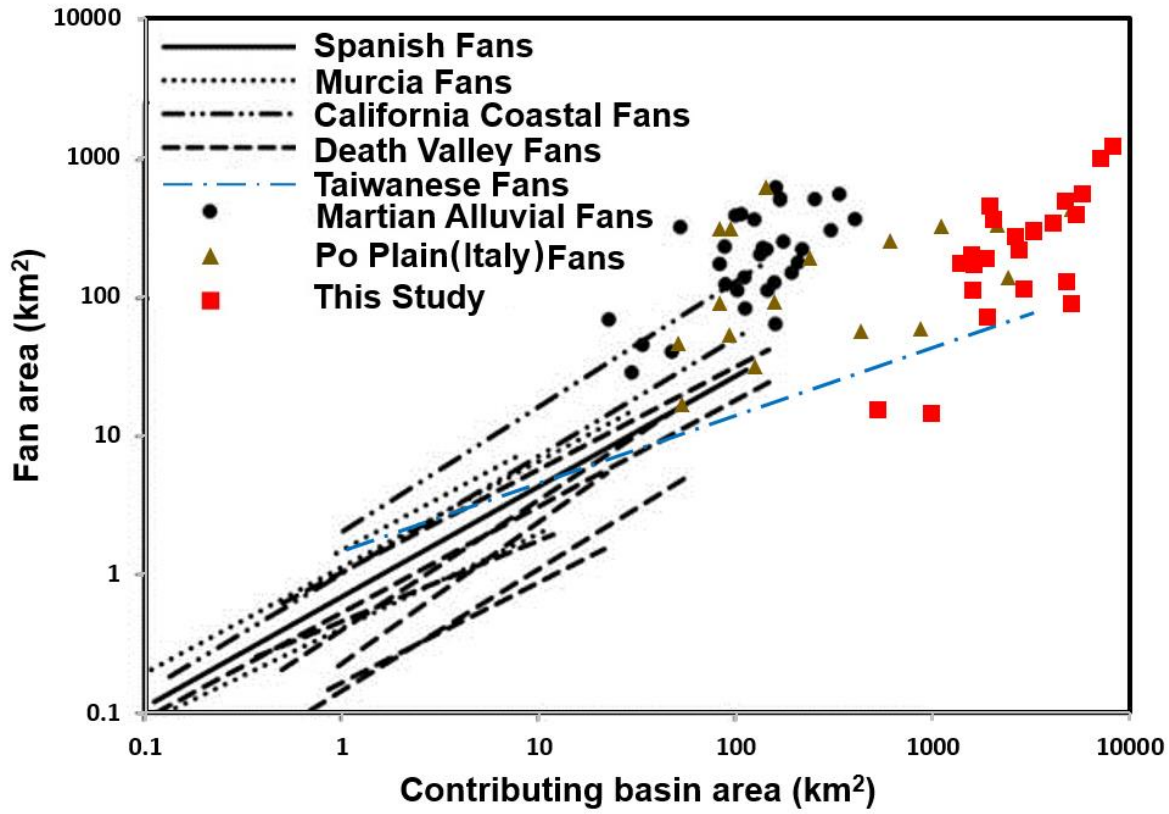

Figure 6-2 Alluvial fan area versus contributing basin area. The western Arabian fans tend to be larger than most of the other fans. (Data for the Italian Po Plain fans are from Guzzetti et al., 1997; Spanish fans, Murcia fans, California coastal fans, Death Valley fans from Harvey, 1997; Martian fans from Moore and Howard, 2005; Taiwanese fans from Lin et al., 2009)

The values of the exponent of the fan area–basin area relationship (n in $A_f = cA_d^n$) from several studies in arid regions are between 0.80 and 0.90 (e.g., Hooke, 1968; Oguchi and Ohmori, 1994), which is higher than humid regions that ranges between 0.50 and 0.60 (Oguchi and Ohmori, 1994; Lin et al., 2009), and also higher than the Mediterranean regions (0.3–0.4; Guzzetti et al., 1997). The exponent *n* from the result of this study (**Figure 5-10a**) is much higher (1.21), implying that larger basins supply a greater amount of sediments per unit area than smaller basins. This agrees with the inference from PC1: large basins have sufficient flow to enhance channel incision, resulting in higher drainage density and hence more sediment supply per unit area.

The fan slope may also relate to the contributing basin area with a power law. Primarily the fan slope is controlled by debris calibre and is generally determined by conditions in the source area (Hooke, 1968). In many previous studies, the fan slope–basin area relationship is shown by a negative correlation (Bull, 1964; Hooke, 1968; Harvey, 1997). However, in the present study, no significant correlation between the fan slope and the basin area is observed (**Figure 5-10d**), whereas the fan slope is dependent on drainage basin slope (**Figure 5-10c**). **Figure 6-3**

shows the fan slope versus basin area plot from this study along with some published data from different climatic settings. The large systems in the Po Plain also do not possess a significant correlation. It can be assumed that the negative correlation between the fan slope and basin area becomes less distinct in larger systems. This agrees with the analysis of Taiwanese fans by Lin et al. (2009); basins smaller than 80 km^2 have a negative correlation between the fan slope and basin area, while the fan slope tends to be constant irrespective of the basin area if it the basin larger than 80 km^2. However, **Figure 6-3** shows that such tendency of constant slope is more apparent for the Po Plain fans than the Arabian fans. This may reflect different climatic conditions. In humid regions like Italy and Taiwan, the fan slope is more constant because the fan–basin systems are more organized close to a characteristic form under faster and long-term geomorphic processes due to abundant rainfall. By contrast, in arid regions like Arabia, the system may be less organised due to weaker geomorphological processes related to water. Blissenbach (1954) noted that fans in arid regions are steeper than humid environment where the precipitation affects the fan slope, which also holds true for the study area (**Figure 5-10d**). Some studies have attributed variations in the fan slope to lithology (e.g., Hooke, 1968); however, for the present study, no significant influence of lithology on the fan slopes is observed. Similarly, other morphometric relationships between the fans and source basins do not show consistent differences according to geology (**Figure 5-10**), although landforms of the source basins show some differences corresponding to geology. This suggests that geology does not significantly affect the average sediment yield per unit area.

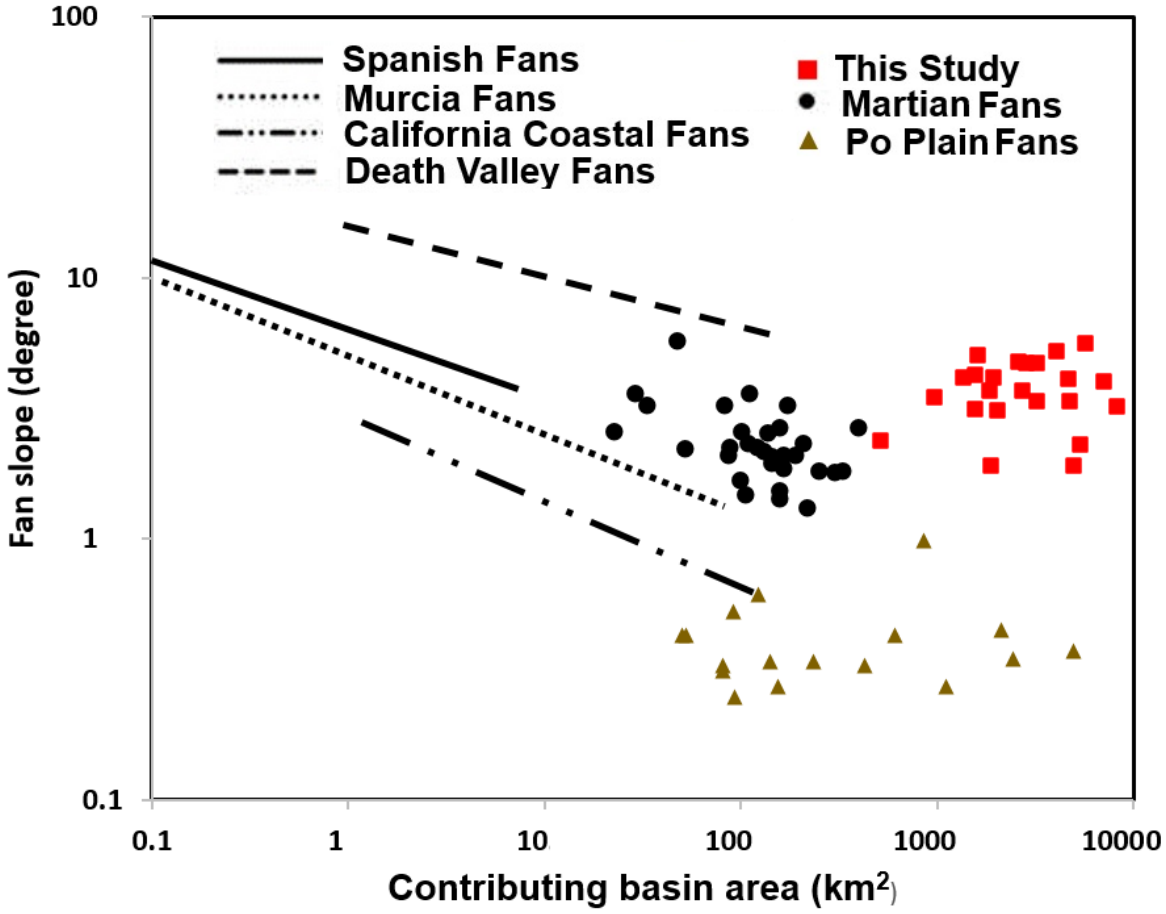

Figure 6-3 Fan slope versus contributing basin area. No significant relationship is observed for the slope of the Western Arabian fans and their contributing area. Their slope is steeper than most of the other fans.

6.3 **Knickzones in relation to climate, hydrology and lithology**

The analyses of longitudinal profiles demonstrate that the knickzones in the 36 main rivers occur anywhere along the reaches. However, they are more abundant at higher altitudes close to the river head (**Figure 5-16**). The knickzone height, length, and gradient, inferred from the results also show that large knickzones tend to be more abundant in the upstream steep reaches. These observations agree with the findings of Hayakawa and Oguchi (2006). The role of strong stream hydraulics in higher steeper reaches (e.g., Wohl, 2000; Chin and Wohl, 2005) may facilitate knickzones formation. However, in the study area of the Arabian Peninsula with an arid to semi-arid climate, the effect of hydraulics in small basins may be questionable, although flash floods of high intensity and short duration occur in the higher altitudes of Hijaz, Asir and Yemen. One possible interpretation is more enhanced erosion under a wetter climate in the past. At least three events of wet period in the Pleistocene and one wet event in the Holocene have been reported around the study area (Chapman, 1978; Vincent, 2008).

However, even if such past events facilitated knickzones formation particularly in the upstream areas, the effects do not look comparable to those in humid regions. **Figure 6-4** shows the knickzone frequencies for the bedrock channels underlain by volcanic and crystalline rocks in Japanese basins (Hayakawa and Oguchi, 2006) and those in the Arabian Peninsula. It is noted that the knickzone frequencies are significantly higher in Japan for the same lithology type. Although Japan is in the active tectonic margin, the effect of tectonics on the development of knickzones is limited (Hayakawa and Oguchi, 2009). Therefore, the difference between Japan and the Arabian Peninsula is ascribable to the climatic difference. The knickzone frequency is exceptionally high (>10 km^{-1}) for lower order streams in the South Fork Eel River, northern California, where the mean annual rainfall exceeds 1500 mm (Foster and Kelsey, 2012). Furthermore, within the study area, the knickzone frequency tends to be positively correlated with mean annual precipitation (**Figure 5-19**). All these indicate that knickzones are more abundant where hydrological processes are stronger due to higher rainfall. At the same time, a moderate amount of knickzones can be produced even under a dry climate as in the Arabian Peninsula.

Geology also plays an important role in controlling river profiles in the study area including knickzones. Hack (1973) pointed out that channel gradient is often correlated with underlying lithology. In this study, volcanic rocks tend to have higher steepness and lower concavity than crystalline rocks (**Figure 5-12**). Moreover, knickzone frequencies along channels underlain by volcanic rocks (0.088 km^{-1}) are almost twice as those along the crystalline channels (0.049 km^{-1}). **Figure 5-18c** indicates that a large drainage area is required to have a high knickzone frequency in crystalline rocks; whereas, the volcanic rocks tend to have high knickzone frequency even in small drainage areas. This difference may be attributed to more uneven erosion in the volcanic rocks; an unevenly eroded channel has more knickzones. The accumulated layers of lava flows that filled the valleys (Vincent, 2008) and associated alternating bands of hard and soft volcanics may facilitate the formation of knickzones as suggested by Hayakawa and Matskura (2003) and Hayakawa and Oguchi (2009). Some previous studies have also identified numerous knickzones in basaltic rocks (e.g., Kale and Shejwalker, 2008; Lima and Binda, 2013).

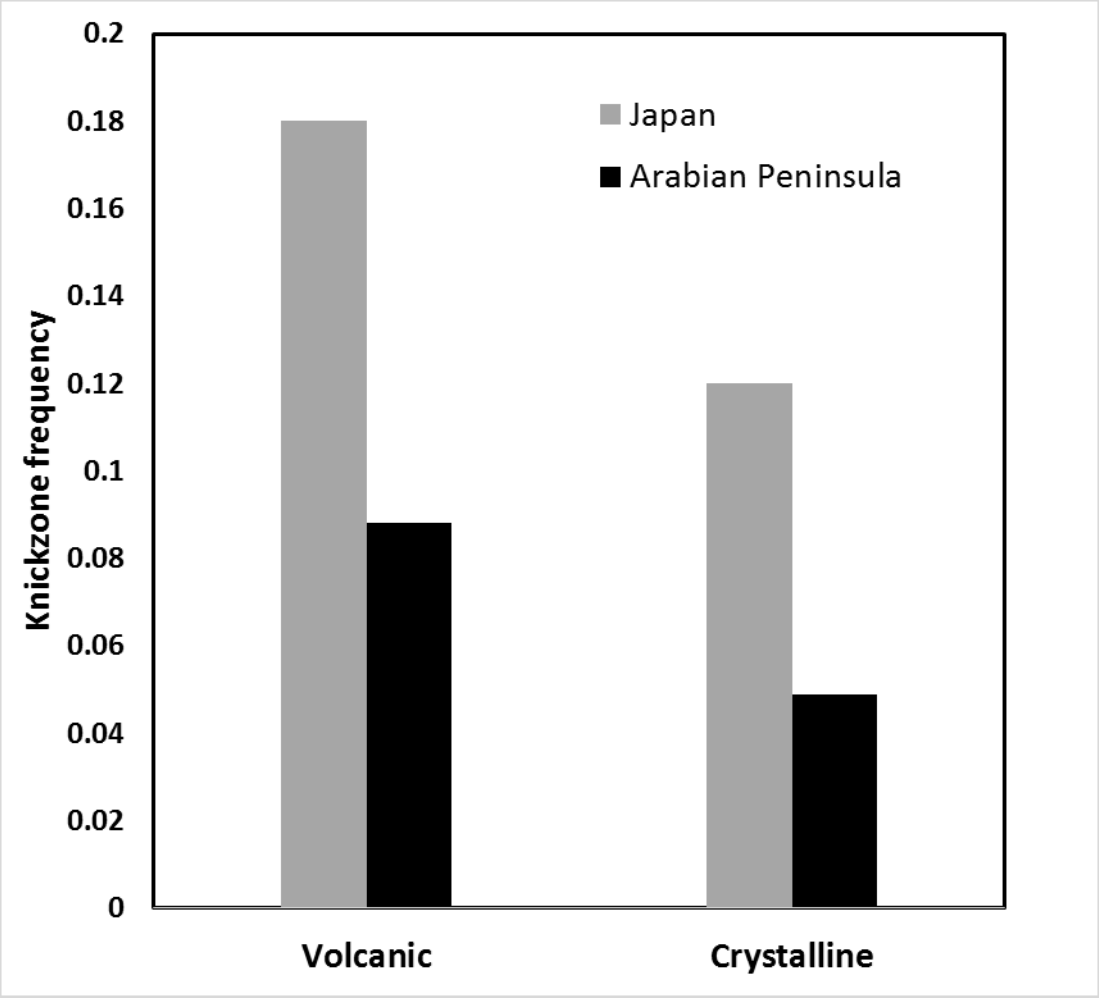

Figure 6-4 Comparison of knickzone frequencies for channels in two different rocks types in two different climatic environments. Data for Japanese drainage basins are from Hayakawa and Oguchi (2006).

6.4 Effect of geology on *HI*, erosion, and sediment yield

As noted, PC2 is related to *HI* and bedrock geology, suggesting that geology strongly affects *HI*. This issue is discussed below. It has been noted that *HI* values of a drainage basin are influenced by various parameters such as drainage area, tectonics, lithology and climate (Lifton and Chase, 1992; Masek et al., 1994; Hurtrez et al., 1999; Chen et al., 2003). Because the Western Arabian Peninsula is a passive continental margin (Matmon et al., 2002), the significance of tectonics on *HI* can be ruled out. Moreover, *HI* for 97% of the major basins and 93% of sub-basins are less than 0.5, indicating no significant neotectonic activity according to Keller and Pinter (2002). The results described in Section 5.3 also indicate that *HI* for the studied basins are independent of basin geometry and no particular spatial trend occurs for *HI* at different Strahler orders. These results are similar to the observation of Walcott and Summerfield (2007) but are in contrast with some other studies (Hurtrez et al., 1999; Hancock and Willgoose, 2001; Chen et al., 2003; Cheng et al., 2012).

It is evident that basins located in the volcanic rocks have higher *HI* values compared to those in the crystalline rocks (**Figure 5-8**). Also, the basins in the volcanic rocks have convex and S-shaped hypsometric curves, while those in the crystalline rocks have concave hypsometric curves (**Figure 5-7**). These suggest that the basins with crystalline rocks are more eroded than those with volcanic rocks. Nevertheless, the alluvial fan analyses suggest that long-term sediment yields per unit area are not strongly dependent on geology. In addition, more knickzones along rivers in volcanic terrains may indicate active hydraulic action and erosion there. All these observations can be explained from the more uneven erosion in volcanic terrains as noted above. Davison et al. (1998) and Vincent (2008) suggest that the volcanic rocks act as cap rocks in Western Arabia, which may have led to the relatively high *HI* values and S-shaped and convex curves. However, very deep incision along some channels in volcanic terrains is observed, and thus the distribution of erosion rate is highly uneven. In contrast, more homogeneous and intensively weathered crystalline rocks are widely reported along the highways in the mountainous parts of Asir terrain (Vincent, 2008), and such a condition is favorable for more evenly distributed erosion, low *HI* values due to the lack of cap-rocks, and concave hypsometric curves.

CHAPTER 7: Conclusions

Geomorphology in the Western Arabian Peninsula, particularly the steep drainage systems, have not been studied carefully enough and therefore the fundamental aspects of geomorphic processes there are still not well understood. Although qualitative appraisal of geomorphic processes in the western Arabia was stated in some previous studies, a comprehensive quantitative analysis is essential to understand detailed characteristics of landforms and discuss their development processes. A major reasons for the limited scientific knowledge so far is the inaccessibility of locations for field research due to limited road network, poor mapping base, harsh terrain and a dry climate. This makes geomorphic mapping and their interpretation in western Arabia exceedingly unstable. *Henceforth;*

This study has concentrated on interpreting geomorphic processes mainly using digital elevation models from remotely sensed data. Since rivers and streams provide the most significant greatest volume of information on geomorphic processes, the emphasis is primarily given upon drainages and drainage basins.

This study has conducted extensive morphometric analyses for the 36 drainage basins and 1046 sub-basins in the Western Arabian Peninsula. Drainage basins and stream networks were delineated using the ASTER GDEM and GIS with the constant threshold contributing area method. Principal component analysis (PCA) and cluster analysis (CA) were applied to 21 morphometric parameters derived from the DEM. PCA results for the 1046 sub-basins is analogous to that for the 36 major basins.

The results indicate that the three major principal components can be interpreted in relation to drainage basin development through fluvial and hillslope erosion, under the influence of geology.

(1) PC1 accounts for 39% of the variance of the 21 parameters and it represents the dimensions of basins such as *A*, *P*, *Nu*, *Lu*, and *Lb*, and the drainage texture as defined by *Fs*, Fs_1, R_{P1}, *Dd*, and *Mc*.

(2) PC2, which explains 21% of the total variance, represents parameters *HI*, *C*, *Re* and *Ff*, reflecting the general shape of a basin. PC2 is also correlated with geology, which differs from the other PCs.

(3) PC3 explains 13% of the total variance, and represents mainly the variances in basin relief.

PC1 strongly reflects basin dimensions and drainage texture; their positive correlations indicate enhanced erosion in large basins as well as limited stream incision in small basins under an arid climate. In an arid climate, the production of marked channelization with large and relatively frequent flow requires a large upstream area. If such channelization occurs along the trunk stream, it leads to channelization along tributaries due to a fall in the local base level; this brings about positive correlations between basin dimensions and drainage texture.

PC2 mainly reflects the effect of bedrock geology, suggesting that volcanic rocks tend to produce more elongated and less eroded immature basins than crystalline rocks. In statistical analyses of geomorphological units such as drainage basins, lithology is usually represented as a categorical variable, because its quantification as a continuous variable, including a representative index for rock strength or weathering vulnerability, is difficult. Therefore, PCA and CA usually do not incorporate geological parameters. *However:*

If geological differences are considered along with the results from PCA and CA, it may be possible to discuss the potential lithological influence on landforms, as demonstrated in this study

PC3 mainly reflects the basin relief, slope and the length of each stream segment which may indicate the effect of mass wasting on stream development. It also better explains the secondary level variation observed in the CA result. The result of the drainage basin classification from CA is consistent with the results of PCA.

Compared with previous drainage basin analyses using PCA, this study has used a greater number of drainage basins and morphometric parameters to obtain a statistically more significant result and to include the possible effects of absolute basin dimensions on geomorphic processes. The results show the importance of including parameters that represent absolute basin size in statistical analyses of drainage basins.

Basin hypsometric results shows that *HI* for the basins in the Western Arabian Peninsula neither correlates with basin area nor with the circularity.

It is noticed that the differences in HI result from lithological variations including the erosional resistance of one rock unit with respect to another or uneven erosion. In summary, in the Western Arabia, HI appear to be sensitive to lithology rather than basin geometry.

The shape of hypsometric curves also leads to the same inference. Thus, Strahler's cycle of the hypsometric curve gives a reasonable relative stages for the development of drainage basins.

In the study area, some large alluvial fans were identified at the mouth of the major drainage basins. The results of analyses of the alluvial fans were compared with those from different climatic settings.

As far as the author knows, no studies have been carried on a comprehensive analysis of alluvial fans in the region. Although the fans in Western Arabia are found to be larger than most of the fans analyzed in other regions, the contributing areas of Arabian fans are also larger and the studied fans are located along the overall trend of the fan area–basin area relationships from various regions.

Also the value of the exponent of the fan area–basin area relationship is higher than the previously reported values and even more than unity, showing that larger basins supply a greater amount of sediments per unit area than smaller basins. This reflects the arid climate that requires a large basin area to enable fast erosion. Regarding fan slope–basin area relationship, no significant correlation is observed, and the slope is less constant compared to some examples in humid regions due to less organized geomorphic systems in the arid region.

The results of longitudinal profile analysis throw light on the effect of climate and lithology in shaping the river profiles.

A total of 325 knickzones were identified, and their abundance in the upstream reaches of rivers is confirmed from the analysis of locational factors. The relatively high frequency of knickzone abundance in arid basins however is surprising.

The relationships between precipitation and knickzone frequencies for different climatic settings show the influence of large stream hydraulics for their origin. Variation in lithology seems to have affected the development of the knickzones at least in three ways: 1) the presence of volcanic lava flows that fill the valley, 2) differences in hard and soft rocks within the region, and 3) uneven erosion within the volcanic rocks. In contrast, the effect of faults on knickzone abundance are weak.

Originality of this research includes:

(i) The comprehensive explanation of various geomorphic variables,

(ii) New investigations for Western Arabia such as alluvial fan morphometry and knickzone analyses, which have never been conducted in the region,

(iii) The present study has revealed the importance of considering geology when interpreting the results of statistical analyses such as PCA and CA using only from morphometric parameters,

(iv) Some of the results appear to be unique to arid regions; for example, the influence of basin size on erosion may be less significant in humid regions because even small basins can generate sufficient flow to produce marked fluvial erosion.

Further studies into drainage basins in varying environmental conditions are necessary to address the geomorphological issues in detail. For example, it would be useful to investigate the knickzone frequencies related to precipitation variety; particularly, the use of more detailed meteorological data reflecting the intensity of each rainfall event rather than the mean value would be important particularly in arid regions like the study area (e.g., Monlar et al., 2006). Although it seems apparent from topography that fluvial processes are dominant in shaping landforms in the study area, it is also necessary to evaluate the effects of other processes such as eolian processes and rock weathering.

Acknowledgement

First and foremost, I would like to give huge thanks to my supervisor Prof. Takashi OGUCHI. I am greatly appreciative of the time and commitment he have invested in me, his help and guidance over the last three years has been instrumental to the success of this thesis.

I would also like to thank Dr. Yuichi S. HAYAKAWA for all his help, on this thesis and other manuscripts and all other technical aspects. His experience has been invaluable.

In addition, I would like to express my sincere appreciation to Prof. Toshihiko SUGAI, Prof. Juichiro ASHI and Prof. Kaoru SAITO for their valuable comments and suggestions that have helped in improving this manuscript.

This research was supported by Japanese Government (Monbukagakusho) scholarship offered by the Ministry of Education, Culture, Sports, Science, and Technology, Japan.

I thank Mr. Uttam PAUDEL for his gracious support. To my lab-mates and roomies, thanks for the fun and extended assistance.

Finally, I would like to say a huge thank you to my parents, family and friends for their constant encouragement.

References

Abbühl LM, Norton KP, Jansen JD, Schlunegger F, Aldahan A, Possnert G. Erosion rates and mechanisms of knickzone retreat inferred from 10Be measured across strong climate gradients on the northern and central Andes Western Escarpment. Earth Surf Process Landforms 2011;36(11):1464-1473.

Adams MJ. The Principles of Multivariate Data Analysis. Analytical Methods of Food Authentication, edited by Ashurst, P.R, Dennis, M.J.: Blackie Academic & Professional, London, UK 1998. p. 308.

Alberto WD, María del Pilar D, María Valeria A, Fabiana PS, Cecilia HA, María de los Ángeles, Bistoni. Pattern Recognition Techniques for the Evaluation of Spatial and Temporal Variations in Water Quality. A Case Study: Suquía River Basin (Córdoba–Argentina). Water Res 2001;35(12):2881-2894.

Alharbi T, Sultan M, Sefry S, El Kadiri R, Ahmed M, Chase R, et al. An assessment of landslide distribution in the Faifa area, Saudi Arabia, using remote sensing and GIS techniques. Natural Hazards and Earth System Sciences Discussions 2013;1:6685-6717.

Almazroui M. Calibration of TRMM rainfall climatology over Saudi Arabia during 1998–2009. Atmos Res 2011;99(3):400-414.

Almazroui M, Nazrul Islam M, Athar H, Jones P, Rahman MA. Recent climate change in the Arabian Peninsula: annual rainfall and temperature analysis of Saudi Arabia for 1978–2009. Int J Climatol 2012;32(6):953-966.

Al-Turki S. Water resources in Saudi Arabia with particular reference to Tihama Asir province. Durham University: PhD Thesis 1995.

Ambili V, Narayana AC. Tectonic effects on the longitudinal profiles of the Chaliyar River and its tributaries, southwest India. Geomorphology 2014;217:37-47.

Aruga R, Gastaldi D, Negro G, Ostacoli G. Pollution of a river basin and its evolution with time studied by multivariate statistical analysis. Anal Chim Acta 1995;310(1):15-25.

Bailey GN, Flemming NC, King GC, Lambeck K, Momber G, Moran LJ, et al. Coastlines, submerged landscapes, and human evolution: the Red Sea Basin and the Farasan Islands. The Journal of Island and Coastal Archaeology 2007;2(2):127-160.

Baker J, Thirlwall M, Menzies M. Sr Nd Pb isotopic and trace element evidence for crustal contamination of plume-derived flood basalts: Oligocene flood volcanism in western Yemen. Geochim Cosmochim Acta 1996;60(14):2559-2581.

Barnes JB, Pelletier JD. Latitudinal variation of denudation in the evolution of the Bolivian Andes. Am J Sci 2006;306(1):1-31.

Bengraine K, Marhaba TF. Using Principal Component Analysis to Monitor Spatial and Temporal Changes in Water Quality. Journal of Hazardous Materials 2003:100 (1):179-195.

Berlin MM, Anderson RS. Modeling of knickpoint retreat on the Roan Plateau, western Colorado. Journal of Geophysical Research: Earth Surface (2003–2012) 2007;112(F3).

Bishop P, Hoey TB, Jansen JD, Artza IL. Knickpoint recession rate and catchment area: The case of uplifted rivers in eastern Scotland. Earth Surf Process Landforms 2005;30(6):767-778.

Blackwelder, E. Desert Plains. J. Geol. (1931):39:133-140

Blair TC, McPherson JG. Alluvial fans and their natural distinction from rivers based on morphology, hydraulic processes, sedimentary processes, and facies assemblages. Journal of sedimentary research 1994;64(3).

Blissenbach E. Geology of alluvial fans in semiarid regions. Geol. Soc. Am. Bull. 1954;65(2):175-190.

Boothroyd JC, Nummedal D. Proglacial braided outwash: a model for humid alluvial-fan deposits. In: Miall AD. (ed.) Fluvial Sedimentology. Canadian Society for Petroleum Geologists, Memoir 1977:641-668.

Bosworth W, Huchon P, McClay K. The red sea and gulf of aden basins. J Afr Earth Sci 2005;43(1):334-378.

Bowman D, Shachnovich-Firtel Y, Devora S. Stream channel convexity induced by continuous base level lowering, the Dead Sea, Israel. Geomorphology 2007;92(1):60-75.

Brown GF. Eastern margin of the Red Sea and the coastal structures in Saudi Arabia. Philosophical Transactions for the Royal Society of London.Series A, Mathematical and Physical Sciences 1970:75-87.

Brown GF, Tectonic Map of the Arabian Peninsula 1: 4,000,000. : US Geological Survey; 1972.

Brown GF, Schmidt DL, Huffman AC Jr. Shield area of western Saudi Arabia Geology of the Arabian Peninsula, US Geol. Surv. Prof. Pap. 1989: (560-A):188.

Bull WB. Geomorphology of segmented alluvial fans in western Fresno County, California. U.S. Geol. Surv. Prof. Pap. 1964: (352-E): 89-129.

Bull WB. The alluvial fan environment. Progress in Phy. Geog. 1977:1(2):220-270

Bull WB. Threshold of critical power in streams. Geol. Soc. Am. Bull. 1979: (90):453-464

Bull WB. Geomorphic responses to climatic change. Oxford University Press, New York, 1991:326

Burns SJ, Matter A, Frank N, Mangini A. Speleothem-based paleoclimate record from northern Oman. Geology 1998;26(6):499-502.

Burkham DE. Hydrology of Cornfield Wash area and the effects of land treatment practices, Sandoval County, New Mexico, 1951-1960: U.S. Geol. Survey Water-Supply Paper 1831. 1966:87.

Burrough PA, McDonnell R, Burrough PA, McDonnell R. Principles of geographical information systems. : Oxford university press Oxford; 1998.

Castillo M, Bishop P, Jansen JD. Knickpoint retreat and transient bedrock channel morphology triggered by base-level fall in small bedrock river catchments: The case of the Isle of Jura, Scotland. Geomorphology 2013;180:1-9.

Chapman RW. Geomorphology of the eastern margin of the Shedgum Plateau. SS Al-Sayari, JG Zötl (Eds.), Quaternary Period of Saudi Arabia: Springer-Verlag, New York 1978.

Chen Y, Sung Q, Cheng K. Along-strike variations of morphotectonic features in the Western Foothills of Taiwan: tectonic implications based on stream-gradient and hypsometric analysis. Geomorphology 2003;56(1):109-137.

Chen MC. Knickpoint retreat and fluvial incision following the 1999 Chi-Chi earthquake: Da-An River gorge, Taiwan: PhD Thesis 2010.

Cheng K, Hung J, Chang H, Tsai H, Sung Q. Scale independence of basin hypsometry and steady state topography. Geomorphology 2012;171:1-11.

Chin A, Wohl E. Toward a theory for step pools in stream channels. Prog Phys Geogr 2005;29(3):275-296.

Cochran JR. A model for development of Red Sea. AAPG Bull 1983;67(1):41-69.

Cole G, Abu-Ali M, Aoudeh S, Carrigan W, Chen H, Colling E, et al. Organic geochemistry of the Paleozoic petroleum system of Saudi Arabia. Energy Fuels 1994;8(6):1425-1442.

Coleman RG. Geologic background of the Red Sea. : Springer Berlin Heidelberg 1974.

Costa-Cabral MC, Burges SJ. Digital elevation model networks (DEMON): A model of flow over hillslopes for computation of contributing and dispersal areas. Water Resour Res 1994;30(6):1681-1692.

Crosby BT, Whipple KX. Knickpoint initiation and distribution within fluvial networks: 236 waterfalls in the Waipaoa River, North Island, New Zealand. Geomorphology 2006;82(1):16-38.

Davison I, Tatnell M, Owen L, Jenkins G, Baker J. Tectonic geomorphology and rates of crustal processes along the Red Sea margin, north-west Yemen. Sedimentation and Tectonics in Rift Basins Red Sea:-Gulf of Aden: Springer; 1998. p. 595-612.

de Andrade EM, Palácio HAQ, Souza IH, de Oliveira Leão, Raimundo Alípio, Guerreiro MJ. Land use effects in groundwater composition of an alluvial aquifer (Trussu River, Brazil) by multivariate techniques. Environ Res 2008;106(2):170-177.

Diaconu C. Probleme ale scurgerii aluviunilor pe râurile din România. Studii de Hidrologie 1971;30:307.

DiBiase RA, Whipple KX. The influence of erosion thresholds and runoff variability on the relationships among topography, climate, and erosion rate. Journal of Geophysical Research: Earth Surface (2003–2012) 2011;116(F4).

Dietrich WE, Bellugi DG, Sklar LS, Stock JD, Heimsath AM, Roering JJ. Geomorphic transport laws for predicting landscape form and dynamics. Prediction in geomorphology 2003:103-132.

Duvall A, Kirby E, Burbank D. Tectonic and lithologic controls on bedrock channel profiles and processes in coastal California. Journal of Geophysical Research: Earth Surface (2003–2012) 2004;109(F3).

Ehlen J. Statistical Analysis of Geomorphic, Petrographic and Structural Characteristics of the Dartmoor Tors, Southwest England U.S. Technical report. Army Corps of Engineers Topographic Engineering Center Fort Belvoir; Virginia 1993: 22060-5546

Fairfield J, Leymarie P. Drainage networks from grid digital elevation models. Water Resour Res 1991;27(5):709-717.

Figueroa AM, Knott JR. Tectonic geomorphology of the southern Sierra Nevada Mountains (California): Evidence for uplift and basin formation. Geomorphology 2010;123(1):34-45.

Fitzpatrick FA, Waite IR, D'Arconte PJ, Meador MR, Maupin MA, Gurtz ME. Revised methods for characterizing stream habitat in the National Water-Quality Assessment Program. : US Department of the Interior, US Geological Survey; 1998.

Fleitmann D, Matter A, Pint JJ, Al-Shanti MA. The speleothem record of climate change in Saudi Arabia. Saudi Geological Survey, Jeddah, Kingdom of Saudi Arabia 2004.

Flint J. Stream gradient as a function of order, magnitude, and discharge. Water Resour Res 1974;10(5):969-973.

Foster MA, Kelsey HM. Knickpoint and knickzone formation and propagation, South Fork Eel River, northern California. Geosphere 2012;8(2):403-416.

Fournier M, Massei N, Mahler B, Bakalowicz M, Dupont J. Application of multivariate analysis to suspended matter particle size distribution in a karst aquifer. Hydrol Process 2008;22(13):2337-2345.

Fourniguet J, Alabouvette B, Kluyver H, Ledru P, Robelin C. Evolution of Western and Central Saudi Arabia during Late Tertiary and Quaternary. A Bibliographic Review.Open-File Report BRGM-OF-05–10.Jiddah, Ministry of Petroleum and Mineral Resources 1985.

Frankel KL, Pazzaglia FJ, Vaughn JD. Knickpoint evolution in a vertically bedded substrate, upstream-dipping terraces, and Atlantic slope bedrock channels. Geological Society of America Bulletin 2007;119(3-4):476-486.

Freeman TG. Calculating catchment area with divergent flow based on a regular grid. Comput Geosci 1991;17(3):413-422.

Frey H, Paul F. On the suitability of the SRTM DEM and ASTER GDEM for the compilation of topographic parameters in glacier inventories. International Journal of Applied Earth Observation and Geoinformation 2012 8;18(0):480-490.

Frissell CA, Liss WJ, Warren CE, Hurley MD. A hierarchical framework for stream habitat classification: viewing streams in a watershed context. Environ Manage 1986;10(2):199-214.

Fryberger SG, Al-Sari AM, Clisham TJ, Rizvi SA, Al-Hinai KG. Wind sedimentation in the Jafurah sand sea, Saudi Arabia. Sedimentology 1984;31(3):413-431.

Gardiner J. River catchment planning for land drainage, flood defence and the environment. Water and Environment Journal 1990;4(5):442-450.

Gardner TW. Experimental study of knickpoint and longitudinal profile evolution in cohesive, homogeneous material. Geological Society of America Bulletin 1983;94(5):664-672.

Gettings ME, Blank H, Mooney W, Healey J. Crustal structure of southwestern Saudi Arabia. Journal of Geophysical Research: Solid Earth (1978–2012) 1986;91(B6):6491-6512.

Glennie KW. Desert sedimentary environments. : Elsevier; 2010.

Gregory K, Gardiner V. Drainage density and climate. Zeitschrift fur Geomorphologie 1975;19(3):287-298.

Gregory K, Walling D. The variation of drainage density within a catchment. Hydrological Sciences Journal 1968;13(2):61-68.

Guzzetti F, Marchetti M, Reichenbach P. Large alluvial fans in the north-central Po Plain (Northern Italy). Geomorphology 1997;18(2):119-136.

Hack JT. Studies of longitudinal stream profiles in Virginia and Maryland: US Geological Survey Professional Paper 1957:294, 45-97.

Hack JT. Stream-profile analysis and stream-gradient index. Journal of Research of the US Geological Survey 1973;1(4):421-429.

Hancock G, Willgoose G. Use of a landscape simulator in the validation of the SIBERIA catchment evolution model: Declining equilibrium landforms. Water Resour Res 2001;37(7):1981-1992.

Harvey AM. The occurrence and role of arid-region alluvial fans. Arid Region Geomorphology 1989:136-158.

Harvey AM. Factors influencing quaternary alluvial fan development in southeast Spain, in Alluvial Fans: A Field Approach, edited by A. H. Rachocki and M. Church, John Wiley, Hoboken, N.J 1990: 109–129,

Harvey AM. The role of alluvial fans in arid zone fluvial systems. Arid zone geomorphology (2nd edition).John Wiley & Sons 1997:231-260.

Haviv I, Enzel Y, Whipple K, Zilberman E, Matmon A, Stone J, et al. Evolution of vertical knickpoints (waterfalls) with resistant caprock: Insights from numerical modeling. Journal of Geophysical Research: Earth Surface (2003–2012) 2010;115(F3).

Hayakawa YS, Oguchi T. GIS analysis of fluvial knickzone distribution in Japanese mountain watersheds. Geomorphology 2009;111(1):27-37.

Hayakawa YS, Oguchi T. DEM-based identification of fluvial knickzones and its application to Japanese mountain rivers. Geomorphology 2006;78(1):90-106.

Hayakawa Y, Matsukura Y. Recession rates of waterfalls in Boso Peninsula, Japan, and a predictive equation. Earth Surf Process Landforms 2003;28(6):675-684.

Holm DA. Desert Geomorphology in the Arabian Peninsula. Science 1960;132(3437).

Hötzl H, Maurin V, Zötl JG. Geologic history of the Al Hasa area since the Pliocene. In: S.S. Al-Sayari & J.G. Zötl, (eds.). Quaternary Period in Saudi Arabia. Vienna: Springer-Verlag. pp. 1978: 58–74.

Hotzl H. Groundwater recharge in an arid karst area (Saudi Arabia). IAHS Publications-Series of Proceedings and Reports-Intern Assoc Hydrological Sciences 1995;232:195-210.

Hooke RL. Steady-state relationships on arid-region alluvial fans in closed basins. Am J Sci 1968;266(8):609-629.

Hooke RL, and Rohrer RW. Geometry of alluvial fans: Effect of discharge and sediment size, Earth Surface Processes 1979: (4):147-166.

Horton RE. Erosional development of streams and their drainage basins; hydrophysical approach to quantitative morphology. Geological Society of America Bulletin 1945;56(3):275-370.

Horton RE. Drainage-basin characteristics. Transactions, American geophysical union 1932;13:350-361.

Howard AD. Role of hypsometry and planform in basin hydrologic response. Hydrological Processes 1990: 4(4):373-385.

Howard AD, Dietrich WE, Seidl MA. Modeling fluvial erosion on regional to continental scales. Journal of Geophysical Research: Solid Earth (1978–2012) 1994;99(B7):13971-13986.

Hurtrez J, Sol C, Lucazeau F. Effect of drainage area on hypsometry from an analysis of small-scale drainage basins in the Siwalik Hills (Central Nepal). Earth Surf Process Landforms 1999;24(9):799-808.

Imhof E. Cartographic relief presentation. : ESRI, Inc.; 2007.

Jansen JD, Fabel D, Bishop P, Xu S, Schnabel C, Codilean AT. Does decreasing paraglacial sediment supply slow knickpoint retreat? Geology 2011;39(6):543-546.

Jenson S, Domingue J. Extracting topographic structure from digital elevation data for geographic information system analysis. Photogramm Eng Remote Sensing 1988;54(11):1593-1600.

Johnson PR, Woldehaimanot B. Development of the Arabian-Nubian Shield: perspectives on accretion and deformation in the northern East African Orogen and the assembly of Gondwana. Geological Society, London, Special Publications 2003;206(1):289-325.

Johnson P. The structural geology of the Samran-Shayban area, Kingdom of Saudi Arabia. Saudi Arabian Deputy Ministry for Mineral Resources Technical Report 1998.

Kale VS, Shejwalkar N. Uplift along the western margin of the Deccan Basalt Province: Is there any geomorphometric evidence? Journal of earth system science 2008;117(6):959-971.

Keller EA, Pinter N. Active Tectonics: Earthquakes, Uplift and Landscape, 2nd ed. Prentice-Hall, Upper Saddle River 2002:362

Kirby E, Whipple K. Expression of Active Tectonics in Erosional Landscapes. Journal of Structural Geology 2012: 44: 54-75.

Kirby E, Whipple K. Quantifying differential rock-uplift rates via stream profile analysis. Geology 2001;29(5):415-418.

Kochel RC. Geomorphic impact of large floods: review and new perspectives on magnitude and frequency." Flood Geomorphology. John Wiley & Sons New York. 1988: (9):169-187.

Koppen W. Das geographische System der Klimate. vol. 1, part C. Koppen, W., & R.Geiger.Handbuch der Klimatologie.Gebr.Borntrager, Berlin 1936.

Li P, Shi C, Li Z, Muller J, Drummond J, Li X, et al. Evaluation of ASTER GDEM ver2 using GPS measurements and SRTM ver4. 1 in China. 2012.

Liang C, MaCkay DS. A general model of watershed extraction and representation using globally optimal flow paths and up-slope contributing areas. Int J Geogr Inf Sci 2000;14(4):337-358.

Lifton NA, Chase CG. Tectonic, climatic and lithologic influences on landscape fractal dimension and hypsometry: implications for landscape evolution in the San Gabriel Mountains, California. Geomorphology 1992;5(1):77-114.

Lima AG, Binda AL. Lithologic and structural controls on fluvial knickzones in basalts of the Paraná Basin, Brazil. Journal of South American Earth Sciences 2013;48:262-270.

Lin Z, Oguchi T, Chen Y, Saito K. Constant-slope alluvial fans and source basins in Taiwan. Geology 2009;37(9):787-790.

Maidment DR. Arc Hydro: GIS for water resources. : ESRI, Inc.; 2002.

Masek JG, Isacks BL, Gubbels TL, Fielding EJ. Erosion and tectonics at the margins of continental plateaus. Journal of Geophysical Research: Solid Earth (1978–2012) 1994;99(B7):13941-13956.

Matmon A, Bierman P, Enzel Y. Pattern and tempo of great escarpment erosion. Geology 2002;30(12):1135-1138.

McGillivray J, Husseini M. The Paleozoic Petroleum Geology of Central Arabia (1). AAPG Bull 1992;76(10):1473-1490.

Melton MA. Debris-covered hillslopes of the southern Arizona desert: Consideration of their stability and sediment contribution. J Geol 1965:715-729.

Melton MA. An analysis of the relations among elements of climate, surface properties, and geomorphology Proj 1957: NR 889-042 Tech. Rep. 11, 7

Merritts D, Vincent KR. Geomorphic response of coastal streams to low, intermediate, and high rates of uplift, Medocino triple junction region, northern California. Geological Society of America Bulletin 1989;101(11):1373-1388.

Miller JR. The influence of bedrock geology on knickpoint development and channel-bed degradation along downcutting streams in south-central Indiana. J Geol 1991:591-605.

Miller JR, Ritter DF, Kochel RC. Morphometric assessment of lithologic controls on drainage basin evolution in the Crawford Upland, South-Central Indiana. Am J Sci 1990;290:569-599.

Miller RP. Drainage lines in bas-relief. J Geol 1937:432-438.

Miller SR, Sak PB, Kirby E, Bierman PR. Neogene rejuvenation of central Appalachian topography: Evidence for differential rock uplift from stream profiles and erosion rates. Earth Planet Sci Lett 2013;369:1-12.

Miller VC. A quantitative geomorphic study of drainage basin characteristics in the Clinch Mountain Area, Virginia and Tennessee. Columbia University. Department of Geology Technical Report 1953: 3

Ministry of Agriculture and Water. Water Atlas of Saudi Arabia. Riyadh. 1984: 111.

Molnar, P., Anderson, R. S., Kier, G., & Rose, J. Relationships among probability distributions of stream discharges in floods, climate, bed load transport, and river incision. Journal of Geophysical Research: Earth Surface (2003–2012), 2006:111(F2).

Montgomery DR, Balco G, Willett SD. Climate, tectonics, and the morphology of the Andes. Geology 2001;29(7):579-582.

Montgomery DR, Dietrich WE. Channel initiation and the problem of landscape scale. Science 1992;255(5046):826-830.

Moore ID, Turner AK, Wilson JP, Jenson SK, Band LE, Goodchild M, et al. GIS and land-surface-subsurface modeling. Environmental modeling with GIS. 1993:196-230.

Moore JM, Howard AD. Large alluvial fans on Mars. Journal of Geophysical Research: Planets (1991–2012) 2005;110(E4).

Morisawa ME. Relation of discharge and stream length in eastern United States. Proceedings International Hydrology Symposium, Fort Collins, Colorado 1967: 1: 173-176

Morisawa ME. Quantitative geomorphology of some watersheds in the Appalachian Plateau. Geological Society of America Bulletin 1962;73(9):1025-1046.

Morisawa ME. Accuracy of determination of stream lengths from topographic maps. Transactions, American Geophysical Union 1957;38:86-88.

Nanson G, Gibling M. Anabranching and anastomosing rivers. Encyclopedia of Geomorphology 2004:21-25.

Nehlig P, Genna A, Asfirane F. A review of the Pan-African evolution of the Arabian Shield. GeoArabia-Manama 2002;7:103-124.

Nogami M. Geomorphometric measures for digital elevation models. Zeitschrift fur Geomorphologie 1995.

O'Callaghan JF, Mark DM. The extraction of drainage networks from digital elevation data. Computer vision, graphics, and image processing 1984;28(3):323-344.

Oguchi T. Drainage density and relative relief in humid steep mountains with frequent slope failure. Earth Surf Process Landforms 1997;22(2):107-120.

Oguchi T. Ohmori H. Analysis of relationships among alluvial fans area, source basin area, basin slope, and sediment yield. Zeitschrift fur Geomorphologie Neue Folge 1994;38:405-420.

Ohmori H. Changes in the hypsometric curve through mountain building resulting from concurrent tectonics and denudation. Geomorphology 1993;8(4):263-277.

Olivetti V, Cyr AJ, Molin P, Faccenna C, Granger DE. Uplift history of the Sila Massif, southern Italy, deciphered from cosmogenic 10Be erosion rates and river longitudinal profile analysis. Tectonics 2012;31(3).

Ortega JA, Wohl E, Livers B. Waterfalls on the eastern side of Rocky Mountain National Park, Colorado, USA. Geomorphology 2013;198:37-44.

Ouimet WB, Whipple KX, Granger DE. Beyond threshold hillslopes: Channel adjustment to base-level fall in tectonically active mountain ranges. Geology 2009;37(7):579-582.

Pederson JL, Tressler C. Colorado River long-profile metrics, knickzones and their meaning. Earth Planet Sci Lett 2012;345:171-179.

Phillips JD, McCormack S, Duan J, Russo JP, Schumacher AM, Tripathi GN, et al. Origin and interpretation of knickpoints in the Big South Fork River basin, Kentucky–Tennessee. Geomorphology 2010;114(3):188-198.

Pike AC, Mueller TG, Schörgendorfer A, Shearer SA, Karathanasis AD. Erosion index derived from terrain attributes using logistic regression and neural networks. Agronomy Journal 2009:101 (5): 1068-1079.

Pike RJ. A bibliography of terrain modeling (geomorphometry), the quantitative representation of topography. US Geol.Surv.Open-File Rep.02 2002;465.

Pike RJ. Geomorphometry-diversity in quantitative surface analysis. Prog Phys Geogr 2000;24(1):1-20.

Pike RJ. Geomorphometry-process, practice, and prospect. Zeitschrift fur Geomorphologie Supplementband 1995:221-238.

Pike RJ, Wilson SE. Elevation-relief ratio, hypsometric integral, and geomorphic area-altitude analysis." Geological Society of America Bulletin 1971:82(4):1079-1084.

Prima ODA, Yoshida T. Characterization of volcanic geomorphology and geology by slope and topographic openness. Geomorphology 2010;118(1):22-32.

Rappold GD. Precipitation analysis and agricultural water availability in the Southern Highlands of Yemen. Hydrol Process 2005;19(12):2437-2449.

Raux J, Copard Y, Laignel B, Fournier M, Masseï N. Classification of worldwide drainage basins through the multivariate analysis of variables controlling their hydrosedimentary response. Global Planet Change 2011;76(3):117-127.

Reches Z, Schubert G. Models of post-Miocene deformation of the Arabian Plate. Tectonics 1987;6(6):707-725.

Reineck H, Singh IB. Depositional sedimentary environments. Springer-Verlag 1973:439.

Ritter D F, Kochel RC, Miller JR., Process Geomorphology 3rd Ed.: W.C. Brown Publishers, Dubuque 1995: IA, 539 pp

Sagga A. Roundness of sand grains of longitudinal dunes in Saudi Arabia. Sediment Geol 1993;87(1):63-68.

Sarangi A, Madramootoo C, Enright MP. Development of user interface in ArcGIS for estimation of watershed geomorphology. Candaian society for engineering in agricultural, food and biological systems 2003.

Scheidegger A. Mathematical models of slope development. Geological Society of America Bulletin 1961;72(1):37-50.

Schumm SA. Rates of surficial rock creep on hillslopes in Western Colorado. Science 1967 Feb 3;155(3762):560-562.

Schumm SA. Evolution of drainage systems and slopes in badlands at Perth Amboy, New Jersey. Geological Society of America Bulletin 1956;67(5):597-646.

Seeber L, Gornitz V. River profiles along the Himalayan arc as indicators of active tectonics. Tectonophysics 1983;92(4):335-367.

Sen Z. Wadi hydrology. : CRC Press; 2008.

Şen Z, Al-Suba'i K. Hydrological considerations for dam siting in arid regions: a Saudi Arabian study. Hydrological sciences journal 2002;47(2):173-186.

Şen Z, Al-Suba'i K. Seismic hazard assessment in the Tihamat Asir region, southwestern Saudi Arabia. Math Geol 2001;33(8):967-991.

Singh P, Kumar V, Purohit R, Kothari M, Dashora P. Application of principal component analysis in grouping geomorphic parameters for hydrologic modeling. Water Resour Manage 2009;23(2):325-339.

Sklar L, Dietrich WE. River longitudinal profiles and bedrock incision models: Stream power and the influence of sediment supply. Rivers over rock: fluvial processes in bedrock channels 1998: 237-260.

Snyder NP, Whipple KX, Tucker GE, Merritts DJ. Landscape response to tectonic forcing: Digital elevation model analysis of stream profiles in the Mendocino triple junction region, northern California. Geological Society of America Bulletin 2000;112(8):1250-1263.

Sreedevi PD, Subrahmanyam K, Shakeel A. The significance of morphometric analysis for obtaining groundwater potential zones in a structurally controlled terrain. Environmental Geology 2005:43(3): 412-420.

Stern RJ, Johnson P. Continental lithosphere of the Arabian Plate: a geologic, petrologic, and geophysical synthesis. Earth-Sci Rev 2010;101(1):29-67.

Stoeser DB, Frost CD. Nd, Pb, Sr, and O isotopic characterization of Saudi Arabian shield terranes. Chem Geol 2006;226(3):163-188.

Strahler AN. Quantitative geomorphology of drainage basin and channel networks. Handbook of Applied Hydrology 1964.

Strahler AN. Quantitative analysis of watershed geomorphology. Civ.Eng 1957;101:1258-1262.

Strahler AN. Quantitative geomorphology of erosional landscapes. International Geologic Congress; 1954.

Strahler AN. Statistical analysis in geomorphic research. J Geol 1954:1-25.

Strahler AN. Hypsometric (area-altitude) analysis of erosional topography. Geological Society of America Bulletin 1952;63(11):1117-1142.

Strahler AN. Equilibrium theory of erosional slopes approached by frequency distribution analysis. Part I. Am J Sci 1950;248:673-696.

Subyani AM. Hydrochemical identification and salinity problem of ground-water in Wadi Yalamlam basin, Western Saudi Arabia. J Arid Environ 2005;60(1):53-66.

Subyani AM, Qari MH, Matsah MI. Digital elevation model and multivariate statistical analysis of morphometric parameters of some wadis, western Saudi Arabia. Arabian Journal of Geosciences 2012;5(1):147-157.

Subyani N, Bayumi N. Evaluation of groundwater resources in wadi Yalamlam basin, Makkah area. King Abdulaziz University, project no. 203/420, Jeddah, Saudi Arabia 2003.

Tachikawa T, Kaku M, Iwasaki A, Gesch D, Oimoen M, Zhang Z, et al. ASTER Global Digital Elevation Model Version 2–Summary of Validation Results August 31, 2011. 2011.

Talling PJ, Sowter MJ. Drainage density on progressively tilted surfaces with different gradients, Wheeler Ridge, California. Earth Surf Process Landforms 1999;24(9):809-824.

Tarboton DG. A new method for the determination of flow directions and upslope areas in grid digital elevation models. Water Resour Res 1997;33(2):309-319.

Tarboton DG, Bras RL, Rodriguez-Iturbe I. Scaling and elevation in river networks. Water Resour Res 1989;25(9):2037-2051.

Tarboton DG. The analysis of river basins and channel networks using digital terrain data 1989.

Tucker GE, Bras RL. Hillslope processes, drainage density, and landscape morphology. Water Resour Res 1998;34(10):2751-2764.

Tucker GE, Slingerland R. Drainage basin responses to climate change. Water Resour Res 1997;33(8):2031-2047.

VanLaningham S, Meigs A, Goldfinger C. The effects of rock uplift and rock resistance on river morphology in a subduction zone forearc, Oregon, USA. Earth Surf Process Landforms 2006;31(10):1257-1279.

Vincent P. Saudi Arabia: an environmental overview. : Psychology Press; 2008.

Walcott RC. Summerfield MA. Scale dependence of hypsometric integrals: An analysis of southeast African basins." Geomorphology 2008: 96(1):174-186.

Whipple KX, Wobus C, Crosby B, Kirby E, Sheehan D. New tools for quantitative geomorphology: extraction and interpretation of stream profiles from digital topographic data. Geological Society of America, Annual Meeting, Short Course Guide: Boulder Colorado, disponible en www.geomorphtools.org; 2007.

Whipple KX, Tucker GE. Dynamics of the stream-power river incision model: Implications for height limits of mountain ranges, landscape response timescales, and research needs. Journal of Geophysical Research: Solid Earth (1978–2012) 1999;104(B8):17661-17674.

Whittaker AC, Boulton SJ. Tectonic and climatic controls on knickpoint retreat rates and landscape response times. Journal of Geophysical Research: Earth Surface (2003–2012) 2012;117(F2).

Willgoose G, Rafael LB, Rodriguez RI. A coupled channel network growth and hillslope evolution model: 1. Theory." Water Resources Research 1991:27(7):1671-1684.

Wilson JP, Gallant JC. Terrain analysis: principles and applications. : John Wiley & Sons; 2000.

Wilson L. Drainage density, length ratios, and lithology in a glaciated area of southern Connecticut. Geological Society of America Bulletin 1971;82(10):2955-2956.

Wobus CW, Crosby BT, Whipple KX. Hanging valleys in fluvial systems: Controls on occurrence and implications for landscape evolution. Journal of Geophysical Research: Earth Surface (2003–2012) 2006;111(F2).

Wohl EE. Mountain rivers. : American Geophysical Union; 2000:14

Wohl EE, Greenbaum N, Schick AP, Baker VR. Controls on bedrock channel incision along Nahal Paran, Israel. Earth Surf Process Landforms 1994;19(1):1-13.

Wohl EE, Thompson DM, Miller AJ. Canyons with undulating walls. Geological Society of America Bulletin 1999;111(7):949-959.

Yatsu E. On relief energy of the Chichibu Mountains, Japan. Transactions Otsuka Geographical Association 1950;6:323-330.

Yatsu E. On the longitudinal profile of the graded river. Transactions, American Geophysical Union 1955;36:655-663.

Young R. Waterfalls: form and process. Z.Geomorphol.Suppl 1985;55:81-95.

Youssef AM, Maerz NH, Al-Otaibi AA. Stability of rock slopes along Raidah escarpment road, Asir Area, Kingdom of Saudi Arabia. Journal of Geography and Geology 2012;4(2):p48.

Zaprowski BJ, Evenson EB, Pazzaglia FJ, Epstein JB. Knickzone propagation in the Black Hills and northern High Plains: A different perspective on the late Cenozoic exhumation of the Laramide Rocky Mountains. Geology 2001;29(6):547-550.

Zaprowski BJ, Pazzaglia FJ, Evenson EB. Climatic influences on profile concavity and river incision. Journal of Geophysical Research: Earth Surface (2003–2012) 2005;110(F3).

Zavoianu I. Morphometry of drainage basins. : Elsevier; 1985.

Zhang H, Zhang P, Fan Q. Initiation and recession of the fluvial knickpoints: A case study from the Yalu River-Wangtian'e volcanic region, northeastern China. Science China Earth Sciences 2011;54(11):1746-1753.